THESIS

EVALUATION OF CONTROLLED END GAS AUTO IGNITION WITH EXHAUST GAS RECIRCULATION IN A STOICHIOMETRIC, SPARK IGNITED, NATURAL GAS ENGINE

Submitted by

Scott Michael Bayliff

Department of Mechanical Engineering

In partial fulfillment of the requirements

For the degree of Master of Science

Colorado State University

Fort Collins, Colorado

Spring 2020

Master's Committee:

Advisor: Daniel B. Olsen

Bret Windom
Daniel Baker

Copyright Scott Bayliff 2020

All Rights Reserved

ABSTRACT

EVALUATION OF CONTROLLED END GAS AUTO IGNITION WITH EXHAUST GAS RECIRCULATION IN A STOICHIOMETRIC, SPARK IGNITED, NATURAL GAS ENGINE

Many stationary and heavy-duty on-road natural gas fueled engines today operate under stoichiometric conditions with a three-way catalyst. The disadvantage of stoichiometric natural gas engines compared to lean-burn natural gas and diesel engines is lower efficiency, resulting primarily from lower power density and compression ratio. Exhaust gas recirculation (EGR) coupled with advanced combustion controls can enable operation with higher compression ratio and power density, which yields higher efficiency. This also results in engine operation between the limits of knock and misfire. Operation between these limits has been named controlled end gas auto-ignition (C-EGAI) and can be used to improve the brake efficiency of the engine.

Various methods of cylinder pressure-based knock quantification were explored to implement C-EGAI. The indicated quantification methods are used for the implementation of a control scheme for C-EGAI with a relation to the fractional heat release due to auto-ignition. A custom EGR system was built and the effect of EGR on the performance of a stochiometric, spark ignited, natural gas engine is evaluated. C-EGAI is implemented and the optimal parameters are determined for peak performance under EGR and C-EGAI conditions.

In this study, knock detection is used for the recognition, magnitude, and location of the auto-ignition events. Cylinder pressure-based knock detection was the primary method for determining the occurrence and location of knock but was also used for implementing the ignition control scheme for controlled end gas auto-ignition. The combustion intensity metric

(CIM) enabled parametric ignition timing control which allowed for the creation of a relationship between fractional heat release due to auto-ignition and CIM.

Both exhaust gas recirculation and controlled end gas auto-ignition were analyzed with a cooperative fuel research (CFR) engine modified for boosted fuel/air intake. The data was interpreted to provide a proper evaluation of unique analytical methods to quantify the results of C_EGAI and characterize the live auto-ignition events. The control variables for this method of C-EGAI were optimized with EGR conditions to generate the point of peak performance on the CFR engine under stoichiometric, spark ignited, natural gas conditions.

ACKNOWLEDGEMENTS

I would like to recognize the people and groups who supported during the work presented in this Thesis. The Department of Energy office of Energy and Renewable Energy for sponsoring and funding this study. My advisor, Dr. Daniel B. Olsen, for his support throughout my graduate studies and allowing me to work within his research group. Dr. Bret Windom, Dr. Anthony Marchese, and Dr. Daniel Baker for their interest in this work, for the time they invested on my behalf, and for the guidance they provided me throughout this process. I would also like to thank Robbin Bremmer and Hui Xu from Cummins Inc. for their support with engine test cell issues. Along with Greg Hampson, Suraj Nair, and Jeffery Carlson from Woodward Inc. for their assistance with data processing and installation of their donated LECM on the CFR engine test cell. The powerhouse staff – Mark, Kirk, and James, who guided me through months of troubleshooting and engine test cell development. I would also like to thank many others who assisted me – Alex, Jack, Diego, Matt, Jason, and Chris. Finally, my parents David and Pam along with the rest of my friends and family, who endlessly supported me every step of the way while putting up with the previous stress-ridden year of study.

TABLE OF CONTENTS

LIST OF TABLES

LIST OF FIGURES

CHAPTER 1: INTRODUCTION

1.1 BACKGROUND AND MOTIVATION

Improvements in natural gas (NG) engine efficiencies while maintaining ultra-low NOx emission levels are necessary to realize future NG fuel demand goals and exploit the economic and environmental benefits of NG. Targeting higher efficiencies and NOx emission levels that will compete with future electrified fleet will require technological improvements in areas such as high CR, fast combustion, and advanced combustion phasing so that increased efficiency can be reached. However, the occurrence of end gas auto-ignition (EGAI) prevents using the optimal theoretical values for each of these parameters as an engine is typically designed with a knock margin or safety factor by "backing off" CR or retarding combustion phasing.

EGAI is characterized by low-temperature chemistry and self-heating of the gas ahead of the flame front due to the rising pressure and compressive temperature resulting from the propagating flame. Often viewed as adiabatic compression conditions, this end-gas starts its own low-temperature chemical reactions. If left long enough under these conditions, radical build-up can occur in the end-gas and trigger rapid combustion of the fuel in this vicinity. Radical formation and EGAI are heightened in larger n-alkane hydrocarbon species due to unique low-temperature combustion kinetics, posing challenges to natural gas fuels that have high variability in these species' concentrations. If the flame front is fast enough and the auto-ignition reactions slow enough, then the flame will consume the end gas prior to EGAI. Historical approaches have been to move toward rapid burn rates and slow auto-ignition reactions (e.g., running lean,

diluting with EGR, or controlling fuel chemistry) [1]. The EGAI phenomenon is displayed below in Figure 1.

Engine combustion strategies utilizing lean mixtures or exhaust gas recirculation (EGR) can lead to high cycle-to-cycle ignition variation. Since only the most advanced combustion event might trigger the uncontrolled knock, the average cycles must be retarded to ensure the most aggressive cycle does not knock, translating into a net loss in efficiency. One of the key strategies proposed here is to move the most aggressive cycle closer to the average cycle by cycle resolved control thereby shrinking the knock margin and recovering efficiency benefits. To do this requires an in-depth understanding of the knock/EGAI phenomenon, inherently stable combustion, and a control system that can maintain optimal combustion phasing while fuel, engine, and atmospheric conditions change. Such a system can minimize the knock margin under all conditions and enable maximum efficiency.

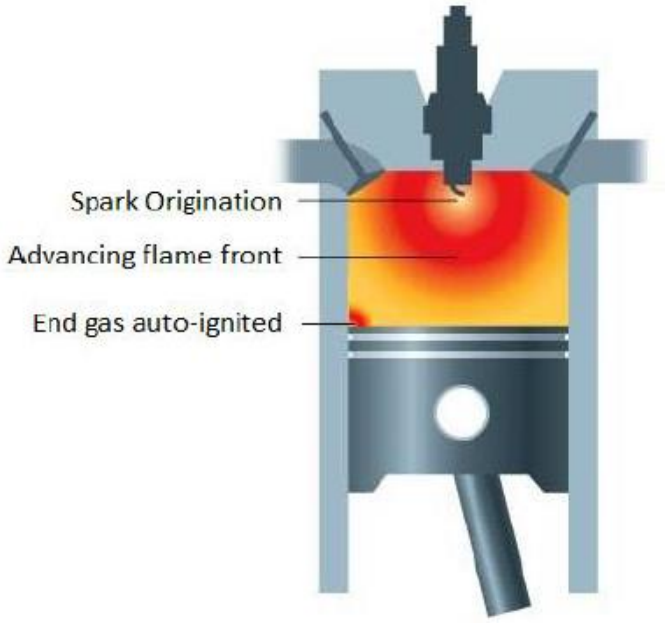

Figure 1: Auto Ignition of End Gas in a Combustion Chamber [2]

For stoichiometric combustion, operating at high compression ratios (CRs), closer to severe knock limited operational conditions, will achieve higher efficiencies and engine power. The decision to run stoichiometric was influenced by the benefit of reduced emission generations from the use of a three-way catalyst with stoichiometric exhaust. Running at high CR will require the use of high concentrations of cooled EGR with advanced real-time controls to monitor and optimize EGR rates and combustion phasing. Increases in EGR, despite allowing for higher CR, slows burn rates (laminar flame speeds decrease 5-fold going from 0 - 30% EGR) shifting a majority of heat release away from minimum volume and potentially preventing complete burn, negatively affecting fuel economy and resulting in unburned hydrocarbon emissions [3]. Furthermore, EGR dilution can increased the cycle to cycle variability and was utilized at levels that maximize CR while achieving stable combustion. Issues related to EGR dilution can be mitigated by increasing flame propagation by way of increased turbulent mixing while also enhancing flame initiation with advanced ignition technologies.

To date, there has been a limited amount of work exploring controlled end gas auto-ignition (C-EGAI), primarily isolated to gasoline SI engines. Nevertheless, improved brake specific power and peak torque have been observed with the successful implementation of C-EGAI [4]. Demonstration of real-time control over a varying engine load speed map is lacking and represents a key challenge towards the adoption of this combustion mode. Furthermore, an improved understanding regarding the coupling between fuel chemistry and turbulent fluid dynamic driven heat and mass transport between the burned and unburned gases are needed before this strategy can be implemented in practice. Given the complex coupling between the fluid dynamics, fuel ignition chemistry, and combustion phasing, the engine and associated are and fuel delivery systems must be designed to operate in this mode to maximize efficiency and

power output. The instability of uncontrolled combustion phasing can be seen in Figure 2, which demonstrated the difference of 1 cylinder in a 4-cylinder engine that lacks proper combustion control (i.e. constant ignition timing) [5].

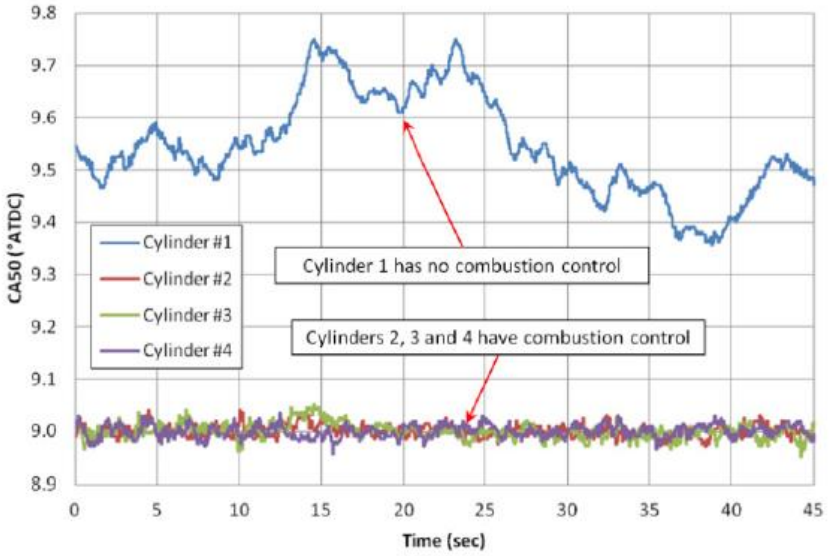

Figure 2: Effects of Continuously Varying Ignition Control on Combustion Phasing for Cylinder 1 – Not Controlled, and Cylinders 2, 3, and 4 Under CA50 Closed-Loop Control.

Real-time optimization strategies for operational parameters related to EGR rate, ignition timing, fuel injection, and boost pressure will be selected from engine models with inputs validated by CFD. As such, the development of these predictive capabilities will require a fundamental understanding of the physics behind misfire, burn rates, and EGAI and must be vetted and validated strategically to ensure they are correctly predicting the in-cylinder physics and chemistry that will allow them to be used as design tools. Using the fundamental knowledge related to EGAI gained during the early phases of the research combined with new sensing and

control strategies will be implemented to demonstrate a pathway to greater efficiency for natural gas engines.

Two compelling reasons to use NG as a substitute for diesel fuel are to reduce particulate matter emissions and fuel costs. Currently in the U.S., the cost of diesel fuel on an equivalent energy basis is approximately 5X the cost of NG [6]. NG engines, however, are typically less efficient than diesel engines, especially in the on-road medium and heavy-duty engine markets.

NG engines offer several advantages over diesel engines including lower particulate matter emissions, lower capital and operating costs, availability of vast domestic NG resources, and lower CO2 emissions. With the appropriate exhaust aftertreatment system both NG and diesel engines can meet ultra-low emission limits. However, the exhaust aftertreatment systems used for diesel engines are much more complex, requiring in many cases an oxidation catalyst, diesel particulate filter, and a selective catalytic reduction system. Most current medium-duty NG engines use a single aftertreatment component, a 3-way catalyst, and therefore the aftertreatment system is less complex and lower cost. Market penetration of NG engines for mobile applications has been slow due to limited fueling infrastructure, lower engine efficiency, and lower power density. The second two limitations are closely related since increasing engine power density, or brake mean effective pressure (BMEP), is a practical approach for increasing engine efficiency [7].

The path to diesel-like efficiencies and low emissions in a stoichiometric SI platform with cooled EGR will be achieved through increased compression ratio, cooler combustion temperatures by way of increased EGR fraction, and enhanced rate of combustion. However, individual improvements are limited by knock, misfire, and emissions and are difficult to optimize due to highly varying fuel reactivity. Currently, NG SI engines are designed for the

worst-case fuel quality, resulting in suboptimal performance for the average fuel reactivity. Fundamental research is needed to better understand the underlying combustion phenomenon to enable optimization of the engine design parameters and develop control algorithms to expand knock, emissions, and misfire limits.

1.2 LITERATURE REVIEW

Exhaust Gas Recirculation:

Exhaust gas recirculation is when part of the exhaust is re-routed into the intake manifold and blended with the fuel/air mixture to dilute the charge, thereby reducing peak combustion temperatures. Methods of exhaust gas recirculation include, low-pressure loop recirculation, high-pressure loop recirculation, and dedicated cylinder recirculation, with a high-pressure loop EGR system depicted below in Figure 3. All three methods provide the same fundamental function of EGR, with the primary difference being in the required hardware [8]. EGR commonly replaces an average of 13% of the intake fluid in natural gas engines, with the maximum commercial EGR rate being 17% [9]. The higher rates lead to increased misfire rates and decreased combustion stability despite the increased compression ratios and intake pressure associated with higher EGR rates. These factors make up the physical limits during engine operation, giving operators proper scale of how far they can push the variables of their engine.

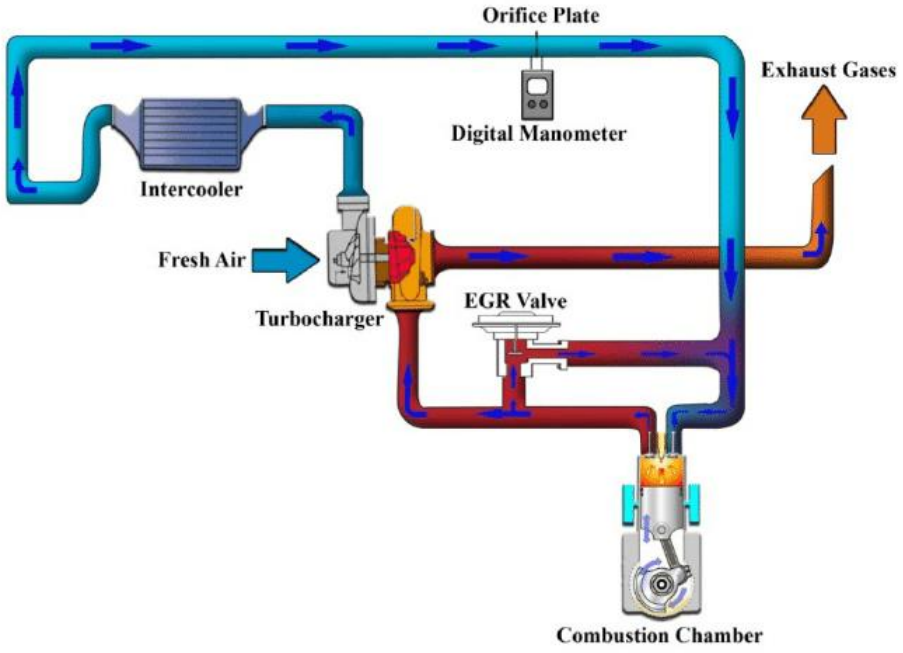

Figure 3: High-Pressure Exhaust Gas Recirculation Diagram [10]

With these physical barriers, engine performance is limited by blocking chemical mechanisms of combustion that commonly occur inside constant volume combustion. Induction of EGR fluid into the intake charge mixes a large amount of H2O and CO2, and a small amount of CO, NOx, and unburned hydrocarbons with the clean combustion air and fuel that make up the initial charge [11]. The CO2 and H2O molecules increase the mixture specific heat, resulting in reduced compression and combustion temperatures. This is because the effect of adding EGR increases the total heat capacity of the charge, which absorbs energy during compression and combustion to limit peak temperatures [12]. However, as the temperature increases in the overall mixture, the readily available H2O, CO, and NOx molecules increase pathways to generate O, OH, O2, and H2O2 molecules and radicals that react readily with H radicals to split fuel molecules [11].

However, with relatively high EGR, a large amount of the intake charge is replaced by exhaust gas, and the number of diluents such as H2O and CO2 become too large to allow complete combustion. This occurs at and above the rated maximum EGR rate for most engines, due to the fact the limiting factor involves combustion instability [13]. The CO2 and H2O molecules absorb up to 40% of the available heat at maximum EGR rates, reducing the available energy for complete combustion. This leads to the simulation of "rich" exhaust components, with increased concentrations of CO and CO2 [14]. During this time, the exhaust gas is still being recycled, which leads to an exponential decrease in combustion efficiency, and the misfire rate continues to climb with exhaust concentrations. To limit this, EGR has been expanded to stoichiometric engines for even greater emissions reductions [3].

EGR provides more benefits than pitfalls, creating the opportunity for increased efficiency through expanding knock limits and boost pressures to create a larger power density, reducing NOx emissions, and increasing knock suppression. The knock suppression is the most compelling reason for EGR utilization, allowing for turbocharged gaseous fuels engines with EGR to create up to 18% more power than turbocharged gaseous fueled engines without EGR [6].

1.2.2 Natural Gas Auto Ignition:

Auto-ignition, also known as engine knock, is a combustion event where unburned fuel molecules mixed with air are introduced to enough energy through heat transfer and pressure to combust spontaneously. These knocking events occur in engines after the initial ignition event, where the flame front is propagating throughout the cylinder, thus exposing the mixture that has yet to burn to the higher energy environment. When the temperature is enough, a secondary

ignition site is created, and the resulting pressure oscillations from end gas spontaneous combustion is what creates the characteristic “knock” or “ringing” to occur that gives these auto-ignition events their name [15] [16]. Engine knock has been known since 1916 and has been long seen as a negative consequence of extreme operating conditions. Within the last four decades, studies have arisen that demonstrate that early onset of engine knock and even light knock can be beneficial to engine performance [13]. Figure 4 shows two different knocking cases of varying intensities, highlighting the pressure fluctuations classified as knock ripples.

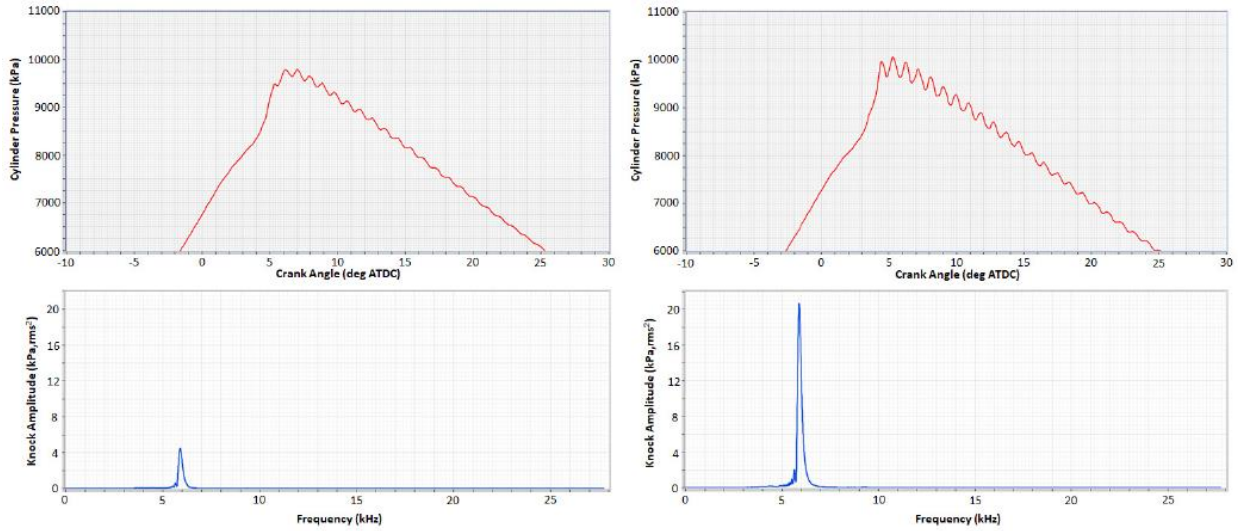

Figure 4: Different levels of knock in CFR engine – medium knock (left) and heavy knock (right)

A large influencer on the auto-ignition of natural gas in the fuel composition. This study examined a worst-case scenario fuel blend with a methane number of 69. The methane number is a measure similar to octane number for liquid fuels that represents the likelihood of auto-ignition to occur under given conditions. Higher methane numbers represent fuels that are less likely to auto-ignite. This is because higher methane numbers contain larger percentages of methane

compared to larger hydrocarbons that slows down the flame speed while the larger hydrocarbons also shorted the ignition delay. The factors of reduced ignition delays and faster flame speeds for fuels with lower methane numbers is what creates the conditions for low temperature combustion chemistry to occur and initiate auto-ignition.

Auto-ignition events commonly occur at the boundary of the combustion chamber. The "cooler" quench layer that exists at the edges of the combustion chamber burns and the boundary layer is disrupted, resulting in high local heat transfer that can cause cylinder damage. Continuous and gradual damage to the combustion chamber walls can lead to reduces lifespans.

A detrimental effect of auto-ignition is the stripping of the quench layer. The quench layer protects the walls of the combustion chamber from the extreme temperatures in the heart of the combustion event. When there is no quench layer, the walls can see temperatures at or above 1000 Celsius [17]. These temperatures create a corrosive reaction with the material of the wall, gradually diminishing the structural integrity of the walls [17]. Another concern with auto-ignition is that the resulting pressure oscillations can be higher than the threshold peak pressure of the engine. This can occur if the auto-ignition event is early enough in the combustion process, while there is a majority of unburned mass still in the cylinder. These large pressure fluctuations paired with wall erosion can lead to cracks and failures of physical components [18].

1.2.3 EGR Effects on Auto-Ignition:

One researcher reported that the frequency of knock occurrence drops by a minimum of 57% for combustion reactions containing EGR gasses [9]. For EGR rates that do not cause frequent cylinder misfire, EGR allows combustion to continue out from the ignition source but restrains any secondary ignition events from occurring unless the combustion intensity is too

high. As previously stated, EGR can reduce the combustion temperature during the reaction, and due to this, cut the NOx emissions in the exhaust stream. In general, there is a trade-off with other pollutant emissions such that as NOx is reduced, CO and unburned hydrocarbons increase [19].

Under "light" EGR conditions, auto-ignition can occur and lack suppression. With this, the volatility and intensity of the auto-ignition event is reduced drastically [8]. In terms of maximum pressure amplitude knock quantification method utilized by companies such as Cummins, Fiat, Briggs and Stratton, and Isuzu; 5% EGR rate displacement of the intake fluid reduces knock intensity from 5 bar to 4 bar variation in the knock ripple, and a 10% EGR rate reduces knock intensity from 5 bar to 2 bar at moderate knock intensity for a 12 L diesel genset engine [14] [17]. Further analysis on this engine shows an exponential decrease in knock intensity by every 5% EGR rate addition, limited at 15% EGR. This knock intensity reduction doubles with every 5% EGR rate addition until 15% EGR is reached, where any further addition leads to misfire and unstable combustion [9] [11].

An additional reason EGR is so effective at knock suppression beyond reduced combustion and end gas temperatures, is that EGR significantly reduces flame speed and increases ignition delay. Conventional combustion with EGR and no auto-ignition results in the need for advanced ignition timing by up to 27 degrees before top dead center (TDC) near idle speeds [20]. The location of 50% heat release occurs near 20 degrees after TDC [19]. With auto-ignition primarily occurring after 50% heat release, the "slow" flame speed related to EGR causes a large part of the heat release to occur while the piston is expanding, increasing the volume, and reducing the pressure and available energy for spontaneous combustion [3]. If EGR and the reduced energy slows down the combustion event enough, knock is unable to occur. The

average knocking event typically occurs between 5 to 15 degrees after TDC, with the heaviest knock intensity occurring around 5 degrees after TDC [21]. This leads to the requirement of parameter adjustments such as advanced timing and high compression ratio to be implemented to induce even light knock while operating with moderate to high EGR rates.

1.2.4 Effectiveness of Knock Suppression:

Knock suppression was an initial byproduct of EGR, but now it is an essential reason for EGR utilization in high-performance engines. Knock suppression, whether it is full suppression of all auto-ignition events or partial suppression and only reducing the intensity of the auto-ignition event, drastically reduces the chances of causing engine damage due to auto-ignition by nearly 96% [20]. The ability to only partially suppress an auto-ignition event, reducing the knock intensity and knock onset location, allows for modern technology to work with auto-ignition to improve engine performance while not inhibiting combustion efficiency through solely EGR utilization.

The effectiveness of knock suppression is a byproduct of the diluents in EGR fluid slowing down the flame speed and increasing the ignition delay so that most of the combustion occurs after the window of heavy auto-ignition. The laminar flame speed of stoichiometric natural gas with a methane number of 75 can be reduced by 10% EGR from approximately 0.50 m/s to 0.32 m/s at 30 bar pressure after the compression stroke [6]. This decrease slows the combustion event down enough through larger bore engine cylinders to minimize the likelihood of auto-ignition [8]. Reduced combustion temperatures, increased ignition delay, reduced overall reactivity, and reduced knock intensity was attributed to combustion phasing. The location of knocking events are vital to their severity, and the spread of combustion phasing over a larger

window of crank angles provide beneficial implementation of knock suppression [15]. A larger combustion window from EGR results in reduced efficiency, but the ability to augment engine performance variables leads to a more substantial efficiency benefit from EGR addition [12] [19].

Despite the suppression of knock intensity from EGR, the fractional heat release due to auto-ignition (f-EGAI) is near constant throughout all levels of EGR substitution. The f-EGAI is the remaining unburned mass fraction remaining in the cylinder after auto-ignition is initiated.

1.3 OVERVIEW AND SPECIFIC AIMS

The objective of this thesis is to determine, describe, and analyze a practical method of controlled end gas auto-ignition (C-EGAI), and its effects on spark ignited, stoichiometric natural gas engine performance. The experiments were conducted on a cooperative fuel research (CFR) engine. Utilizing a premixed natural gas blend with a methane number of 69 (Methane, Ethane, Propane blend verified with the Cummins methane number calculator, and full composition that was replicated shown in appendix D), the CFR engine was controlled under base stoichiometric conditions, then with EGR, then with advanced ignition control to control the level of auto-ignition in the engine. High-speed pressure measurements and crank angle resolved cylinder pressure data characterized the combustion processes and quantify the magnitude of end gas auto-ignition (EGAI) event. Post processing software written in LabVIEW and a Woodward Large Engine Control Module (LECM) enabled in-depth analysis of the required data sets.

The specific objectives of this work are to:

(1) Development and installation of EGR test cart

(2) Investigate knock quantification method to determine the optimal control method for C-EGAI.

(3) Evaluate the impact of EGR variability on the performance of a CFR engine under stoichiometric, spark ignited, natural gas conditions.

(4) Demonstrate the practicality of natural gas engine operation with EGR and C-EGAI and determine optimal levels of C-EGAI for maximum efficiency.

As an overview of this document, Chapter 2 describes the engine and test cell, detailing the associated apparatus and equipment required to collect the outlined data sets. Chapter 3 covers the methods behind the knock quantification utilized to define the knock intensity and fractional heat release due to auto-ignition (f-EGAI). This chapter also outlines the control methods behind C-EGAI. Chapter 4 describes the effect of exhaust gas recirculation (EGR) on a stochiometric, spark ignited, natural gas engine, both under knocking and knock-free conditions and provides insight into the prime operational window for maximum efficiency. Chapter 5 presents the findings on C-EGAI of the CFR engine, utilizing the findings from the previous chapters to guide the efficiency optimization for the optimum level of C-EGAI. This thesis is concluded with a summary and conclusion for the work and explores the applicability of C-EGAI to different applications and offers recommendations for future work.

CHAPTER 2: EXPERIMENTAL APPARATUS AND TESTING METHODS

2.1 COOPERATIVE FUEL RESEARCH ENGINE

The type of engine used in this project is a Cooperative Fuel Research (CFR) F-2 model manufactured by Waukesha Engine, Dresser Industries. It is a stationary, constant speed (~900 rpm), un-throttled, single cylinder, 4-stroke engine with a cylinder bore of 3.250 inches (8.255 cm) and piston stroke of 4.50 inches (11.43 cm). The displacement volume of the engine is 37.33 in^3 (611.7 cm^3). To enable operation at a range of compression ratios from 4:1 to 18:1 the engine is constructed with a can-type casting forming the cylinder and cylinder head as a single part. The exterior of the cylinder is configured with a jack-screw type threaded race allowing an engaged worm-gear to raise and lower the cylinder relative to the piston/connecting rod assembly, held laterally stable in a clamping sleeve. By raising or lowering the cylinder the clearance volume (that volume formed from the top of the piston at TDC, the cylinder wall and the cylinder head) is increased or decreased resulting in an adjustment of the compression ratio. The total vertical travel of the cylinder relative to the fixed position of the crankshaft is 1.235 inches. The engine allows adjustment of compression ratio while operating. Figure 5 provides a cut-away drawing of the engine cylinder and clamping sleeve sections. (Waukesha Engine Division, Dresser Industries, 2003)

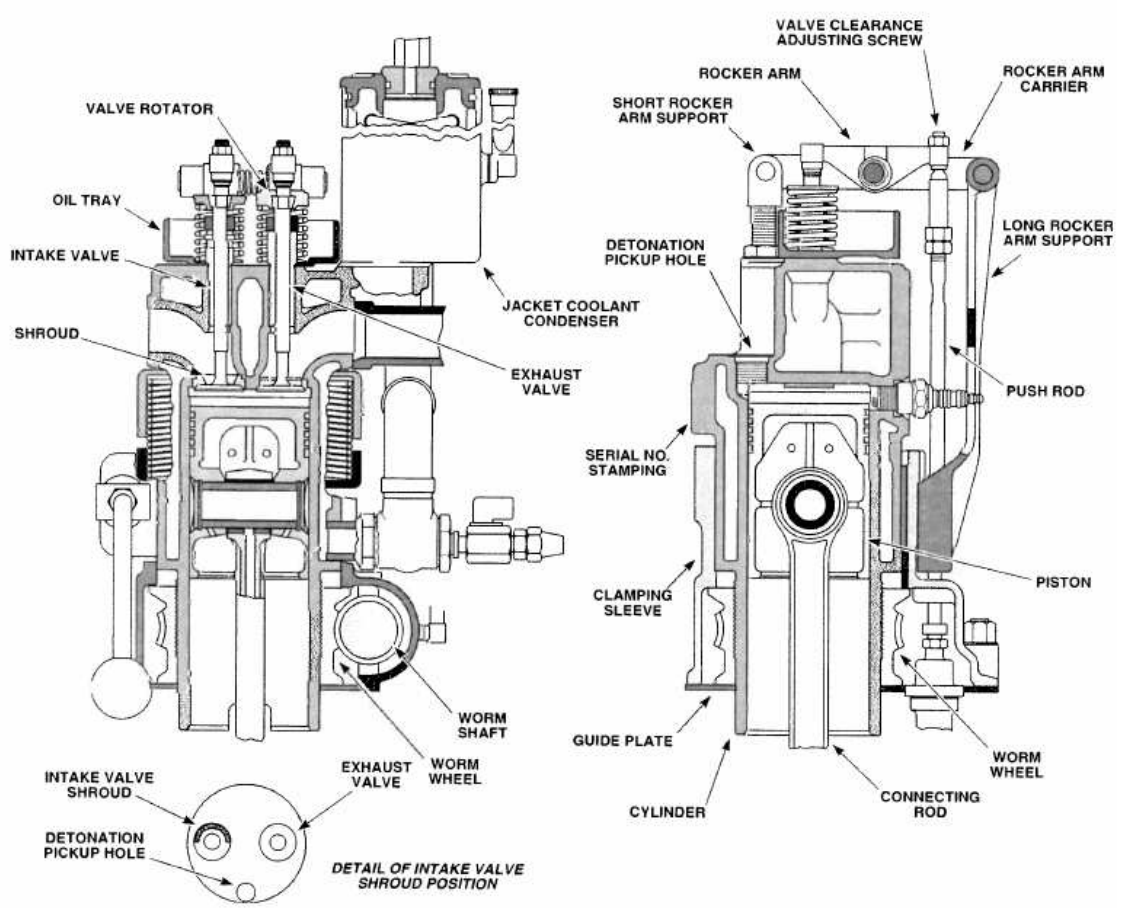

Figure 5: Cylinder and Clamping Sleeve Sections, Waukesha F-2 CFR [22]

The engine used in this project was manufactured in 1957 and is a model still manufactured and sold today, designed specifically for testing knock tendencies of fuels. Initially configured for octane number testing of gasoline blends, the engine is currently configured to burn gaseous fuels. The original CFR engine was designed in 1928 by the (then) Waukesha Motor Company at the request of the Co-operative Fuel Research (CFR) Committee to provide a standardized means to measure and define the combustion characteristics of gasoline blends. The engine was first displayed in January 1929 at the Society of Automotive Engineers annual meeting and served as the standard for fuel testing by both refiners and engine builders. The original design underwent slight modification but the mechanical configuration for the CFR F-2

has remained essentially unchanged since 1952. (Waukesha Engine Division, Dresser Industries, 1980)

The engine is operated through a belt driven connection with a 5-horsepower synchronous motor. On start-up and while operating without producing power (motoring operation) the engine is rotated by the motor, when fueled and producing power the synchronous motor operates as a generator feeding power to the electrical grid (powered operation). Engine speed is limited by the set constant motor speed during motoring operation and corresponding electric grid frequency during powered operation. Figure 6 depicts the current CFR engine used in this study.

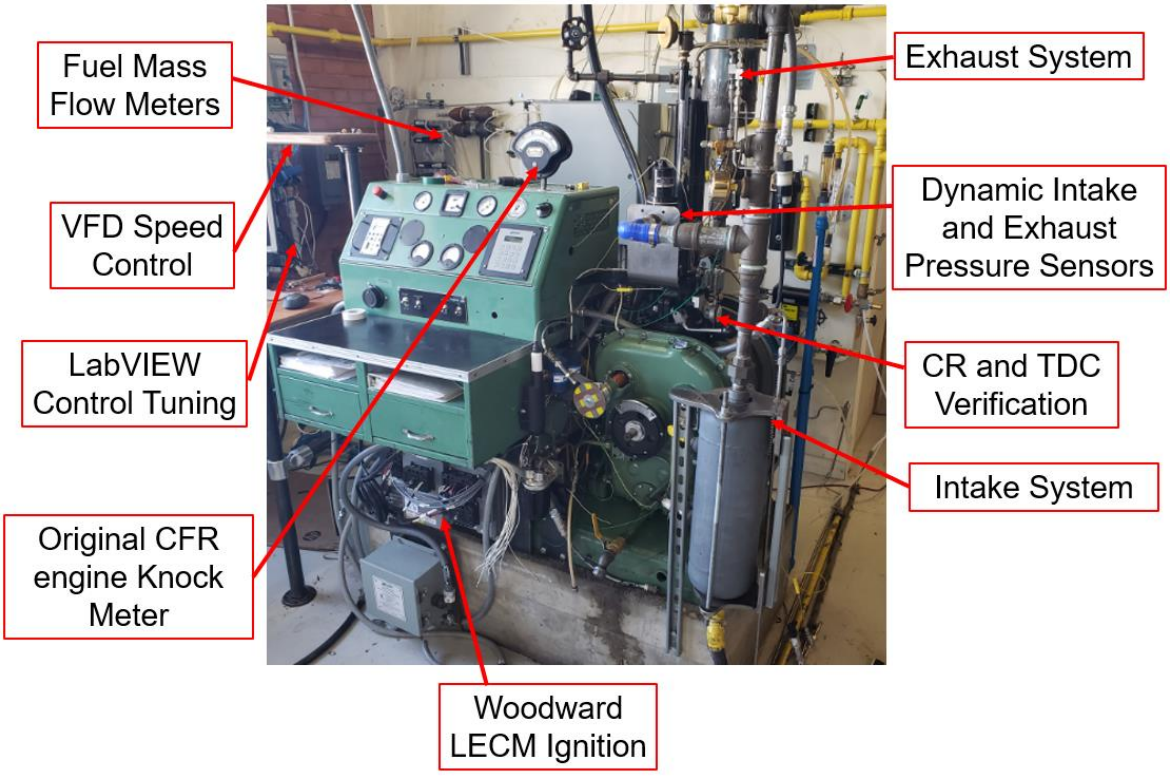

Figure 6: Cooperative Fuel Research Engine at Colorado State University Powerhouse Energy Campus

The differences between the original Waukesha CRF engine and the CFR engine used in this testing, includes numerous modifications. A Yaskawa regenerative Variable Frequency Drive (VFD) was installed for fine speed control at a range of speeds from 600 to 1200 RPM. High-speed Kistler piezo resistive intake (Type 4007D) and water-cooled exhaust (Type 4049B) pressure transducers were installed. These sensors allow for more accurate three pressure analysis (TPA) for 1-D and 3-D model validation for Converge computational fluid dynamic (CFD) and GT-Power models of the engine. Additionally, the engine conversion from liquid fuel testing to gaseous fuel, created the requirement for an in-depth fuel blending system. The fuel blending system included the implementation of Omega specific heat differential flow meters of up to eight different flow constituents, as well as a Coriolis flow meter for total fuel flow. The final upgrade to the original CFR engine includes a Woodward Large Engine Control Module (LECM) ignition system. This system provided more accurate ignition control, and the ability to implement and test various ignition control schemes such as CA50 (control location of 50% mass fraction burned) and Combustion Intensity (Woodward defined metric of combustion control). The final configuration of the CFR engine for this study is shown in the schematic in Figure 7 below. Other modifications from the original engine configuration performed during previous work are described in references [23] [24].

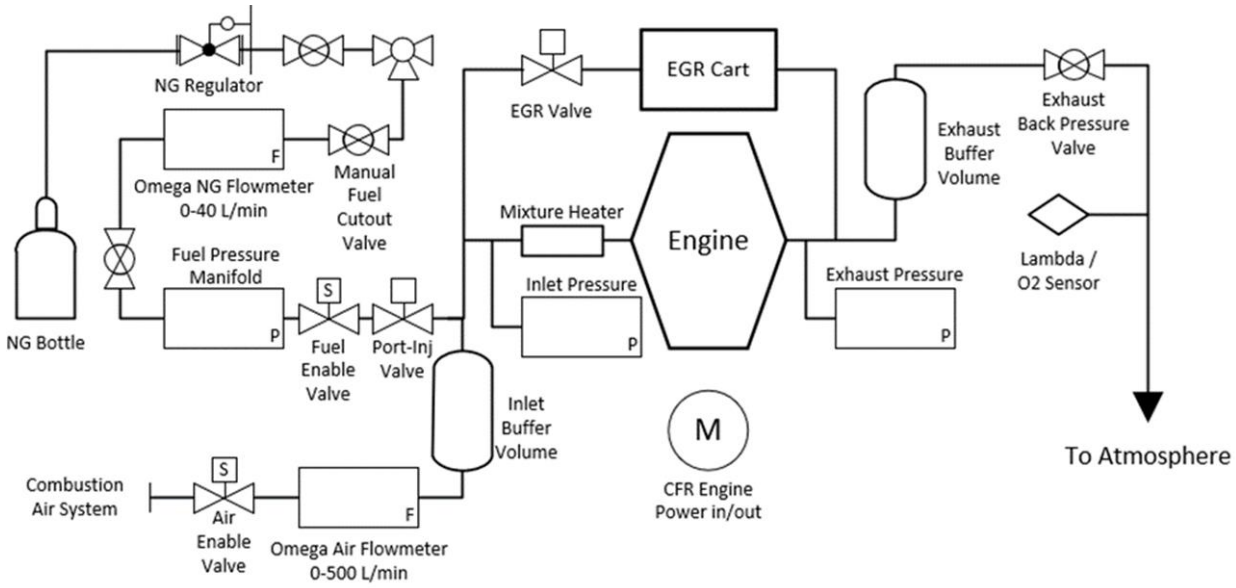

Figure 7: System Schematic of the CFR Engine

2.2 EGR TEST CART

A crucial piece of equipment required for the testing performed for this study, was the Exhaust Gas Recirculation (EGR) test cart that was fabricated for use with the CFR engine. EGR is commonly used for increasing power density, reducing NOx emission concentrations, and causing knock suppression for operation at higher power densities. The CFR engine does not include EGR systems with the base unit, and thus a cart that can replicate the functions of a high-pressure EGR loop while providing a wide range of possible flows was necessary.

For this project, the EGR cart was required to be able to provide the CFR engine with a maximum EGR rate of 40% at maximum load. Utilizing previously supplied engine data from the CFR engine, flow rates were extrapolated to expect ~ 115 grams per minute of exhaust gas at a max load of 3.5 kW. Initial testing after the fabrication of the EGR cart showed that the

maximum optimal EGR rate was only 74 grams per minute at 3.5 kW of electric power output. However, this was more than adequate for the present study. The final EGR cart is shown below in Figure 8.

Figure 8: Exhaust Gas Recirculation Test Cart Constructed for Use with a Cooperative Fuel Research Engine

The EGR cooler is from a 1.8 L diesel Volkswagen engine, that can cool exhaust gas flows up to three times the expected flow range of the CFR engine. The blower is a positive displacement (for lower required shaft speeds) twin-screw super charger capable of providing the full expected flow range and ensuring continuous flow of EGR gasses into the intake of the engine. A 5-hp electric motor coupled with an Eaton 208V, 3-phase, 5-hp variable frequency drive (VFD) runs the blower that provides the various EGR flow rates without the presence of a standard EGR valve used on trucking engines.

The temperature of the EGR fluid was controlled within a window of 60°C to 90°C for causing the full travel length of the system (21 feet) At lower temperatures the water vapor in the exhaust gas could condense on the walls of the EGR test cart, reducing EGR supply to the engine and potentially damaging EGR cart components. A 208V tankless electric water heater was used to raise the temperature of the tap water supply to a minimum of 60°C for use in the EGR cooler. The exhaust gas enters the blower at ~65°C and leaves at ~70°C. A 120-Watt electric heat tape, foam, and fabric insulation was wrapped around the exterior of all pipe surfaces to maintain wall temperatures above 60°C to reduce the chance of water vapor condensing on the walls over the remaining 15 feet of the EGR test cart piping.

The American Gas Association (AGR) Report #3 standard for orifice flow meters was utilized to design the EGR flow meter [25]. Figure 9 shows the required set up and location of sensors for proper calibration of the flow meter. This flow meter utilizes flange taps for pressure locations as well as a stainless-steel orifice plate for minimal thermal expansion. The straight pipe run prior the orifice plate is 24 pipe diameters to properly induce complete laminar flow with no fluctuations in the velocity flow profile. The final details of the flow meter include a 1-inch pipe, 1/8-inch orifice differential pressure of up to 25 kPa and a static inlet pressure of up to 200 kPa with an operating temperature of 60°C to 95°C.

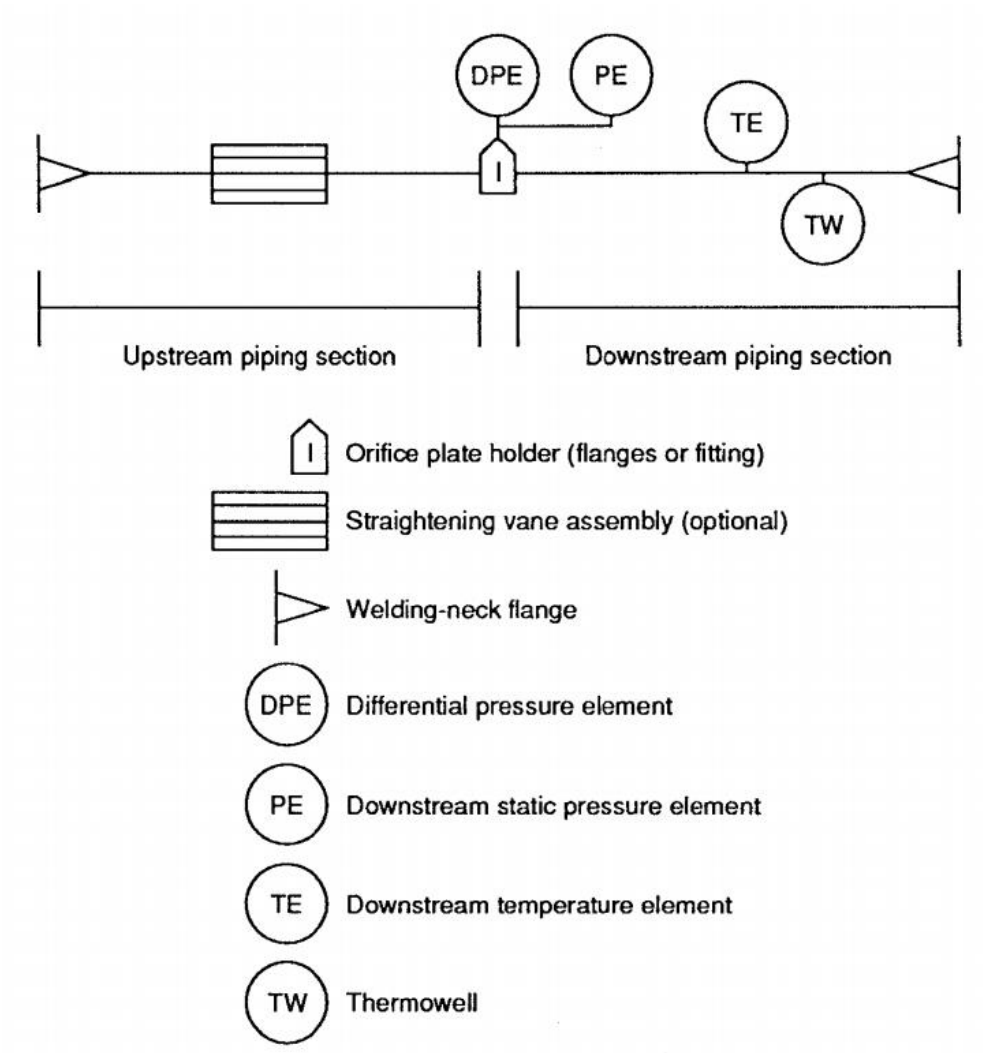

Figure 9: AGA Report #3 Standard Orifice Layout

Equation 1 is the fundamental orifice meter mass flow equation for the AGA report #3 standard flow meters. In this equation, C_d is the orifice plate coefficient of discharge, d is the orifice plate bore diameter, ΔP is the orifice differential pressure, E_v is the velocity of approach factor, N_1 is the unit conversion factor (found from table look ups), q_m is the mass flow rate, ρ_p is the density of the fluid at flowing conditions, and Y is the expansion factor. This equation is valid for the EGR flow ranges expressed for this study.

$$q_m = N_1 C_d E_v Y d^2 \sqrt{\rho_{t,p} \Delta P}$$ Equation (1)

There were several EGR test cart uncertainties observed during testing. During some tests water condensation occurred which reduced the effectiveness of EGR on knock suppression. However, an analysis of total water drop-out over a 10-minute period showed the condensation was ~0.6% of water input. Another uncertainty included the CFR engine intake system. The CFR system simulates a turbocharger for boosted conditions by pulling all dry combustion air from the building compressed air system. This air system is controlled with a proportional – integral – derivative (PID) loop variable butterfly valve, which induces a fluctuation of ±2 kPa in the intake system over time. This fluctuation has a moderate impact on the flow rate of the orifice flow meter because the orifice differential pressure is always less than 25 kPa. At a nominal EGR rate of 15%, nearly 8% change in the discharge pressure of the orifice can vary the EGR rate by ±1%. The use of time average values addresses this issue but caused concern early in the testing for this study.

2.3 KNOCK MEASUREMENT SYSTEM

As originally manufactured and configured the knock measurement system on the CFR engine consists of a power supply, detonation meter, detonation pickup, and knock meter. The pick-up sensor, mounted through the head of the cylinder, offers a thin, flexible diaphragm cover that is exposed to the combustion chamber. As the diaphragm surface reacts to combustion chamber pressure variation the magnetic field varies around a magneto-restrictive alloy wound with a copper wire coil. The magnetic field variance induces a voltage in the coil, which is

directly proportional to the rate of change of cylinder pressure and is output to the detonation meter. The detonation meter is an analog device that can isolate the relative knock amplitude through averaging and filtering the received signal which is then transmitted to the knock meter. The knock meter display reflects the relative intensity of the knock event to establish a comparative scale used as the basis for measuring the intensity of knock experienced in the engine. An analog strip chart recorder may also be attached to provide a permanent record of a data set. Figure 10 shows a signal flow diagram for the original knock measurement system.

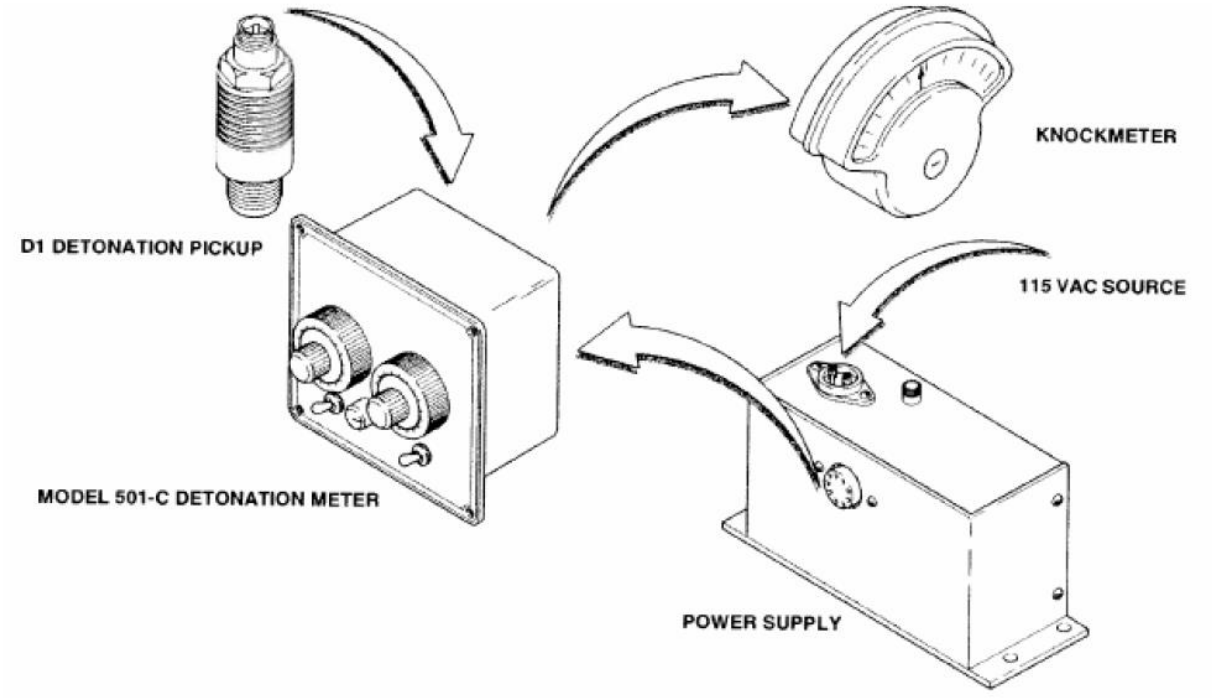

Figure 10: CFR Engine Knock Measurement System, Original. [22]

The original knock measurement system requires that the operator determine the onset of knock audibly and then adjust the meter reading and spread dial settings (controlling resistive networks that adjust the sensitivity of the instrument), establish an operate/zero point, and then select a time constant (1 of 6 positions determining the integration interval). The process and instrumentation force a subjective measurement of knock intensity, which is certainly acceptable for comparing tested fuels to reference blends to assign an octane number. For this project it is desired to establish an objective, quantitative knock intensity measurement less prone to variability due to operator interpretation and sufficiently detailed to allow a more refined analysis of the knocking phenomenon.

The modified knock measurement system begins with a water-cooled, piezoelectric transducer (Kistler model 6061A) mounted in the same cylinder detonation port previously housing the Type D-1 pickup. The signal from the transducer feeds to a charge amplifier which relays pressure signal input to the controlling software. A rotary 0.1° incremental optical engine encoder (BEI model L25) provides positive crank angle position indication enabling real-time display of cylinder pressures as a function of crank rotation. Due to high dynamic response and resolution (3600 discreet data points per engine revolution), detailed pressure history is available allowing direct analysis of the combustion event in the cylinder. Figure 11 provides a signal path depiction of the post-modification knock measurement system.

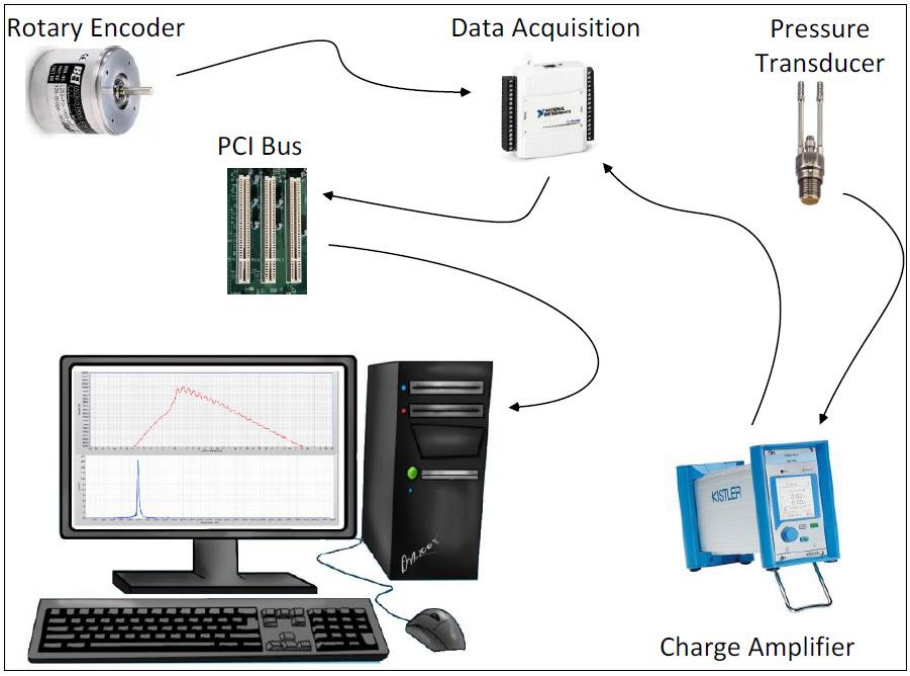

Figure 11: CFR Engine Knock Measurement System Post-Modification

This process is applied to two redundant methods of knock indexing. The first of which is the Fast Fourier Transform (FFT) method, encoded CSU staff and controlled through LabVIEW programing. The Second is the Woodward method Knock Ripple Sum, which is controlled through the Woodward LECM.

2.4 LABVIEW VIRTUAL INSTRUMENTATION (VI) CONTROL

The project test cell monitoring and control system uses a software package developed by the staff of the Colorado State University Engines and Energy Conversion Laboratory written with LabVIEW©. The Virtual Instrumentation software developed specifically for this engine and this project accepts input from installed sensors (flow meters, thermocouples, pressure transducers) and provides automated output to control fuel injector PWM duty cycles in response

to calculated fuel system mass flow, combustion air control valve for controlling intake air pressure and flow rate (also regulating stoichiometry), and calculates desired exhaust backpressure for the engine operator. The VI program displays engine operating status allowing the operator to monitor and control intake air pressure and temperature, fuel mixture, air-fuel ratio, exhaust temperature and pressure, coolant temperature, and power generation level. Figure 12 demonstrates the primary control screen of the LabVIEW VI for the CFR engine.

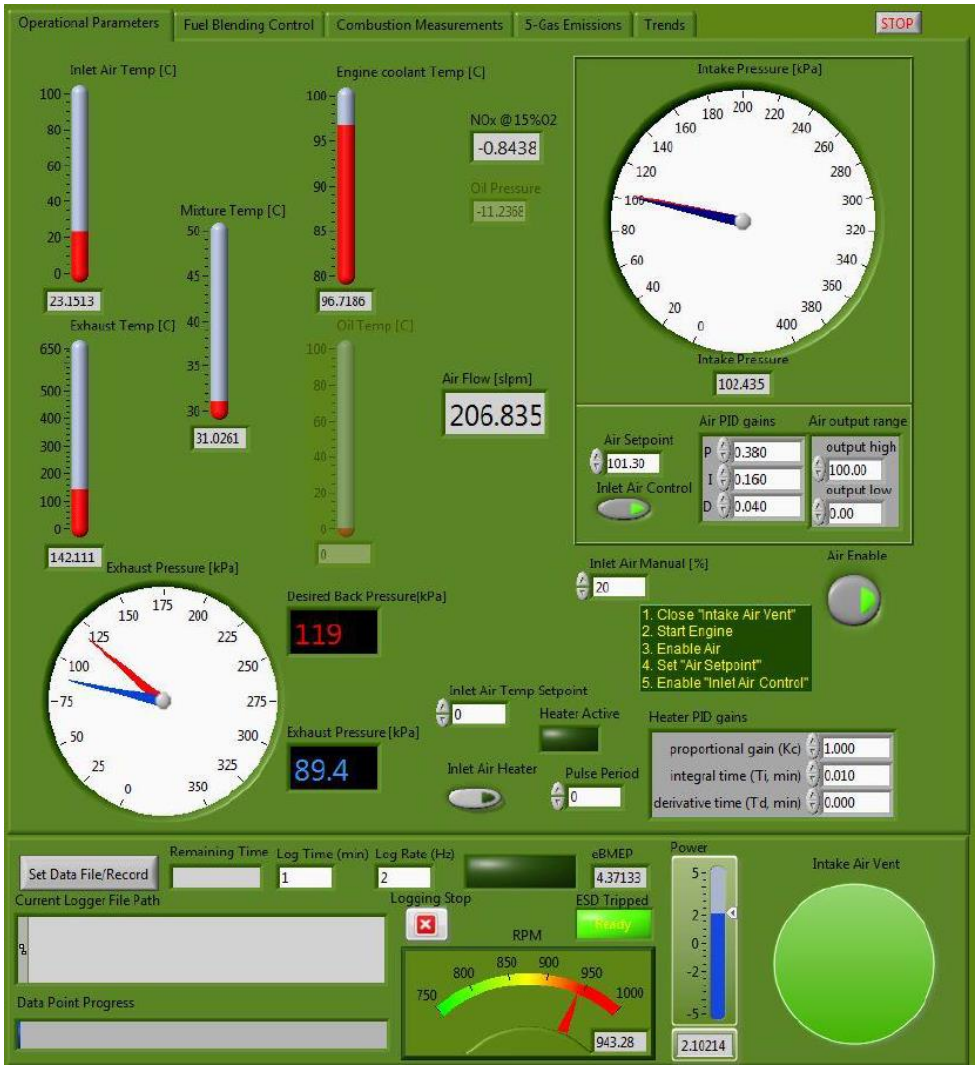

Figure 12: CFR Host VI Operational Parameters Screen

A separate program used in this project, also developed at the CSU Powerhouse and Energy Institute, written with LabVIEW© is the combustion logger. A high-speed data acquisition card receives input from the cylinder pressure transducer, through the charge amplifier, as well as crank shaft position indication from the digital encoder. The information is processed and relayed into real-time monitoring and recording of combustion activity in the operating engine. A synopsis of these programs is provided in Appendix B.

2.5 WOODWARD LECM

A Woodward Large Engine Control Module (LECM) was installed on the CFR engine. The purpose of the LECM was to test control schemes for C-EGAI. The mounted LECM on the CFR engine can be seen in Figure 13.

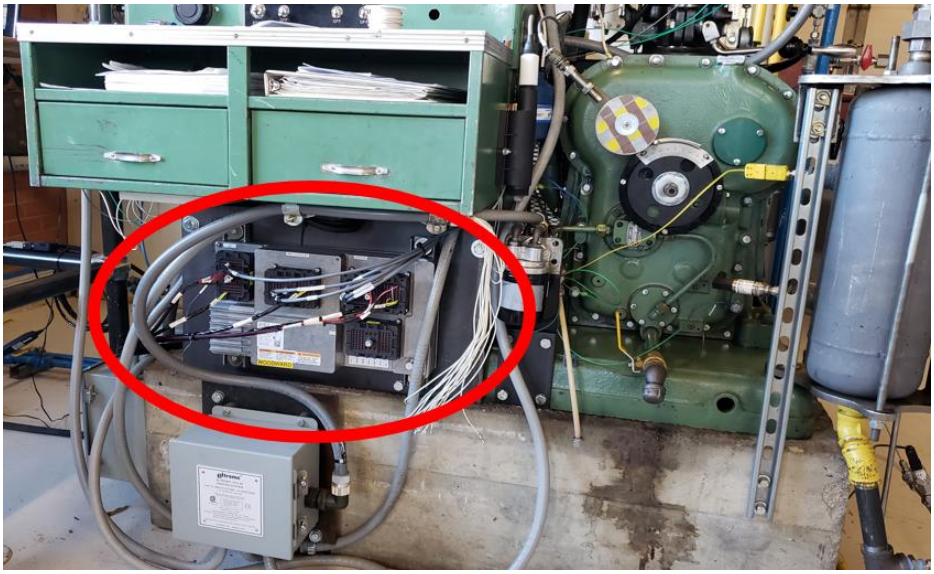

Figure 13: Woodward LECM Front Mounted on CFR Engine

The Woodward LECM manages and controls reciprocating engines (gas, diesel, or dual fuel) used in power generation, marine propulsion, locomotive and industrial engine, and process markets. The LECM provides a single, engine-mounted module that can be used to control all aspects of the engine's operation, including: speed and load control, air/fuel ratio control, ignition or injector control, misfire and knock detection, air/gas/exhaust flow control, the engine's start and stop routines, along with all the monitoring and engine-protection-related alarms associated with each function, as well as on-board data logging and communications. The LECM's software also allows control system designers to insert their own market-differentiating control algorithms.

The LECM provides a single-box approach that can be built up with interlocking modules into a single engine-mountable assembly. This control scheme uses a modular approach for both the electronic control modules and the software they use. These modules can be mixed and matched to address different applications; all use the same software interface. Each module has a microprocessor and runs software routines, written in Woodward's MotoHawk® software, using proven core functions and algorithms. The main module software can also be written in Woodward's Graphical Application Programmer (GAP™). The modules all share their information in a real-time manner, making the entire system act as one fully integrated control.

Utilizing the same cylinder pressure acquisition system and equipment as the LabVIEW control scheme, the LECM is capable of live data processing. The most beneficial parameters to view live include heat release rates, knock intensity, advanced combustion analysis, CA50, combustion intensity, IMEP, NMEP, PMEP, and historical pressure traces, each of which are updated every 1 seconds (~13 cycles). The LECM does not monitor pressures, temperatures, flow rates, power outputs, or EGR rate for the CFR engine because it is primarily controlled

through the LabVIEW control scheme, leaving the LECM's primary function to be cylinder pressure analysis.

CHAPTER 3: EVALUATION OF KNOCK CHARACTERIZATION TECHNIQUES

3.1 CYLINDER PRESSURE BASED KNOCK QUANTIFICATION

Since this study is looking to utilize end gas auto-ignition rather than simply avoid its occurrence, a clear system of classifying the onset and intensity of each knocking event must be defined. The hope is to use auto-ignition to improve the total efficiency of a natural gas, stoichiometric, spark-ignited engine with EGR and C-EGAI. The quantification of engine knock is what allows for the realization of C-EGAI, providing the ability to determine the fractional heat release due to auto-ignition (f-EGAI). In this study, it was assumed that the f-EGAI is equal to the full remaining heat release fraction after the knock onset crank angle. Controlling the f-EGAI to a predetermined level will hold the engine in a steady state beyond the traditional knock limit, thus improving combustion efficiency, reducing combustion durations, thus improving power output and increasing total system efficiency. F-EGAI is the best metric to compare the level of auto-ignition that occurs within the cycle to alternative cycles despite the running conditions.

Five different methods were found within the literature [26][27][28][29] and evaluated for their knock quantification abilities utilizing previously collected CFR engine data. These methods are briefly outlined in table 1 below. The knock intensity quantification methods that were analyzed include: Fast Fourier Transform, knock ripple sum, peak rate of pressure rise (1^{st} derivative), the maximum amplitude of the bandpass filtered cylinder pressure, and the integral of the bandpass filtered cylinder pressure. Each method was evaluated for its ability to detect the

occurrence engine knock, locate the knock onset crank angle, differentiate between the various level of engine knock, and correlate linearly with f-EGAI.

Table 1: Summarization of Cylinder Pressure Based Knock Detection Methods

METHOD	SOURCE	DESCRIPTION
FFT OF BANDPASS FILTERED SIGNAL	Colorado State University	Time averaged analysis of frequencies in knock signal pressure trace
MAXIMUM AMPLITUDE OF BANDPASS FILTERED SIGNAL	Cummins LLC	Knock intensity related to maximum frequency in pressure signal
INTEGRAL OF BANDPASS FILTERED SIGNAL	B. Radu et al. University POLITEHNICA of Bucharest	Knock intensity related to maximum positive value of integral
RATE OF CYLINDER PRESSURE CHANGE	B. Radu et al. University POLITEHNICA of Bucharest	Highest value of pressure trace after first crank angle resolved derivative
THIRD DERIVATIVE OF CYLINDER PRESSURE TRACE	J. Amador Diaz, et al. Universidad del Norte	Rise in amplitude of third derivative correlated to knock onset crank angle
KNOCK RIPPLE SUM	Woodward Inc.	Subtract a running average pressure trace from current knocking trace

3.1.1 Fast Fourier Transform Knock Intensity

The FFT of the cylinder pressure readings to evaluate the dynamics of the pressure trace in the frequency domain. This method is similar in approach to that of Brunt as well as Elmqvist [30] [31]. To demonstrate how this method quantifies auto-ignition events, assume the point of pre-detonation occurs directly across the combustion chamber from the spark plug as a result of excessive temperature in front of the advancing flame front. The event period should correlate to the cylinder geometry and equate to the time required for a pressure wave to travel the cylinder diameter and back – or twice the cylinder diameter. The pressure wave is assumed to travel at the local speed of sound. First, the speed of sound is:

$$c = \sqrt{\gamma RT}$$ Equation (2)

where:

c = speed of sound

γ = ratio of specific heats; cp/cv

R = ideal gas constant

T = temperature of the gas

The period of the event is given by:

$$\tau = 2\ x\ Diameter/c$$ Equation (3)

The frequency is the inverse of the period, so that:

$$f = 1/\tau$$ Equation (4)

And, combining Equations 2-4, the resulting expression is:

$$f = \sqrt{\gamma RT}/2xDiameter$$ Equation (5)

Representative parameter values are:

γ = 1.3

R = 0.2870 kJ/kg·K

T = 2500 K

Bore Diameter = 3.250 inch = 0.08255 m

The anticipated frequency for this case will be 5850 Hz. LabVIEW, the software with which the combustion logger program is written has an FFT function embedded which that can analyze the cylinder pressure signal in real time. In-cylinder pressure measurements are detected as discrete values occurring every 0.1 degrees of crankshaft rotation and grouped corresponding to 2 engine revolutions (one complete thermodynamic cycle with 7200 individual pressure values). An average engine speed is calculated over every two engine revolutions and that value is used for frequency approximation. A band pass filter is applied to the pressure data corresponding to the average engine speed to remove the engine operating frequency and expose pressure data distortion outside of normal operating parameters, those distortions attributable to the effects of knocking. The CFR F2 engine operates at a nominal speed of 900 rpm which corresponds to approximately 15 Hz. When translated to the frequency domain, with the signal filtered of the 15 Hz operating frequency and a Hanning window applied, it is possible to detect ringing corresponding to engine knock. A frequency-domain plot of the signal reveals both the frequency at which knock occurs and magnitude directly corresponding to the energy associated with the knock event, which can be seen in Figure 14.

Figure 14 shows two data plots, the upper display being the measured in-cylinder pressure [kPa] vs. crank angle [°bTDC] and the second being the result of the FFT, amplitude [kPa·rms2] vs. frequency [Hz]. The figure shows recorded data from conditions of heavy engine knock. The FFT plot shows a clear indication or “spike” at the frequency associated with the knock event. The low- and high-end frequency noise is filtered out by the bandpass filter with cutoff frequencies specific to the geometric dimensions of the CFR engine. The location of the frequency spike in the FFT plot corresponds to values near 6 kHz and the magnitude of the spike increases with knock intensity.

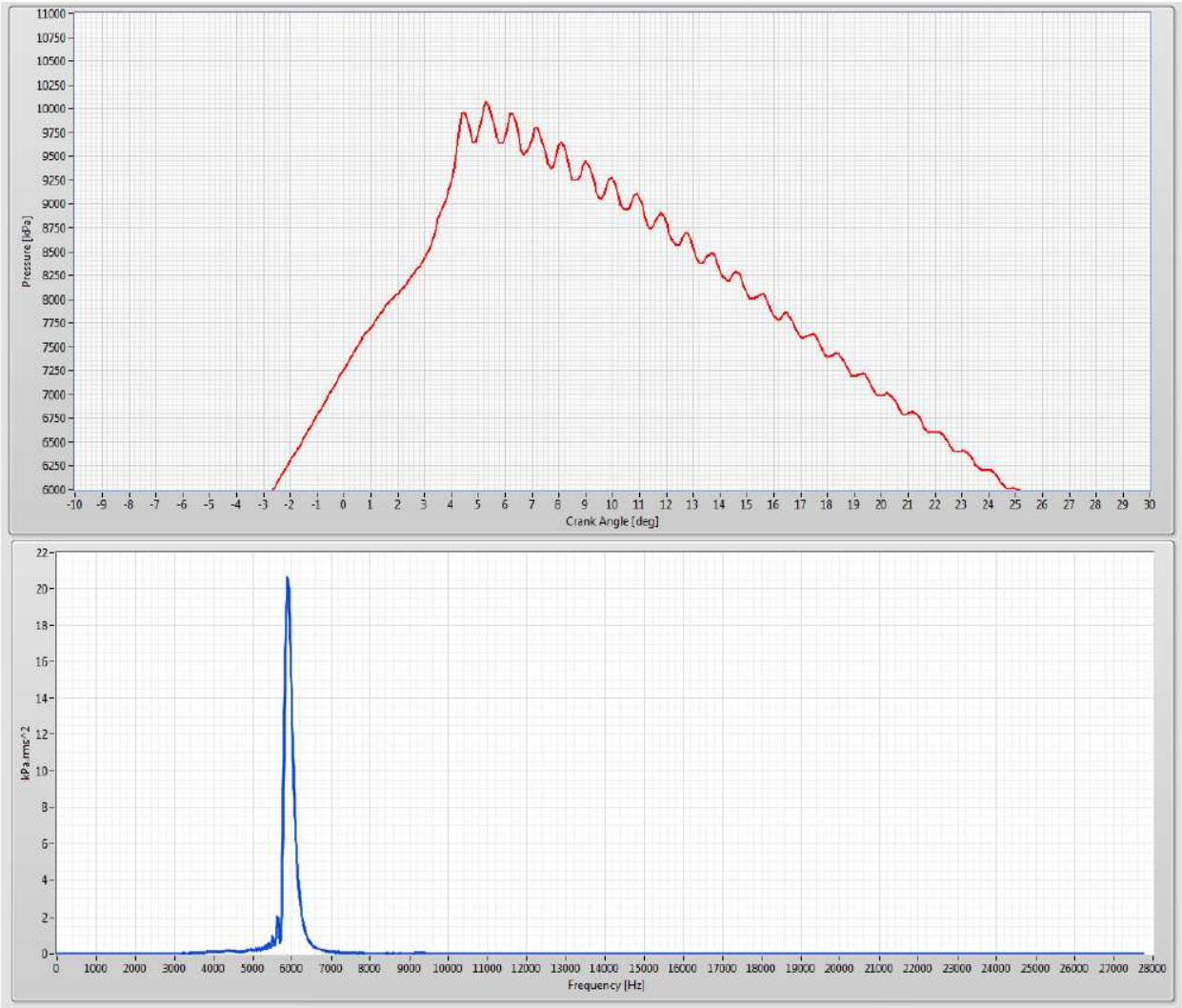

Figure 14: Pressure Trace and FFT Plot - Heavy Knock

The term knock integral refers to the sum of maximum FFT spike magnitudes over a set number of combustion cycles [23]. Since a discreet value for amplitude is known for every cycle the knock integral is given by:

$$KI = Area_{bounded} = \sum_{i=0}^{n} \{(i+1) - i\}\{KL(i+1) + KL(i)\}/2 \quad \text{Equation (6)}$$

where:

n = number of combustion cycles in a data set

KL(x) = knock level magnitude at a given combustion cycle, x

The knock integral is evaluated by summing the cycle FFT magnitudes over a block of successive cycles for each data set, usually 200 cycles. During testing, a real-time summation of the last 200 cycles is displayed. By using the integral value for comparison, both the severity of individual knock events and persistence in recurrence are taken into account. The determination of a knock integral to describe a repeated knock condition offers objective quantification of the phenomena. Figure 15 illustrates how the cyclic FFT magnitudes vary over 1000 cycles of engine data for no knock and three different knock levels. Also provided in Figure 15 are the knock integral knock intensities for each knock level, which are 1000 cycle averages of the 200 cycle knock integral.

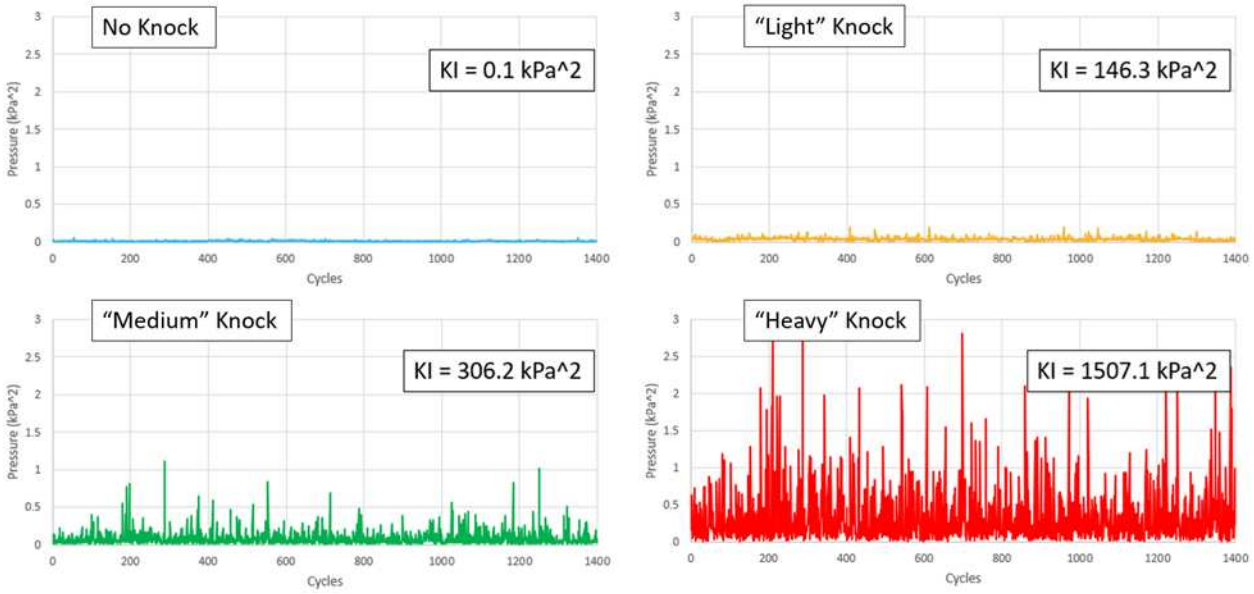

Figure 15: Variation of Cyclic FFT Magnitudes for 1000 Cycles at Various Knock Levels

3.1.2 Peak Rate of Pressure Rise

The peak rate of pressure rise, or first integral of the cylinder pressure trace is a simple concept of knock quantification. By taking the first derivative, a plot is generated to show the rate of pressure rise within the pressure trace. Looking at a knocking trace such as that shown in Figure 14, there is a sharp upturn in the slope of the pressure trace, creating a larger rate of pressure rise right before the occurrence of an auto-ignition knocking event. This increased rate of pressure rise is represented by the peak amplitude on the first derivative knock intensity plot [26]. Figure 16 below shows how plots for the peak rate of pressure rise knock intensity applied to four different levels on knock intensity, defined initially by audible differences.

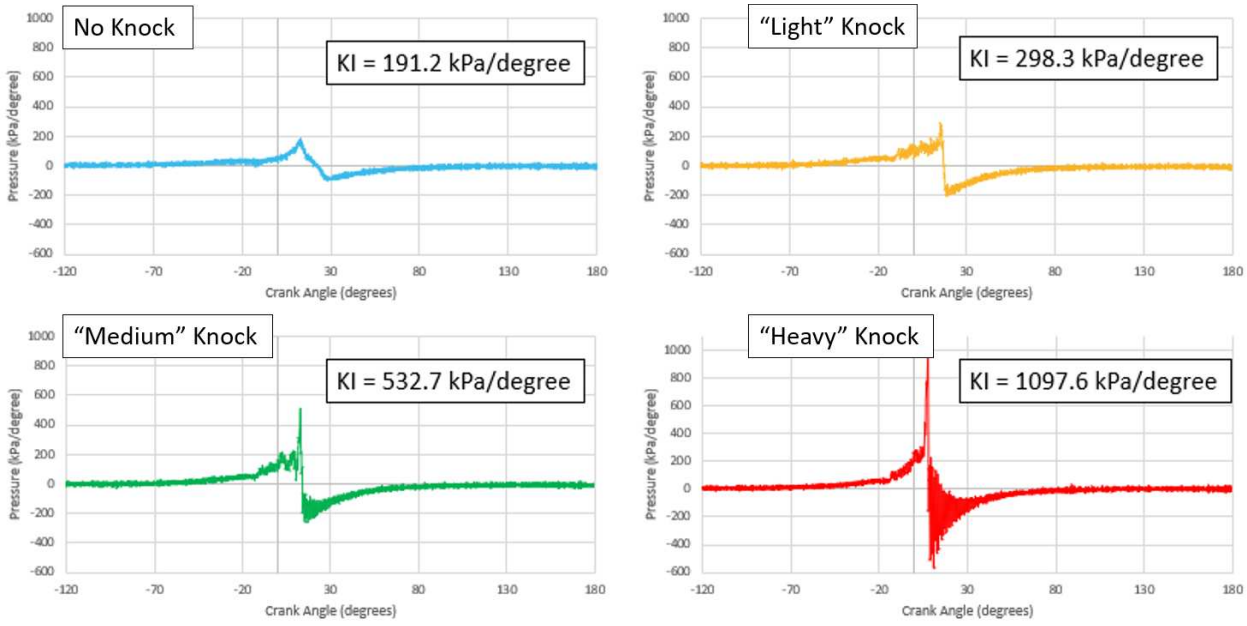

Figure 16: Peak Rate of Pressure Rise Knock Intensity for 1 Cycle of Various Knock Levels

Examining Figure 16 further, the effectiveness of the peak rate of pressure rise as a method of knock quantification is evaluated. A bandpass filter was still required to filter out low-level cylinder noise, recording knock sinusoids between 1000 and 5000 Hz. The filter isolates the pressure trace from all other performance effects such as exhaust peak pressure and compression loads seen within the engine. An “average” knocking trace demonstrated a peak rate of pressure change around 550 kPa/degree at 900 RPM, with the greatest exceeding 1000 kPa/degree. The final plots demonstrate that this method of knock quantification is very good at differentiating between different levels of auto-ignition, while it is known that knock is occurring. However, this method seems to lack in the area of detecting low levels of auto ignition. Since the initialization of C-EGAI will most likely occur within those lighter zones of auto-ignition, this study requires the highest resolution of knock quantification in the “no” to “light” knock zones.

Trace knock for our purposes was arbitrarily defined as occurring when the rms of the rate of pressure change for 20% of the engine cycles exceeded a value twice that for non-knocking cycles. On the knock intensity scale the average trace knock rms value corresponds to 1.4 X 10^3 psi/sec [28]. Note that when trace knock is defined in this manner there is no aural manifestation. The knock intensity, as defined, is useful for any work involving engine knock. The definition permits objective comparisons of knock for different fuels, engines, and investigators. It allows objective comparisons relative to engine performance such as maximum power, trace and audible knock. Due to this, this method of knock quantification will most likely be used as a validation for a more intense auto-ignition event but will not be used as the primary control method behind C-EGAI.

3.1.3 Maximum Amplitude of Bandpass Filtered Cylinder Pressure Trace

The maximum amplitude of the bandpass filtered pressure trace method of knock intensity quantifies knock by analyzing the pressure fluctuations generated by auto-ignition when the multiple ignition events collide within the combustion chamber. These pressure fluctuations are visible in the cylinder pressure traces by the sinusoidal waves that occur after the secondary pressure rise event after especially after the location of peak pressure. The higher the knock intensity, the greater the amplitude of the sinusoidal waves should be [27].

By sending the pressure trace through a bandpass filter with cutoff frequencies defined by the resonance time from one side of the combustion chamber to the other through the combustion fluid at peak combustion temperatures and pressures. Equation 2 demonstrates this calculation of the speed of sound within the combustion chamber. Using the speed of sound from an "average" combustion event and the dimensions of the combustion chamber (bore = 82.55 mm), a fundamental frequency of knock signals is found to be 5.3 kHz with cutoff frequencies of ~ 3450 Hz to 11,050 Hz. Figure 17 demonstrates the application of the bandpass filter to an "average" knocking pressure trace, and the resulting knock intensity plot.

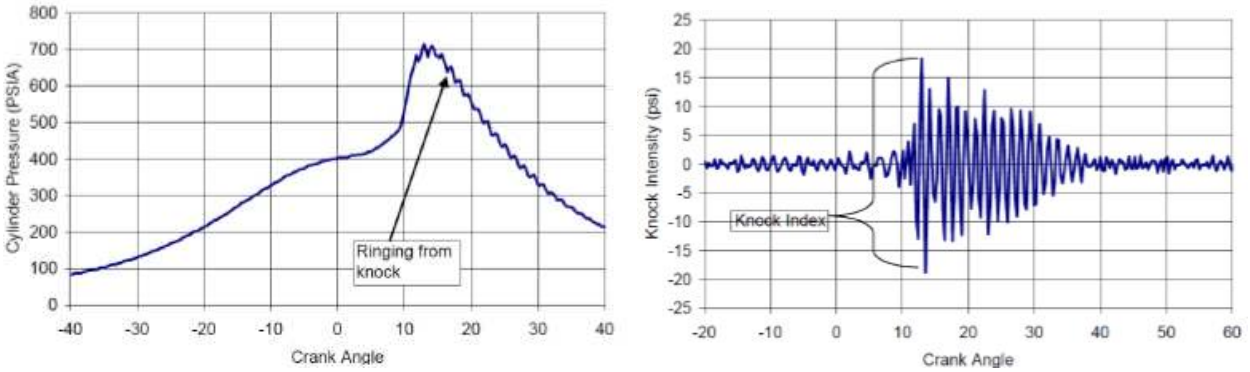

Figure 17: Maximum Amplitude of a Bandpass Filtered Pressure Trace Knock Intensity (right) Applied to a Knocking Pressure Trace (left)

The final knock intensity resulting from this method of knock quantification is equal to the maximum peak-to-peak amplitude occurring from the bandpass filtered plot (right of Figure 17). To show the resolution and functional range of this method, it was applied to the same data sets from the above methods. The results are shown in Figure 18.

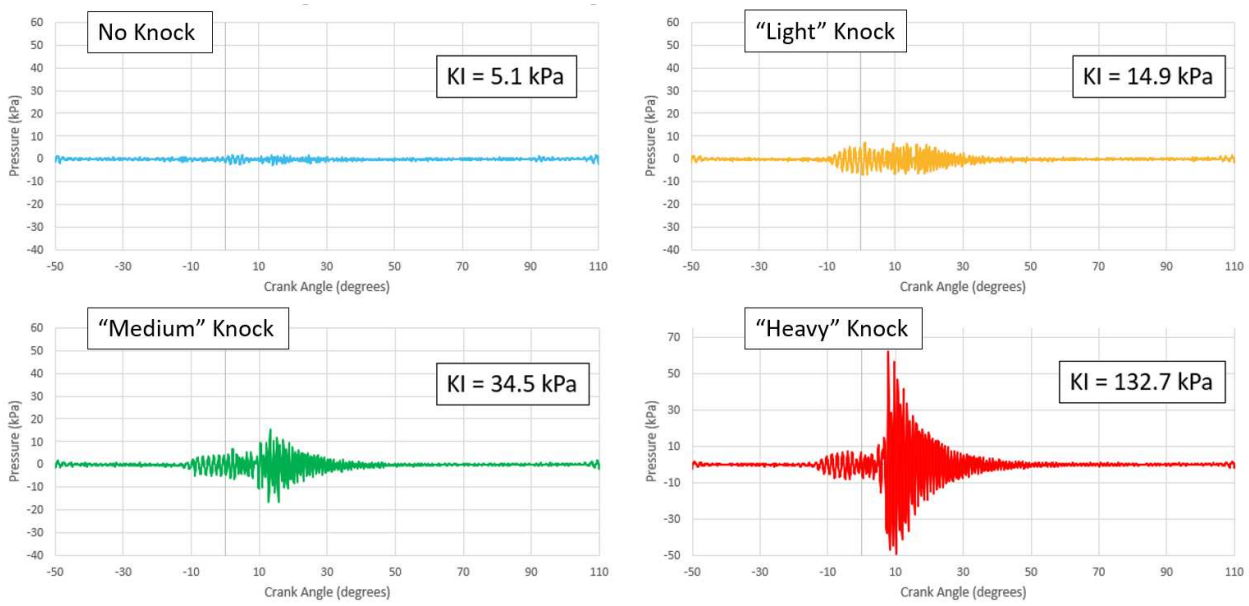

Figure 18: Maximum Amplitude of the Bandpass Filtered Pressure Trace Knock Intensity for One Cycle of Various Knock Levels

This method of knock quantification effectively differentiates between various levels of auto-ignition, but the definition of the onset of auto-ignition is unclear. Figure 16 demonstrates this phenomenon in that the "no" knock pressure trace still resulted in registering a small reading of knock. could be explained by the cutoff frequencies of the bandpass not being adequate for all operating conditions of the CFR engine, but is unlikely due to the minimal variations the resonance time sees over the full load of the CFR engine.

Analyzing the maximum amplitude is a common method of knock quantification, used within the industry, such as engine manufacturing [29]. However, the leading issue is the unsteadiness in the cycle to cycle variations of knocking events. Auto-ignition events are inherently unstable, and can vary in peak pressure, burn duration, and thus the amplitude of the knock sinusoids from cycle to cycle. This phenomenon causes the programmer to believe it is not in the proper knock range even when an alternative indication may indicate otherwise. Attempting to resolve this issue with averaging the knock intensity over a set number of cycles resulted in an overall lower reading in knock intensity than desired.

3.1.4 Integral of Bandpass Filtered Cylinder Pressure Trace

One method that was deemed promising early in the study was the integral of a bandpass filtered cylinder pressure trace. This method is a pairing of the two previous methods, utilizing the previously defined bandpass filter, and taking the integral of the absolute value of the resulting bandpass plot [26]. This method failed in knock quantification, compounding the failures of the two previous methods. Figure 19 shows this method applied to various knock intensities, aligning with the previously utilized data sets.

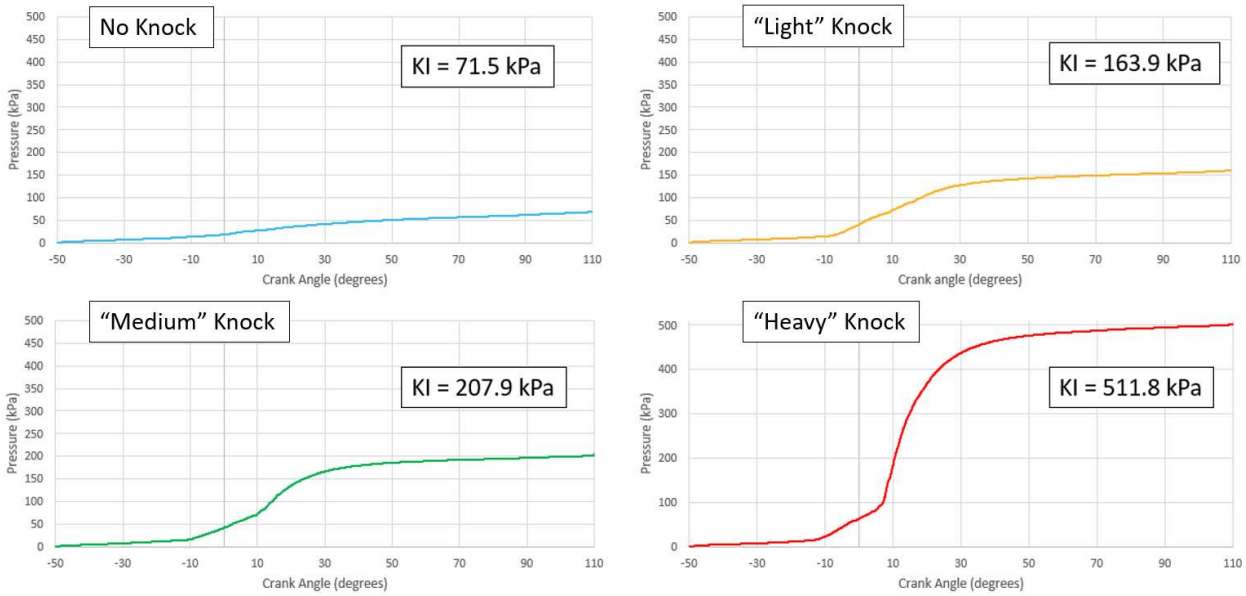

Figure 19: Integral of the Bandpass Filtered Pressure Trace Knock Intensity for One Cycle of Various Knock Levels

This method performed the worst in differentiating between lower levels of knock intensity, being uninterpretable whether knock onset was occurring or not at lower intensities.

3.1.5 Knock Ripple Sum Knock Intensity

An additional knock quantification method that was analyzed within this study was the Woodward defined method of "Knock Ripple Sum" knock intensity [32] [33]. This method operates similarly to the bandpass filtered methods of knock quantification but uses a running average of pressure traces in place of a bandpass filter. While the bandpass locates the center y-axis (y = zero) of the plot with the average of the sinusoids themselves, leaving room for error with where the sinusoids occur on the pressure trace. The knock ripple sum method takes an average of the 50 previous pressure traces, requiring the engine to be running at steady state, and setting y = zero at that average pressure trace location. Additionally, without the use of a

bandpass filter, the full pressure trace can be analyzed for knock ripples without cutting off any high or low spectrum frequencies, while still filtering out any resonance noise created by the engine or additional equipment.

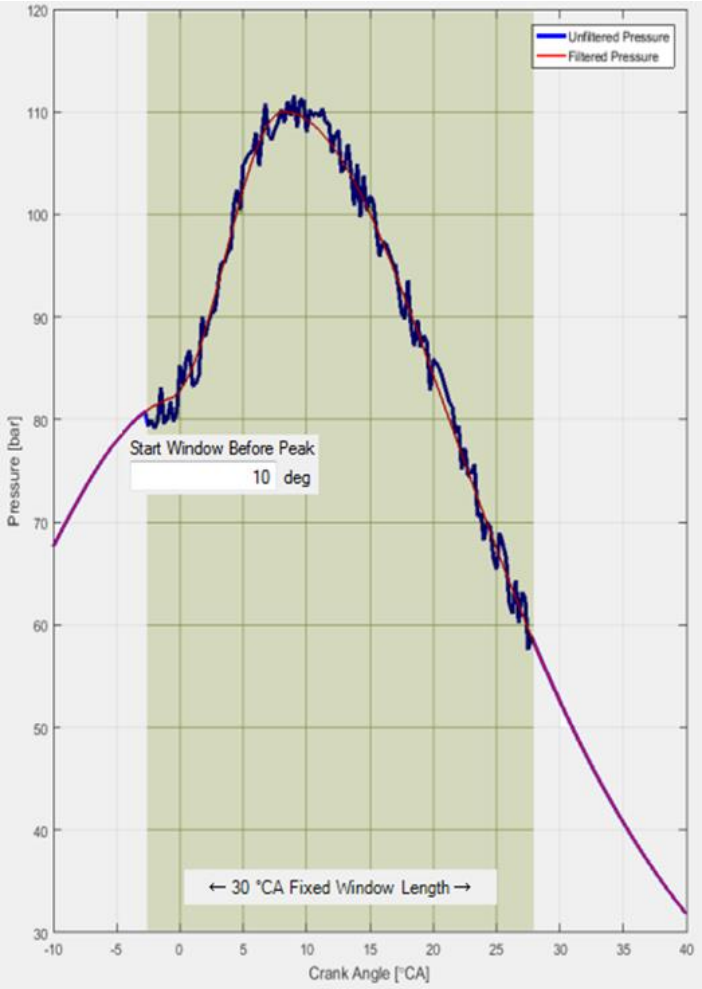

Figure 20: Knock Ripple Sum Demonstrational Difference in Average and Knocking Traces

Figure 20 demonstrates the process of overlaying a knocking pressure trace with a 50-cycle average trace within the proper window of combustion. By subtracting the average trace from the knocking trace, a plot such as what can be seen in Figure 21 is generated.

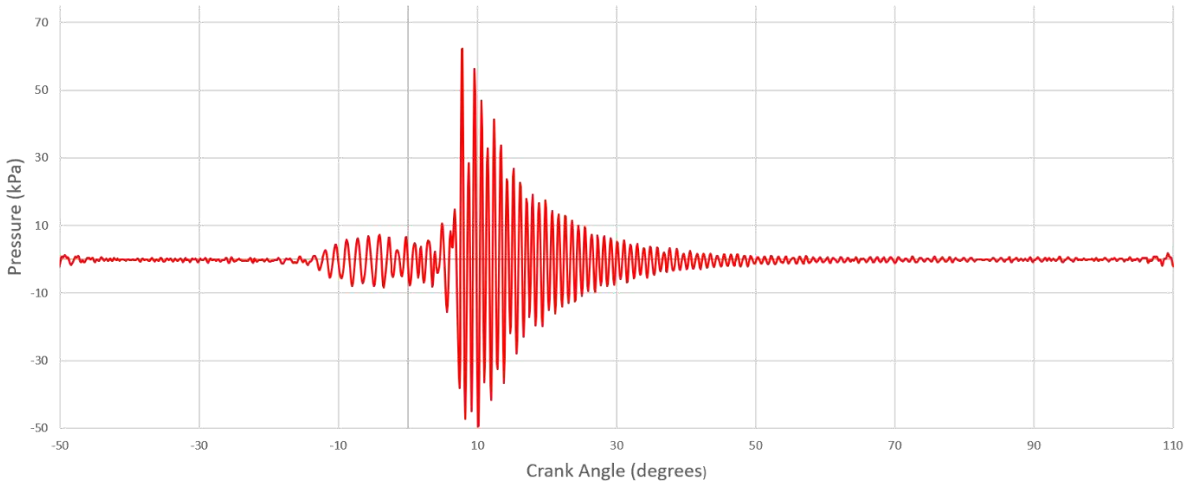

Figure 21: Knock Ripple Sum Knock Intensity Post Average Pressure Trace Subtraction

Knock ripple sum knock quantification is scaled on a 0 to 100% scale of the sum of the absolute value of the resulting plot with Figure 21, creating a finer level of resolution for full-scale operation. Previous methods defined their knock intensities in the associated units, creating an issue with low levels of knock being challenging to differentiate the two. Utilizing a 0 to 100% scale creates a clear cutoff where knock onset begins and what the difference between 10 to 15% knock is as well as the difference between 75 to 80% knock intensity. Previous methods had issues of hitting a plateau at higher knock intensities as well as not clearly defining the occurrence of knock with the differentiation between “no” and “light” knocking cases. This method is more consistent that alternative methods in its average knock intensities, with the knock sinusoids being more appropriately represented for every trace, despite cycle to cycle variations. This method was selected as the primary method of knock quantification for C-EGAI.

3.2 KNOCK ONSET CRANK ANGLE

Each previously outlined method of knock quantification with cylinder pressure data was evaluated for not only their ability to quantify the level of auto-ignition occurring each cycle, but also their ability to locate the knock onset crank angle (KOCA). The KOCA is defined as the crank angle where the combustion event transitions from a propagating flame front originating from the initial ignition source, to an auto-ignition source. The location of knock onset is often classified on the pressure trace with the inflection point where the slope increases to a more aggressive rate of pressure rise. None of the previous knock quantification methods could accurately locate this point clearly for every cycle within a data set and were often removed from the target location by as much as 10 crank angle degrees.

Another method was found within the literature referred to as the KOCA method [34]. This method of knock quantification requires taking the third derivative of the pressure trace, making the inflection point of a rapid increase in pressure rise equal to y = 0 on the plot. Figure 22 below demonstrates the application of the third derivative KOCA method to a “heavy” knocking pressure trace, highlighting the location of the knock onset crank angle with the location of the peak amplitude of the KOCA plot.

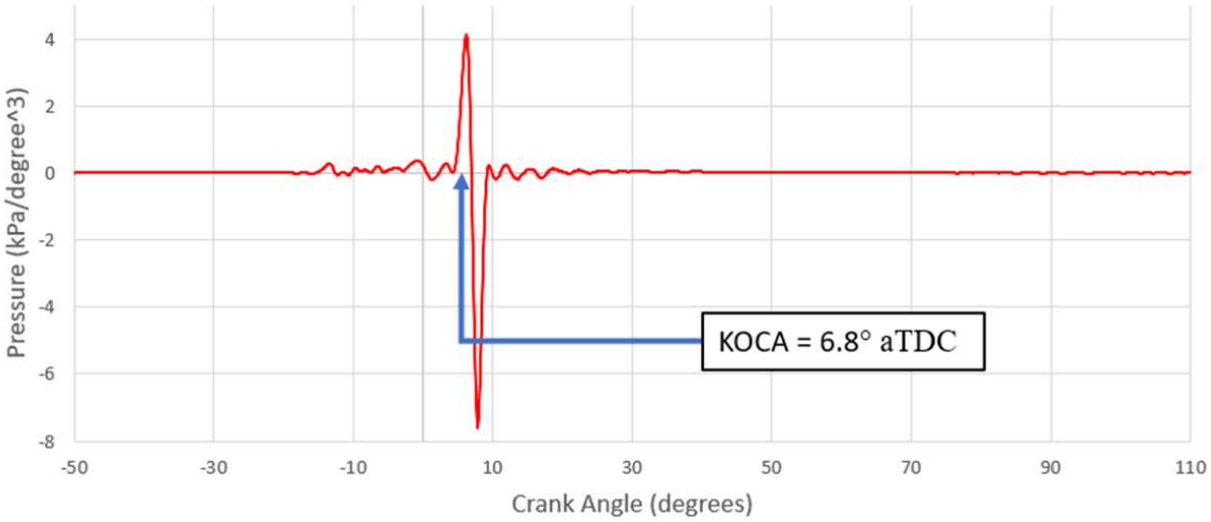

Figure 22: Third Derivative of the Cylinder Pressure Trace Knock Onset Crank Angle Method

Figure 20 shows a KOCA value of 6.8° aTDC, which is the crank angle location where initialization of auto-ignition occurs. To further demonstrate this effect, the KOCA value was found with the third derivative method in Figure 23 for various levels of auto-ignition. The data shows that for cycles where there is no auto-ignition, there is no clear instigation of knock onset, unlike previous methods where false readings of knock onset would be found. Additionally, as the knock intensity increases the KOCA value appears to advance closer to TDC, and thus more of the combustion event occurs as auto-ignition. The third derivative method was applied to 600 cycles of CFR engine data to ensure that this method is accurately providing the KOCA values over repeating cycles of a data set. This plot can be seen in Figure 24.

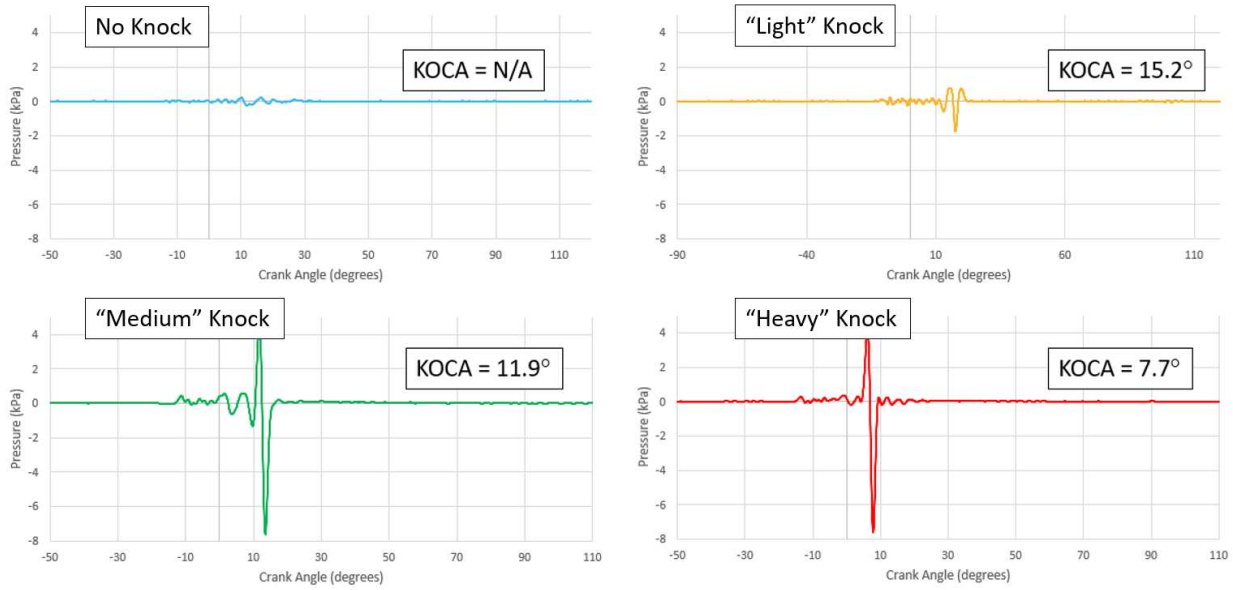

Figure 23: Third Derivative of the Cylinder Pressure Trace Knock Onset Crank Angle Method for 1 Cycle of Various Knock Levels

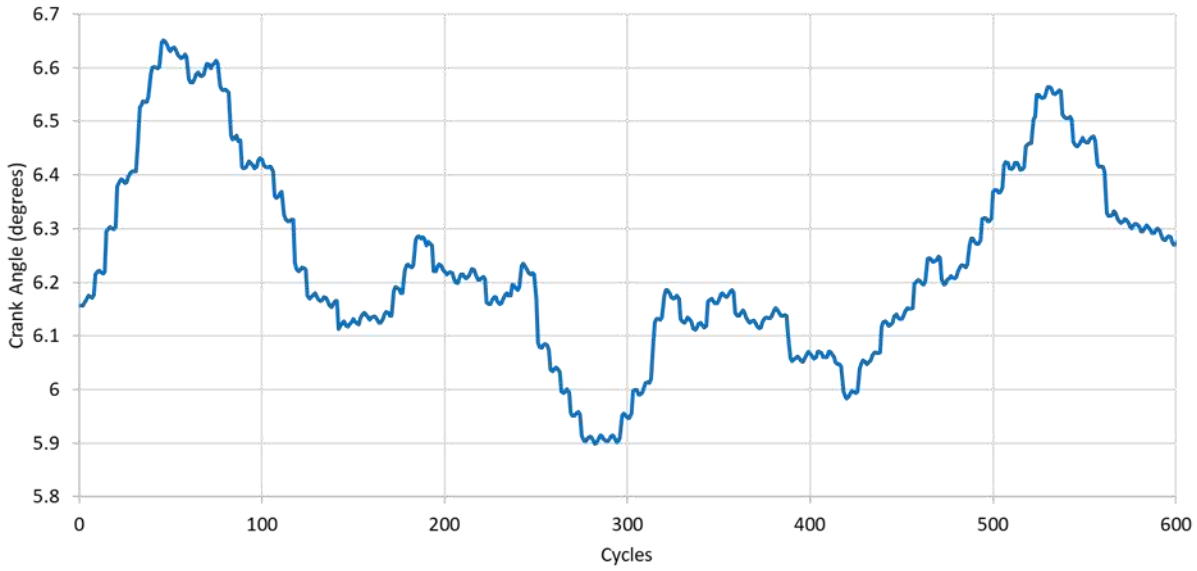

Figure 24: Third Derivative of the Cylinder Pressure Trace Knock Onset Crank Angle Method Applied to 600 CFR Engine Cycles.

The notion of the combustion process being primarily due to auto-ignition for cycles of heavier knock intensities is supported by Figure 25. This figure took the same cycle from Figure 20 that was analyzed with the KOCA third derivative method and applied to the mass fraction burned (MFB) plot for that cycle. By plotting the KOCA value for that cycle on the MFB plot, an intercept between the two lines is generated that corresponds to the MFB of the fuel mixture in the cylinder prior to auto-ignition. Due to the accelerated speed of combustion with auto-ignition, it can be assumed that all heat release from the KOCA forward, is due to auto-ignition. So, for the plot in Figure 25, a KOCA value of 6.8° aTDC corresponds to a MFB of 58.2%, implying that 41.8% of the mixture was consumed during the auto-ignition event. The f-EGAI is a rather large percent heat release due to auto-ignition, which could, in the long run, damage components of the engine. The ability for the KOCA third derivative method to analyze these crank angles with high fidelity and resolution, especially at lower knock intensities, is required to realize C-EGAI and increase overall efficiency.

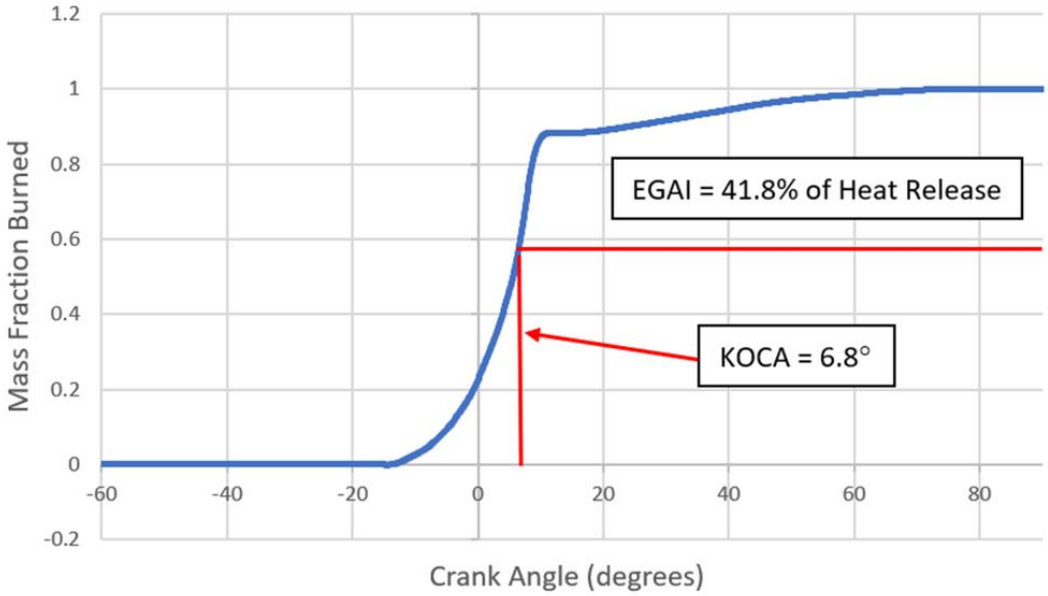

Figure: 25: Application of KOCA Value to MFB Plot for Heavy Knocking Cycle

3.3 COMBUSTION INTENSITY

Through the evaluation of the different knock quantification techniques, the main objective was to define a control scheme for C-EGAI. The most promising method is to utilize ignition timing control, due to its high correlation with knock severity. The Woodward LECM ignition system was utilized to develop and control a parameter programmed into the LECM called “Combustion Intensity” [22]. This method utilizes multiple operational engine parameters and takes a weighted average of each to determine where on a 0 to 100% scale the engine is operating. The results from previously evaluated methods of knock quantification were considered with this method of ignition control.

The key factors in the Combustion Intensity Metric (CIM) are:

- Magnitude of Peak Pressure (bar) – P_max
- Burn duration- (CA ATDC) – BD
- Pressure Rise Rate (bar/deg) – PRR
- Slope of Heat Release Rise Rate (J/deg/deg) – HRRs
- Knock Intensity (Knock Ripple Sum) – KI

These are combined in a scaled linear combination for a reference threshold to determine the CIM as shown in Equation 7:

$$CIM = A_1\left(\frac{P_{max}}{P_{max_{ref}}}\right) + A_2\left(\frac{BD}{BD_{ref}}\right) + A_3\left(\frac{PRR}{Prr_{ref}}\right) + A_4\left(\frac{HRRs}{HRRs_{ref}}\right) + A_5\left(\frac{KI}{KI_{ref}}\right) \qquad \text{Equation (7)}$$

Where A_1 through A_5 are calibration constants.

Transitioning this evaluation over to a natural gas engine, with the CFR engine as the test subject, combustion intensity was analyzed for the application of C-EGAI. The first issue that stood out was at greater engine loads, where all knock quantification techniques showed increased noise levels and reduced accuracy due to random error with the engine. By standardizing knock intensity alongside the other four parameters inside the combustion intensity metric, the operational condition of the engine is more comparable across all loads. These results are demonstrated in figure 25 with a sweep of combustion intensity near peak power, with 0% and 15% EGR substitution. Note that a sweep of combustion intensity is essentially a sweep of ignition timing.

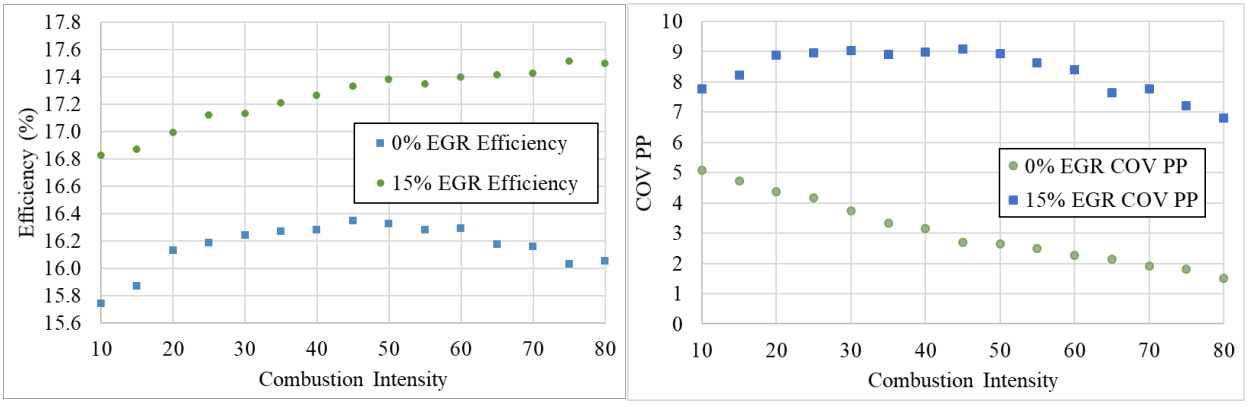

Figure 26: Efficiency (left) and COV of Peak Pressure (right) for Combustion Stability of Combustion Intensity Sweep from 10% to 80%

While Figure 26 demonstrates the combustion stability of the engine near peak power over a sweep of combustion intensity, it begins to highlight a location of maximum efficiency near 44% combustion intensity. Since combustion intensity control is also ignition timing control, and higher combustion intensity values are equal to more advanced timing values, the engine is taken from operating at the threshold of knock onset to an operating point deep within the knock window. Figure 27 below shows this sweep for 0% EGR substitution in the form of the cylinder pressure traces over the 10% to 80% sweep.

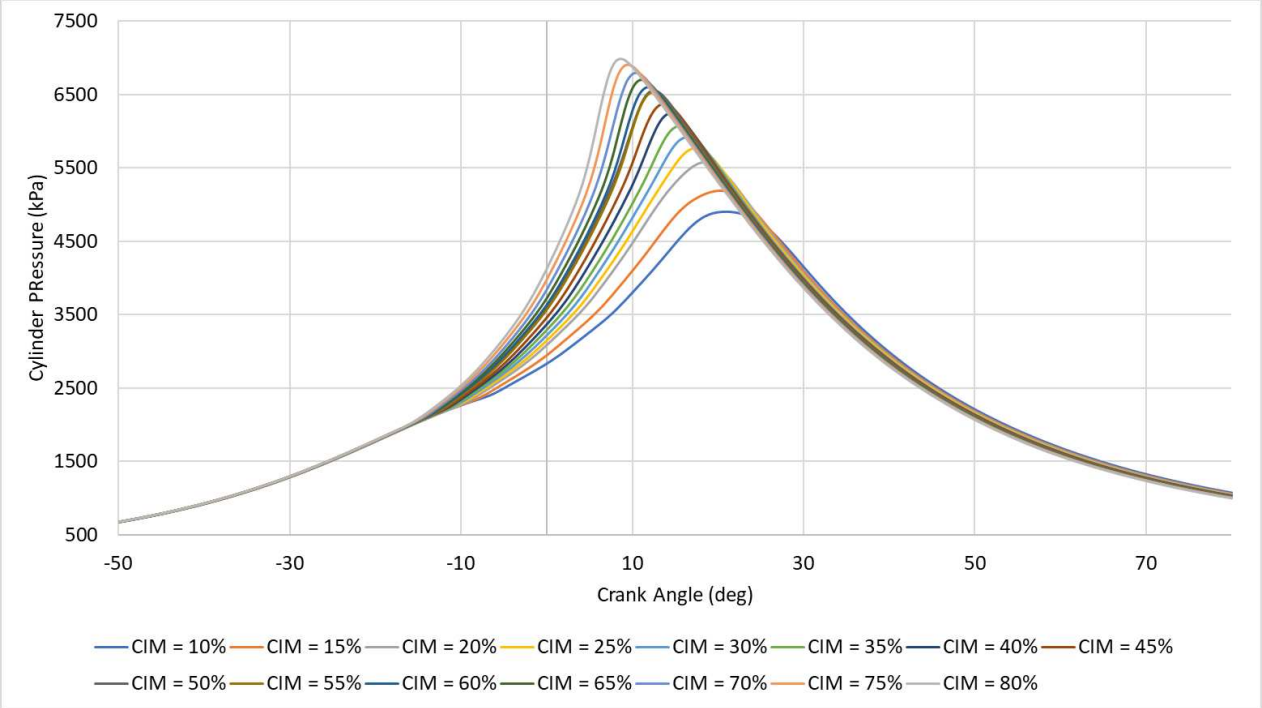

Figure 27: Cylinder Pressure Traces from Combustion Intensity Sweep

Within this figure, not only is the ignition timing sweep visible, but all five variables within the combustion intensity metric are visible. Peak pressure, peak rate of pressure rise, knock intensity, burn duration, and slope of heat release rise rate are all increasing with advancing spark timing and increasing combustion intensity. Further analysis later in the study will develop the control scheme between combustion intensity, f-EGAI, and C-EGAI. The first example of such is shown in Figure 28 with plots between combustion intensity, and the two most promising methods of knock quantification, FFT Power Spectrum and Knock Ripple Sum knock intensities. It can be seen in this figure that both with and without EGR substitution, the knock intensity trends positively with combustion intensity. Therefore, additional combustion metrics are required in combustion intensity to draw a trend with f-EGAI and C-EGAI.

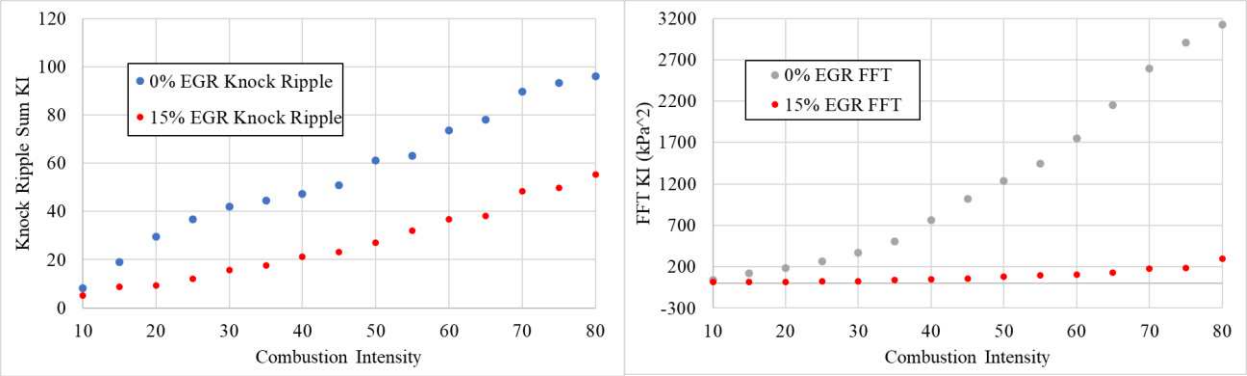

Figure 28: Combustion Intensity Sweep 10% to 80% vs Knock Intensity Methods of FFT Power Spectrum (right) and Knock Ripple Sum (left)

3.4 END GAS AUTO IGNITION FRACTION

To implement C-EGAI using CIM as the control parameter, a correlation between CIM and f-EGAI must be established. A plot of f-EGAI vs combustion intensity (CIM) is presented in Figure 29. The previously shown data for combustion intensity sweeps for 0% and 15% EGR substitution was used for this plot, however, combustion intensities below 20% did not generate any end gas auto-ignition. Yet, after 25% combustion intensity, a near linear trend is generated between combustion intensity and f-EGAI. There was a discrepancy around 55% combustion efficiency, with a plateau effect in f-EGAI. However, 15% EGR substitution remained more linear than 0% EGR. Overall, this provides a valid justification for the use of combustion intensity as the control parameter for C-EGAI.

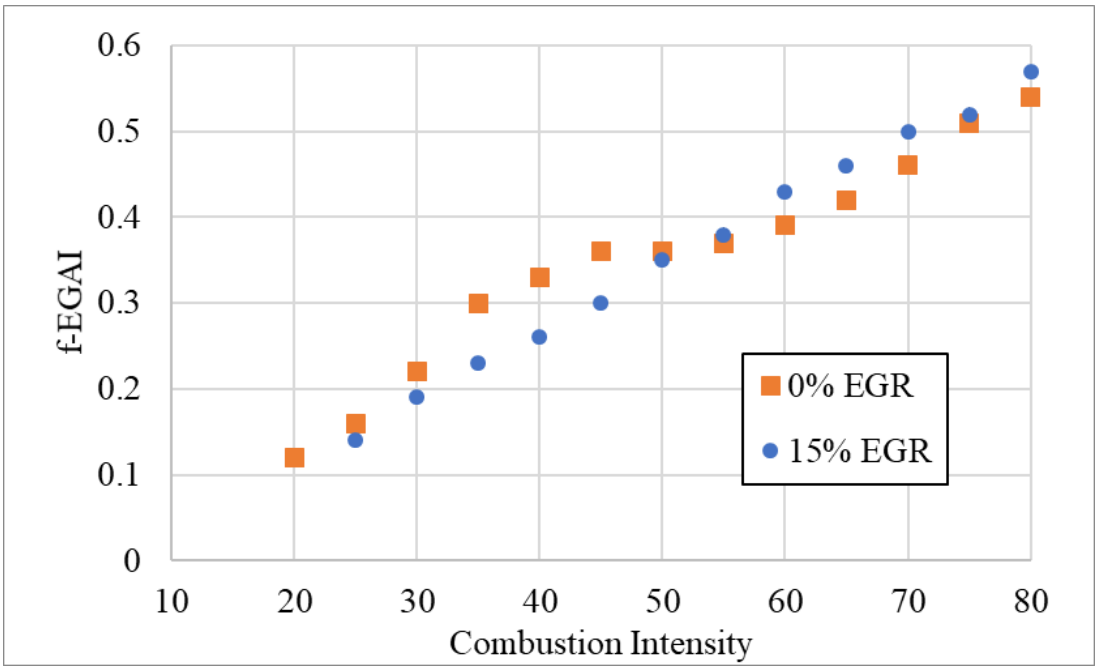

Figure 29: Combustion Intensity vs Fractional Heat Release Due to Auto Ignition for 0% and 15% EGR Substitution

Referring to Figures 26 and 29 together, it can be concluded that the best efficiency for the CFR engine under near peak power conditions while operating as a stoichiometric, spark ignited, natural gas engine with no EGR was with a combustion intensity of ~ 44%, and a f-EGAI of ~ 33%. This indicates the most optimal point occurs while operating in the medium knock window of operation. The application of C-EGAI will hold the f-EGAI to a set value. This value will correspond to an operating point just beyond the knock threshold of the engine, increasing combustion efficiency and power output for each cycle and leading to an increased brake efficiency. The knock threshold was determined by when the FFT power spectrum method demonstrated a net positive value of knock intensity from the increasing pressure ripple sinusoids.

CHAPTER 4: EFFECT OF EGR ON CFR ENGINE PERFORMANCE

4.1 EGR ENGINE TEST PLAN

For future comparative measurements with EGR operational data, a baseline measurement was established on the CFR engine. Table 2 below outlines the conditions and important metrics recorded from the baseline measurements. The values used were derived from conditions similar to those used for methane number measurements in previous work. A standard operating procedure for methane number testing can be found in Wise, et. al. [23]. Figure 30 and Figure 31 shows the cylinder pressure and apparent heat release rate (AHRR), respectively, from the baseline measurements. This data point rendered a total efficiency of 15.2%, providing the metric for comparing the effectiveness of future testing phases and potential improvements.

Table 2: CFR Engine Operational Conditions for Baseline Measurements

Metric	Value
Engine Speed	900 RPM
Intake Boost Pressure	101.3 kPa
Equivalence Ratio	1
Intake Temperature	60 °C
Spark Timing	CA50 = 10.3° aTDC (provides ignition timing near -15° aTDC)
EGR Rate	0%
Compression Ratio	9.5 FFT KI = 20 (knock onset)
Fuel MN	69 (MWM calculator)
Exhaust Temperature	~ 545 °C
IMEP	~ 800 kPa
Brake Efficiency	15.2 %

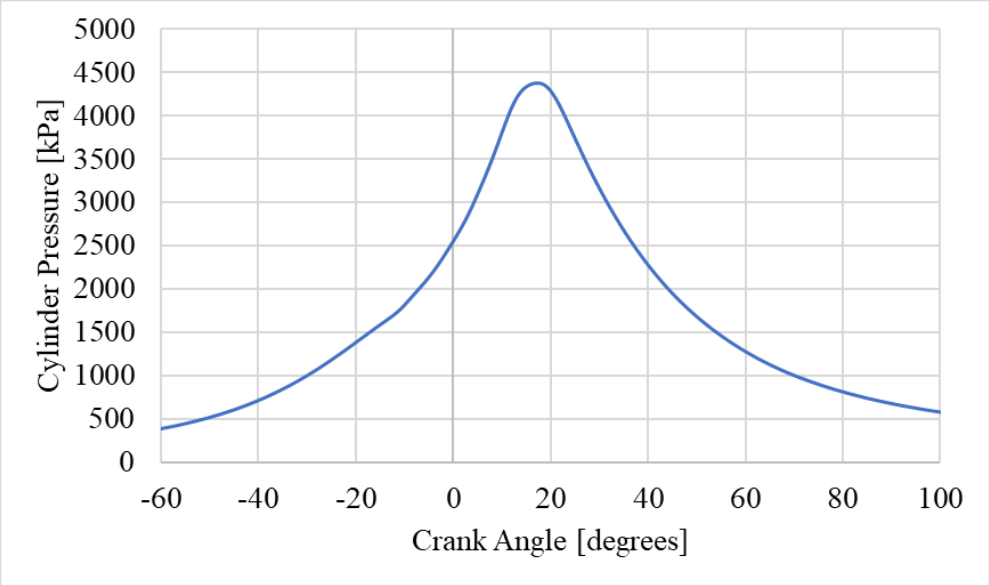

Figure 30: Cylinder Pressure Trace for Baseline CFR Engine Measurements

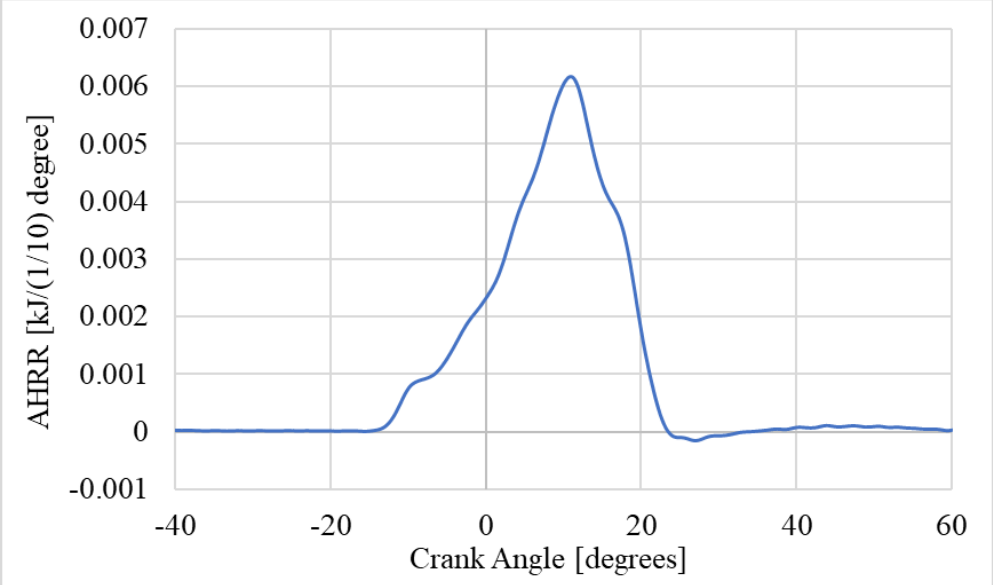

Figure 31: Apparent Heat Release Rate for Baseline CFR Engine Measurements

Measurements within the baseline testing showed a substantially lower knock threshold, brake efficiency, and compression ratio than expected. Figure 30 shows the combustion event with a smooth pressure trace, no auto-ignition, and a non-extended heat release period due to EGR. These trends will be more evident moving forward as EGR and auto-ignition levels increase with each testing phase. For all explorative EGR tests shown within this chapter, the baseline data will be represented as the 0% EGR case at the beginning of each figure, to demonstrate the available benefits of EGR introduction.

The fuel blend with a methane number of 69 was used throughout all testing within this study. This fuel blend was selected as the worst-case scenario for pipeline natural gas within the continental United States. A synthetic natural gas blend was used in place of straight pipeline gas to ensure consistent composition throughout the entire testing period. The blend consisted of 85% methane, 12% ethane, and 3% propane. The methane number was verified with the Cummins methane number calculator [35].

The testing was divided into four main phases with each implementing another step towards an optimized system, while analyzing the full range of EGR. Table 3 outlines the major changes implemented with each testing phase. Phase 1 begins with the parameters outlined for baseline testing, then EGR is added with 5% step sizes. The EGR test cart for the CFR engine is capable of providing up to 40% EGR at full load. The full range of EGR was tested initially, and the effects of this EGR sweep is shown in Figure 32. Phase 2 involved a repeat of the EGR sweep data points, but with increasing the compression ratio of the CFR engine to a new critical compression ratio (at FFT Knock Intensity value of 100 ~ light knock onset) for that EGR rate. Phase 3 operated at the same points from Phase 2 with a unit of 1 decrease in compression ratio, and then increasing the boost pressure and fuel flow to find the new critical power density for

knock onset (same FFT knock intensity as above). Then Phase 4 was a CA50 ignition control sweep from 6° to 21° aTDC at the previous two points of greatest efficiency from Phase 3.

Table 3: EGR Introduction Testing Phases for CFR Engine Efficiency Data

	Compression Ratio	EGR Rate	CA50 Timing	Output Power
Baseline	9.5	0	10.3° ATDC	800 kPa
Phase 1	9.5	0 to 35%	10.3° ATDC	800 kPa
Phase 2	9.5 to XXX	0 to 30 %	10.3° ATDC	800 kPa
Phase 3	Critical CR - 1	0 to 30%	10.3° ATDC	800 to 1250 kPa
Phase 4	Critical CR - 1	15%, 20%	6° to 21° ATDC	100 kPa under critical IMEP

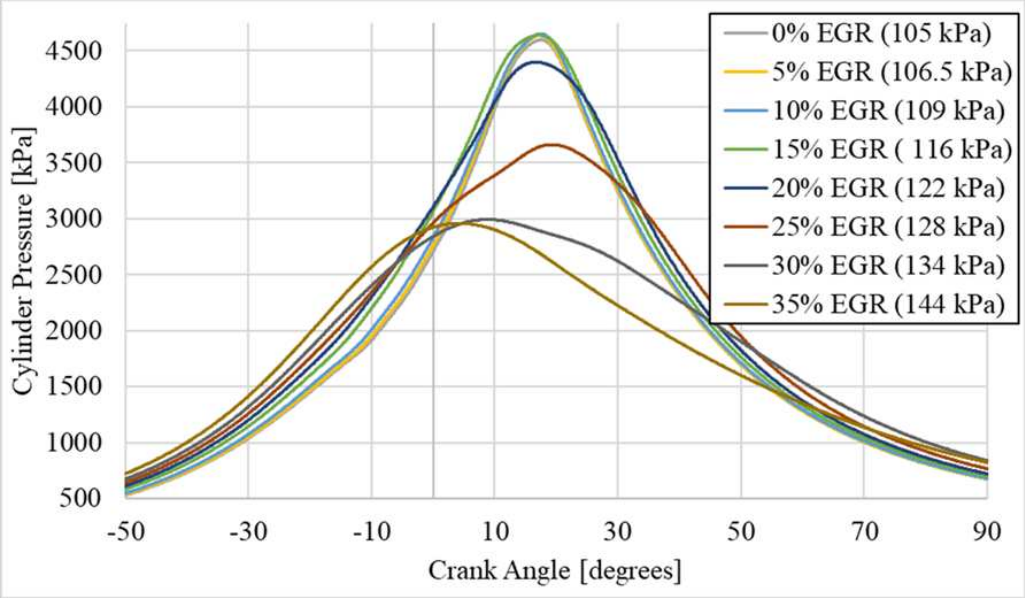

Figure 32: Cylinder Pressure Traces from Phase 1 of EGR Testing

Figure 32 demonstrates the basic effects of the EGR sweep applied to the CFR engine. The initial conditions prior to the EGR rate sweep were far from the max load and below the knock limit of the engine. Hence, the primary effect of the EGR sweep was an increase in combustion durations and a reduction in combustion stability. The reduction in combustion

stability is seen in the reduction in peak pressure for the higher EGR rate cases, despite the constant compression ratio, and increased boost pressures (equating to a greater amount of trapped mass) of the higher EGR rates to maintain constant power. These effects will be addressed further in the subsequent section.

4.2 COMBUSTION STABILITY AND EGR LIMITS

The limiting factor behind the use of EGR in natural gas, stoichiometric, spark-ignited engines is combustion stability. The EGR limit is defined as the highest rate of EGR that can be run through the engine before the combustion process gets too. The EGR limit is located at the onset of excessive combustion instability. More specifically, this location of combustion instability is when the coefficient of variance (COV) of peak pressure exceeds a value of 10%, and/or the misfire rate exceeds a value of 10%. A misfire event occurs when the engine fails to ignite the mixture. Higher rates of EGR creates a larger fraction of noncombustible components in the intake charge, therefore requiring more energy to ignite the air/fuel mixture and slowing flame propagation. Figure 32 in the previous section demonstrates the dilution effect with the diminishing peak pressure with higher EGR rates.

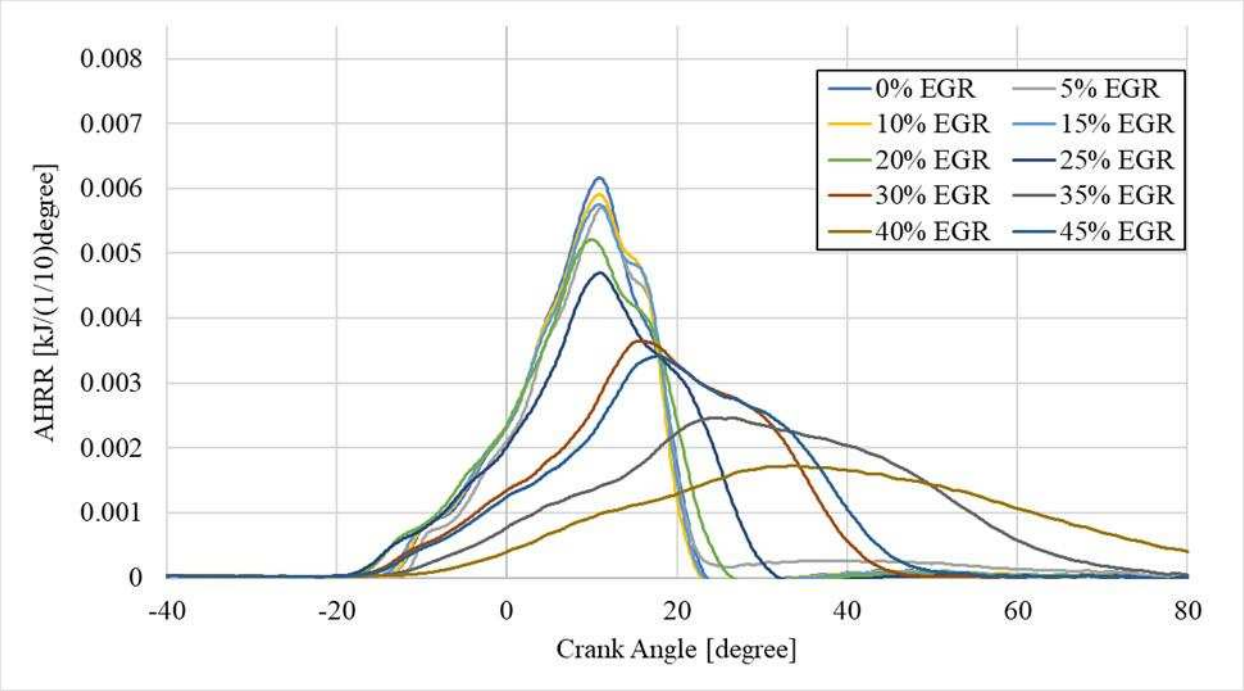

Figure 33: Apparent Heat Release Rates from Phase 1 of EGR Testing

Figure 33 shows the heat release rate from the same data set as Figure 30. The plots demonstrate a delayed ignition event similar to auto-ignition with a secondary heat release plateau. However, unlike auto-ignition, this event is not greater in heat release than the initial combustion event. Instead the EGR ignition delay appears to be an extension of combustion duration, most likely caused by the dilution effect slowing flame propagation through the combustion chamber. From this data set, the EGR limits due to combustion instability and misfire is likely between 25% and 30% EGR. All cases with an EGR rate over 30% exhibited a peak pressure one third the magnitude or lower than the baseline data point, and demonstrated combustion occurring well into the expansion stroke with elevated pressures beyond 40° aTDC. This is illustrated in Figure 34, where the misfire rates and COV of peak pressure are displayed with the brake efficiency for each data point.

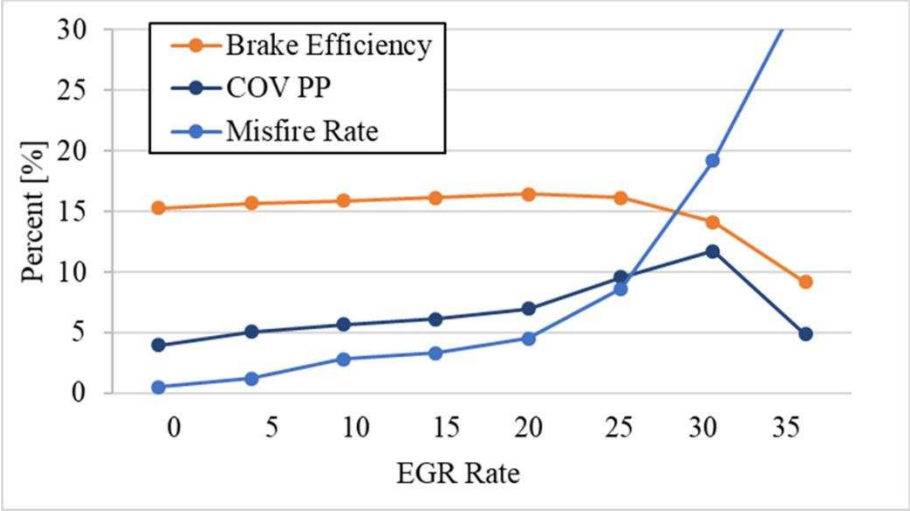

Figure 34: Combustion Stability Metrics for Phase 1 of EGR Testing

The EGR limit in Figure 34 becomes more evident within the window of 25% to 30% EGR. The plot also demonstrates that any EGR rate above 30% is impractical. The EGR limit is because the COV of peak pressure exceeds 10% between 25% and 30%, while the misfire rate also crosses that threshold at about the same EGR level. At EGR rates above 30%, the COV of peak pressure falls below 10%, while the misfire rate jumps rapidly to a rate of over 50%, meaning the majority of cycles for that data point are misfires. The improvement of COV of peak pressure above 30% EGR results from most of the cycle being misfires, or motored pressure events, which are very consistent from cycle to cycle. The optimal EGR rate is not within the window of 25% to 30%, where the EGR limit is located. The optimal EGR rate is located where the highest brake efficiency occurs, which for this data set is around an EGR rate of 20%.

All preceding testing phases focus on the areas of the EGR limit as well as the optimal EGR window. Any operating point outside of those locations exhibits decreased brake efficiencies due to decreased reactivity of the charge in the combustion chamber. At constant

CA50, increasing the EGR rate results in advanced spark timing of the CFR engine, causing what appears to have a larger portion of the combustion event near TDC of the combustion chamber, generating a higher compression force. Higher EGR rates beyond the optimal EGR window create too large of a dilution effect, where the higher rate of misfires decreased total brake efficiency below baseline recordings. These effects can be seen in Figure 35, where the combustion durations of phase 1 of the EGR testing are presented. Both ignition delay and burn duration increase as the EGR rate increases.

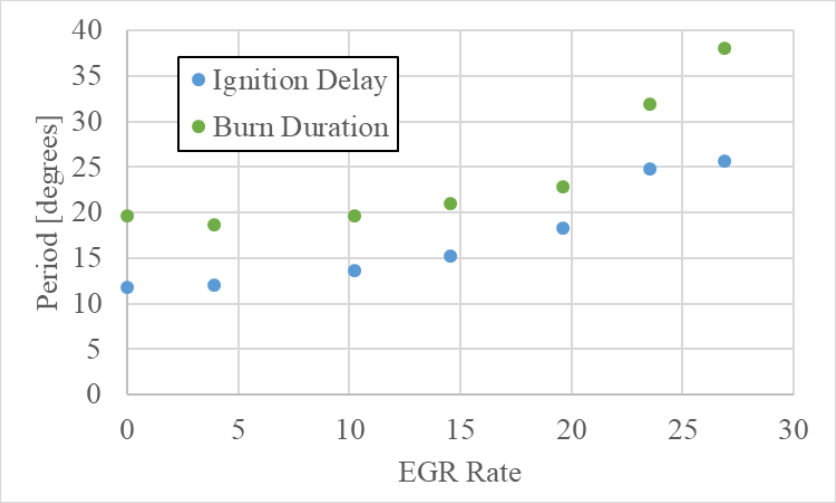

Figure 35: Combustion Phasing for Phase 1 of EGR Testing

Concluding the work done within phase 1 of the EGR testing, the EGR sweep affected several aspects of engine performance. These include the knock threshold, brake efficiency, combustion stability, combustion phasing, and exhaust temperature. The last metric, exhaust temperature is a leading factor contributing to power density limits in engines. For the CFR engine, the exhaust temperature limit is 650 °C, which was higher than baseline testing conditions. Figure 36 below demonstrates the effect EGR had over the sweep on exhaust

temperature, and it can be seen that the temperature was reduced by 80 °C over the 30% EGR rate sweep. The dilution effect in the combustion chamber due to the CO2 and H2O in the EGR fluid cause the combustion temperature to lower by a factor of ~ 0.18, which thus translates to a reduction in the temperature of the exhaust stream. These cooler constituents in the exhaust allow the engine to increase the power density and thus the efficiency, which was performed in phase 3 of the EGR testing.

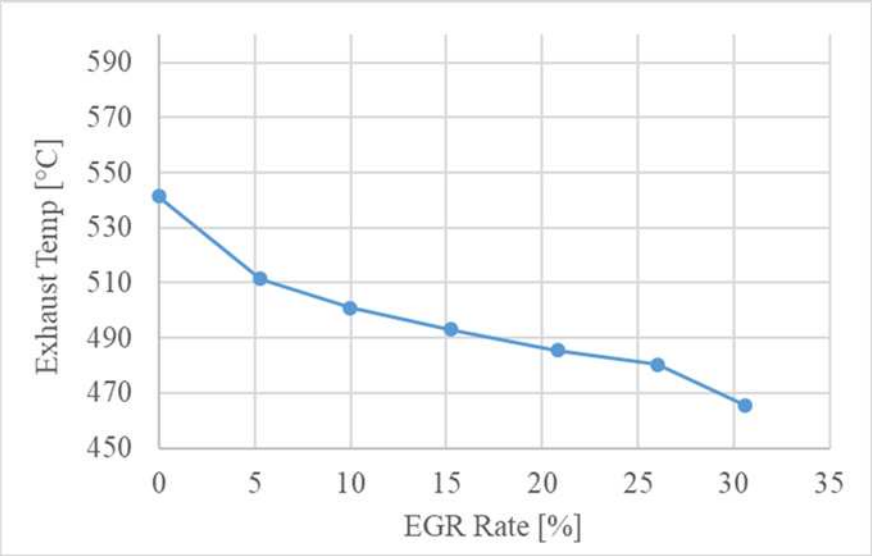

Figure 36: Exhaust Temperature with EGR Rate from Phase 1 of EGR Testing

Phase 2 involved repeating the viable EGR rate data points from phase 1 but increasing the compression ratio to the new critical compression ratio. The cylinder pressure traces and heat release data from this set can be seen in Figures 37 and 38 respectively. The magnitude of peak pressures is greater with increased compression ratios. Additionally, the AHRR occurs over a shorter duration when the cycles are closer to the knock limit. The optimal EGR rate was also increased by ~1% at a higher compression ratio. However, at and above 25% EGR replacement

rate, a compression ratio near the limit of the CFR engine was required to maintain steady combustion, and the maximum efficiency still occurred at the 20% EGR rate data point.

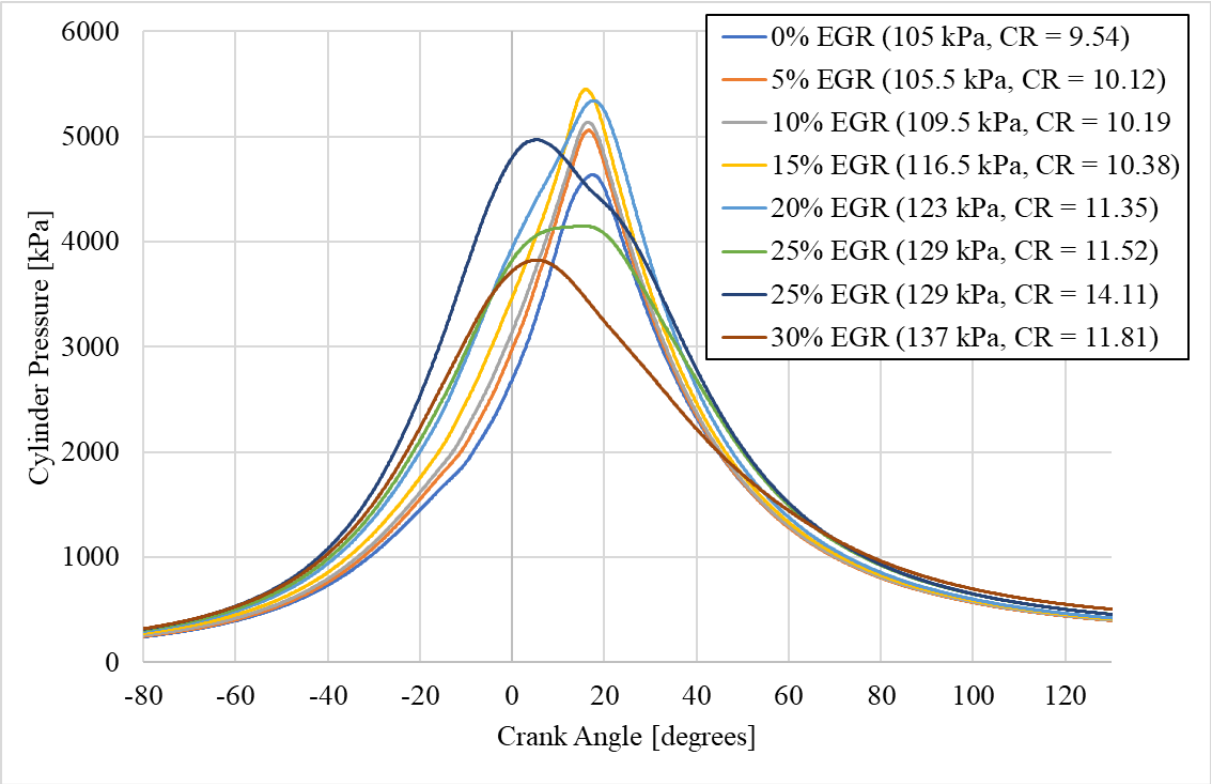

Figure 37: Cylinder Pressure Traces from Phase 2 of EGR Testing

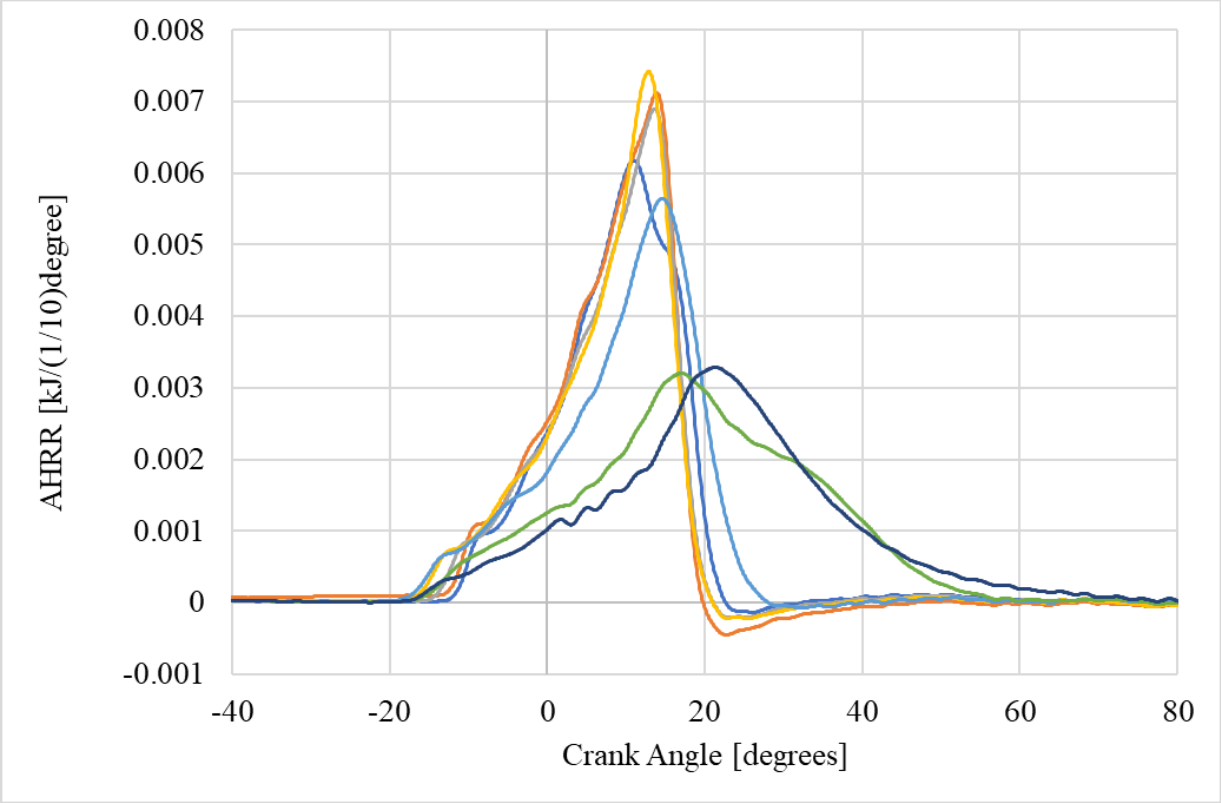

Figure 38: AHRR from Phase 2 of EGR Testing

The greatest performance benefits with EGR operation were found in Phase 3 testing, which involved a repeat of Phase 2 data points in finding the maximum power density with a compression ratio of 1 unit below the critical compression ratio. Figure 39 shows the cylinder pressure traces from this phase. The magnitude of peak pressure again rises about 22 bar above the baseline peak pressure. This increased power density rendered the largest efficiency gain with a maximum brake efficiency of 20.1%. The inclusion of EGR in the combustion process increased the knock threshold compared to baseline. The maximum power density of the CFR engine lies near 1300 kPa IMEP, and the most efficient data point rendered an IMEP of 1162 kPa.

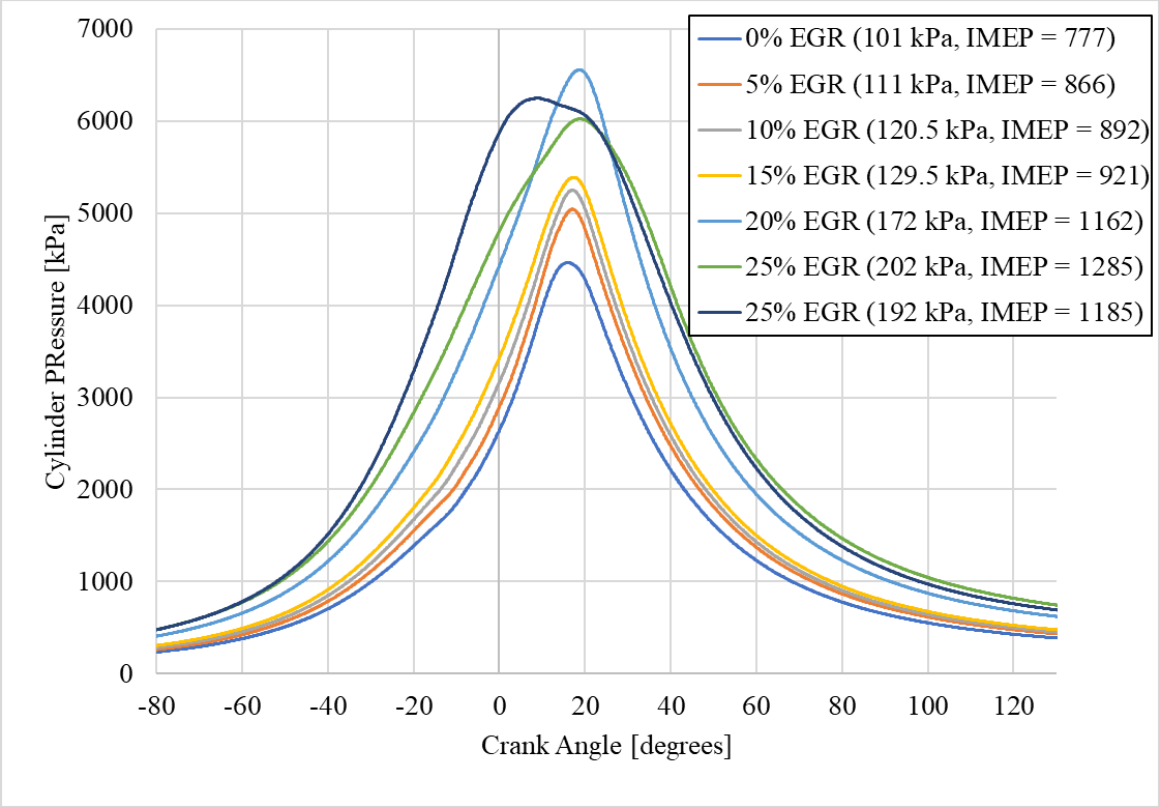

Figure 39: Cylinder Pressure Traces from Phase 3 of EGR Testing

The final phase of EGR testing took the 15% and 20% EGR rate data points from phase 3 and fixed all variables except for CA50, which was swept across a viable window of engine operation. The cylinder pressure traces from the 15% EGR rate CA50 sweep is shown in Figure 40. This data shows that advancing the CA50 control values resulted in the peak cylinder pressure advancing towards 0° TDC. Additionally, advanced CA50 control values such as the 6° aTDC required advanced spark timing that was great enough to induce slight auto-ignition within the cycles. Through this CA50 ignition control sweep, it was found that for both the 15% and 20% EGR rate cases, the optimal CA50 control was 10.9° aTDC. This 0.6° shift in CA50 was enough to raise the brake efficiency by 0.1% and provide the highest efficiency value for the EGR testing of 20.2%.

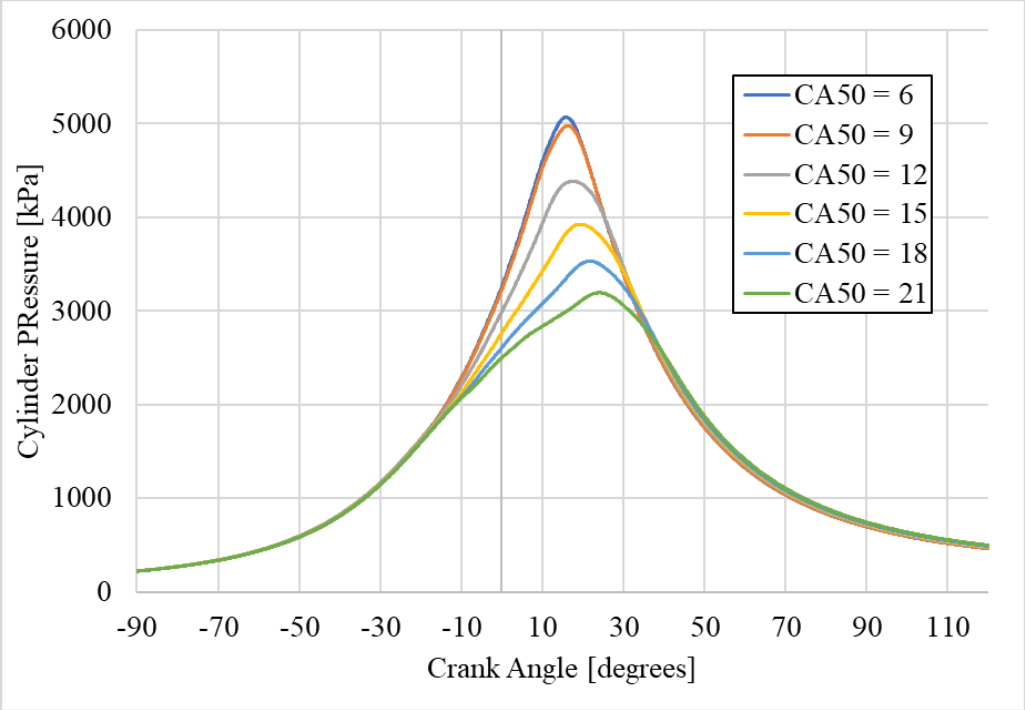

Figure 40: Cylinder Pressure Traces from First CA50 Sweep of Phase 4 of EGR Testing

Combustion pressure traces for select points from EGR testing can be found in Figure 41. This plot shows the pressure traces of the highest efficiency for each phase. The efficiency values for Phases 1 through 3 as a function of EGR rate are shown in Figure 42. This plot indicates that the optimal EGR rate is around 20% EGR. The values for brake specific efficiency was calculated using Equation 8.

$$\eta_b = \frac{W_b}{\sum(m_f Q_{LHV})}$$

Equation (8)

where:

Wb = work available at the engine crankshaft

mf = mass flow rate of fuel

QLHV = lower heating value of fuel.

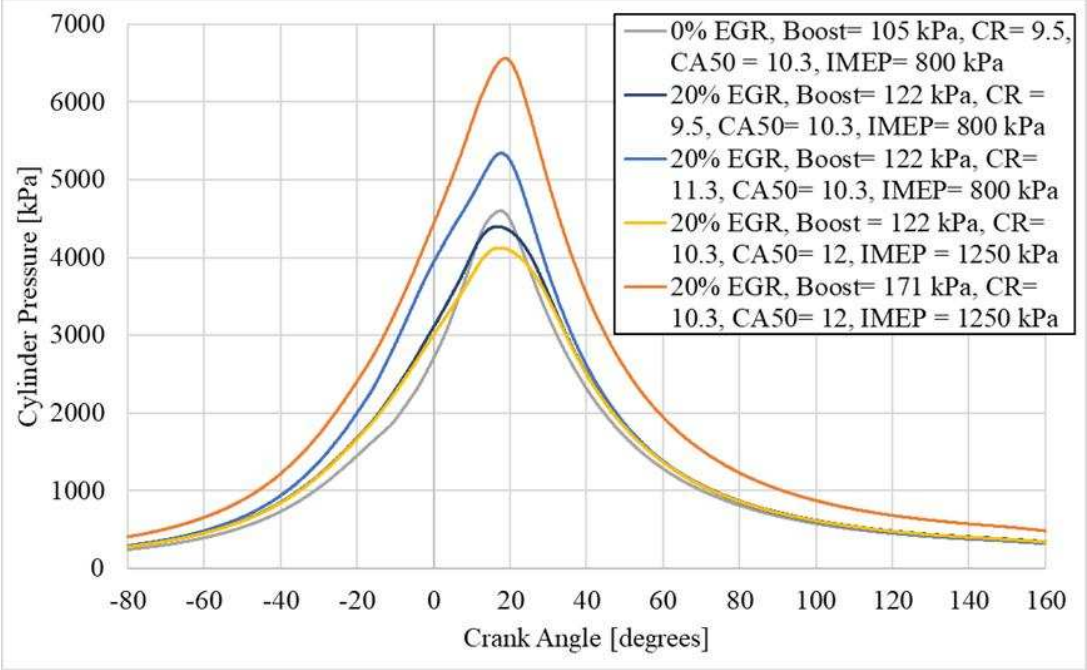

Figure 41: Cylinder Pressure Traces of Greatest Efficiency from EGR Testing Phases 1-4

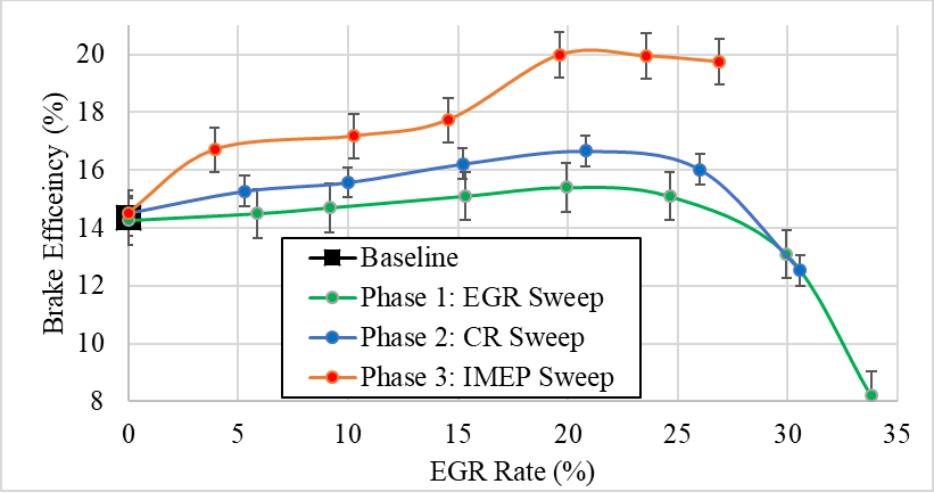

Figure 42: Brake Efficiency vs. EGR for Testing Phases 1 Through 3

4.3 EXPANSION OF KNOCK THRESHOLD

EGR has many fundamental effects including increasing the thermal efficiency of an engine, reducing harmful emission concentrations, and acting as a knock suppressant. This study demonstrates the effectiveness of EGR as a knock suppressant and its ability to expand the knock threshold. From Phases 2 and 3 of EGR testing, the critical compression ratio, and critical IMEP (power density) was found, and this data is displayed in Figure 43. Taking the optimum EGR rate of 20%, the compression ratio was able to increase by 2.3 units before knock onset, and the IMEP was able to be increased by 360 kPa. The entirety of this data was taken at the knock threshold.

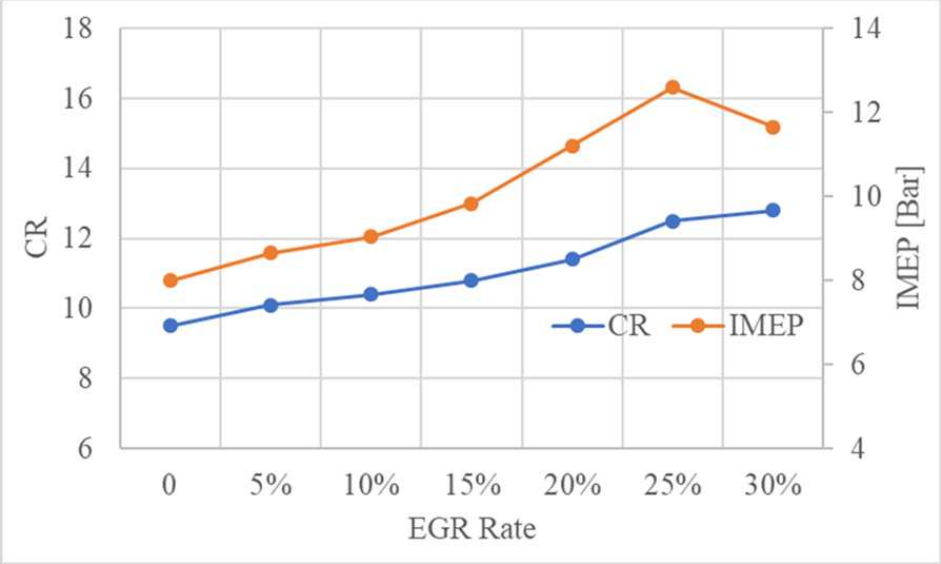

Figure 43: Critical Compression Ratio and Critical IMEP Values vs. EGR Rate

Figure 44 shows the knock intensity for Phase 1 EGR rate sweep, using the knock ripple sum quantification technique. As the EGR rate increases at constant IMEP and speed, the knock amplitude decreases. To provide context, the FFT power spectrum deals in units of kPa·rms^2, and a value of 20 signifies the earliest onset on auto-ignition. Baseline testing produced a knock intensity of 22, and a non-knocking case displays an average value of knock intensity of 5 kPa·rms^2. At a 20% EGR rate, and no other variable changes from baseline measurements, the knock intensity was ~ 5 kPa·rms^2. Over the 35% EGR rate sweep, an 80% reduction in knock intensity is realized.

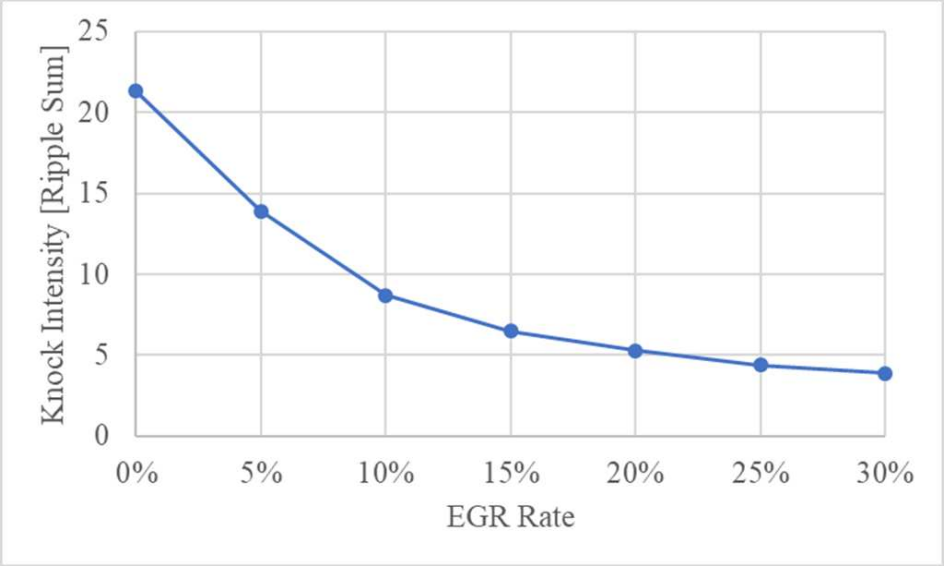

Figure 44: Effect of EGR Rate on Knock Intensity (FFT)

Due to the EGR knock suppression effect, the implementation of C-EGAI on a stoichiometric, spark-ignited, natural gas engine will require more intense operational conditions than expected. However, the knock suppression effect will ensure more consistent cycle to cycle combustion pressure for modes of greater combustion intensity. Inherently, auto igniting cycles

with greater knock intensities cause inconsistencies in subsequent cycles, but the presence of minor dilution with EGR provides stability by inhibiting knock. The expanded knock threshold overall appears to provide an ability to operate at a greater combustion intensity, and thus produce a greater brake efficiency through knock suppression.

4.4 EFFECT OF EGR ON EMISSIONS CONCENTRATIONS

The last potential benefit of EGR implementation is the reduction in harmful emission concentrations. EGR is a powerful modern tool to meet strict Environmental Protection Agency (EPA) emission regulations, especially with NOx emissions. The primary species in question are Carbon Monoxide (CO), Total Hydrocarbons (THC), and Oxides of Nitrogen (NOx). Stoichiometric natural gas engines paired with a 3-way catalyst can meet most stringent emission standards [3].

Emissions of CO, THC, and NOx concentrations are displayed in Figure 45. A trade-off is observed in the data. As CO and THC increase, NOx decreases. Emissions levels of all three are equivalent at around 20% EGR.

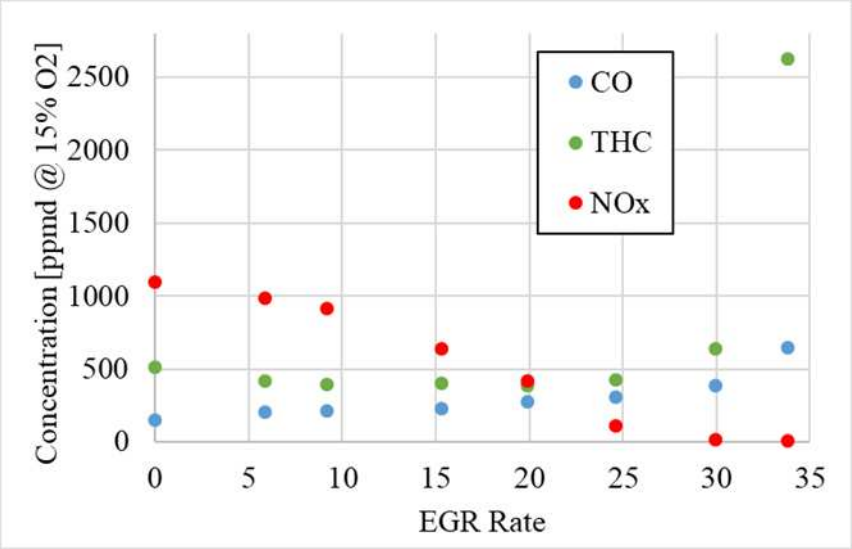

Figure 45: Emission Concentrations for CO, THC, and NOx from Phase 1 of EGR Testing

The rise in THC emissions as EGR rate increases is consistent with the increased misfire rate with greater EGR rates. The increase in CO emissions is consistent with the lower combustion temperatures and increased combustion variability. The decrease in NOx is consistent with the reduced combustion temperatures from the EGR dilution. This is further displayed in Figure 46 with the emissions concentrations from the critical power density Phase 3 of EGR testing.

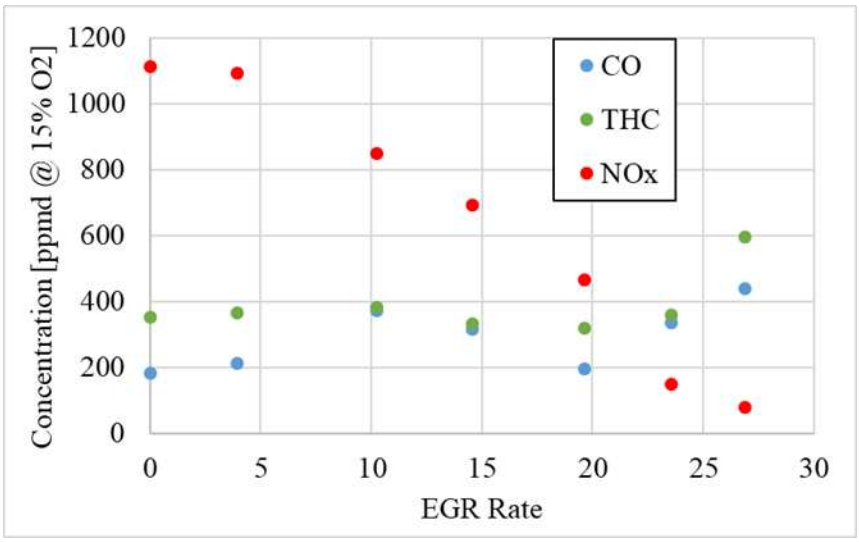

Figure 46: Emission Concentrations for CO, THC, and NOx from Phase 3 of EGR Testing

Formaldehyde is a known carcinogen, which can be formed by partial combustion. Higher EGR rates can cause partial combustion and can potentially lead to large concentrations of formaldehyde. However, rising EGR rates shown in Figure 47, decrease formaldehyde concentrations until the EGR limit is reached and the misfire percentage increases. This emission was measured during each engine test using a Fourier Transform Infrared Spectroscopy (FTIR) emissions probe. These emissions were approximately two orders of magnitude lower than regulated emissions of NOx, CO, and THC so the concentration has been displayed in units of mg/bkW-hr.

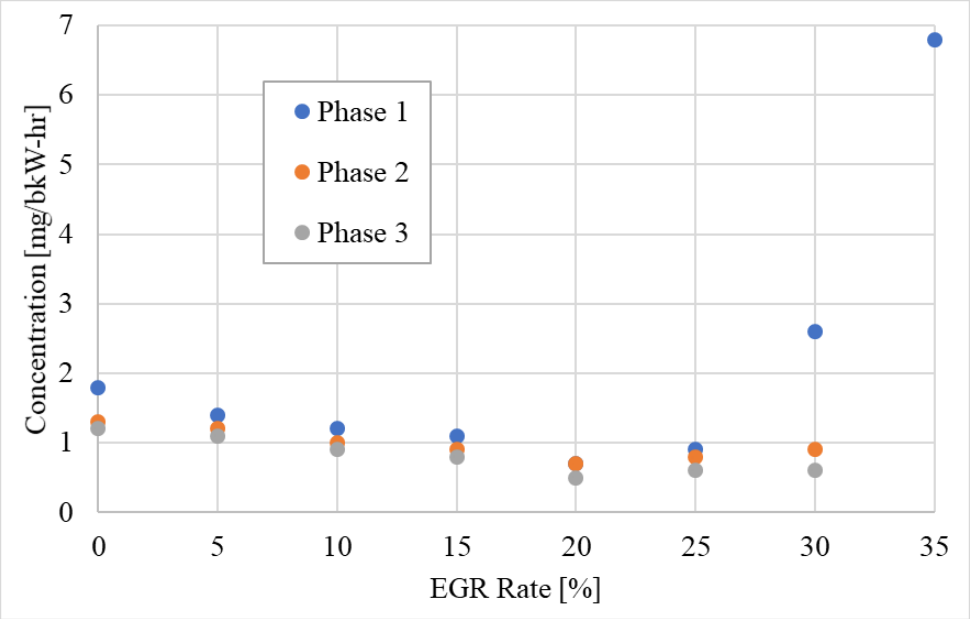

Figure 47: Formaldehyde Concentrations for Phases 1 Through 3 of EGR Testing

CHAPTER 5: DEMONSTRATION OF C-EGAI ON A CFR ENGINE

5.1 DETERMINATION OF PERCENT END GAS AUTO IGNITION AND C-EGAI IMPLEMENTATION

Additional CFR engine testing was conducted with the implementation of C-EGAI. This testing required the utilization of the previous knock intensity quantification data as well as the previous EGR explorative data. To control end gas auto-ignition to a set value, the f-EGAI must be calculated and maintained to a set level. C-EGAI requires a correlation between the previously outlined knock quantification methods and a set of variable controls on the CFR engine. The best method found through said testing in Chapter 3 included the combustion intensity metric (CIM), the FFT power spectrum knock intensity, and the knock ripple sum knock intensity. These methods were analyzed moving forward for their correlation to f-EGAI.

Due to the fact that the knock ripple sum knock intensity method is a variable within the combustion intensity metric, the FFT power spectrum knock intensity became the primary method of verification for knocking cases, and the CIM in conjunction to the knock ripple sum knock intensity became the method of ignition control to instigate C-EGAI. Figure 28 in Chapter 3 plotted a sweep of combustion intensity vs both knock intensity methods, demonstrating how the increase in combustion intensity causes an advancement in spark timing, while increasing the knock intensity. The inclusion of the four other variable inputs for the CIM cause knock intensity to not be the primary cause of increases in CIM and considers other factors of engine operation that influence the severity of recurring auto-ignition events.

The CIM parameter was selected as the control parameter. Figure 29 in chapter 3 demonstrates the effect of CIM control on fractional heat release due to auto-ignition. It was previously demonstrated that the CIM control method relates to a linear trend of f-EGAI. Because C-EGAI controls to a set value of f-EGAI, a relationship can be created that allows for C-EGAI through CIM control. The relation was tested with C-EGAI baseline testing before a full efficiency optimization. Figure 48 is a cylinder pressure trace from the CFR engine that demonstrates heavy knock. This is the same pressure trace analyzed earlier in Figure 25, where the calculation of f-EGAI is demonstrated in the MFB plot. This MFB plot is also shown in Figure 49.

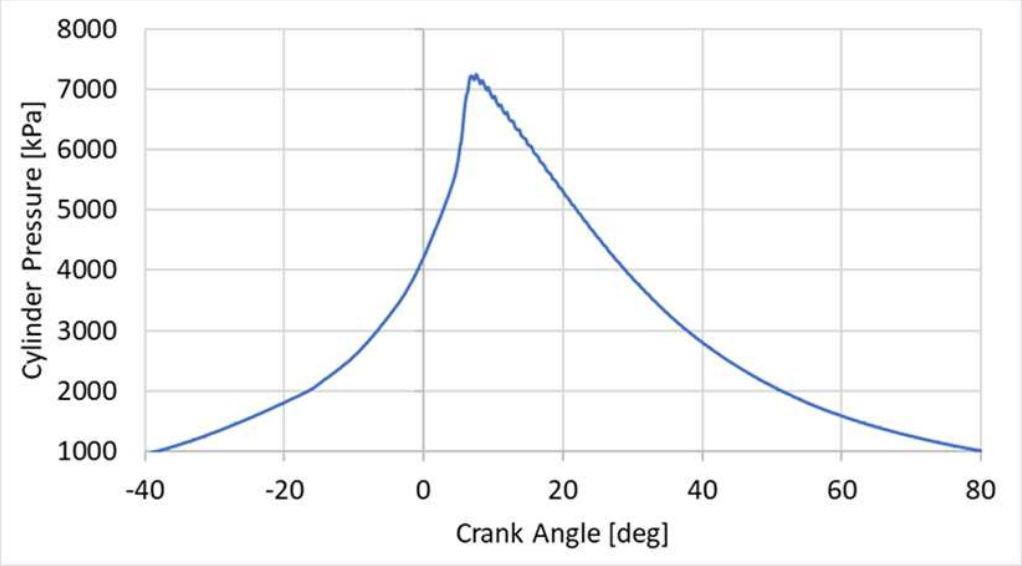

Figure 48: Heavy Knocking Pressure Trace from CFR Engine

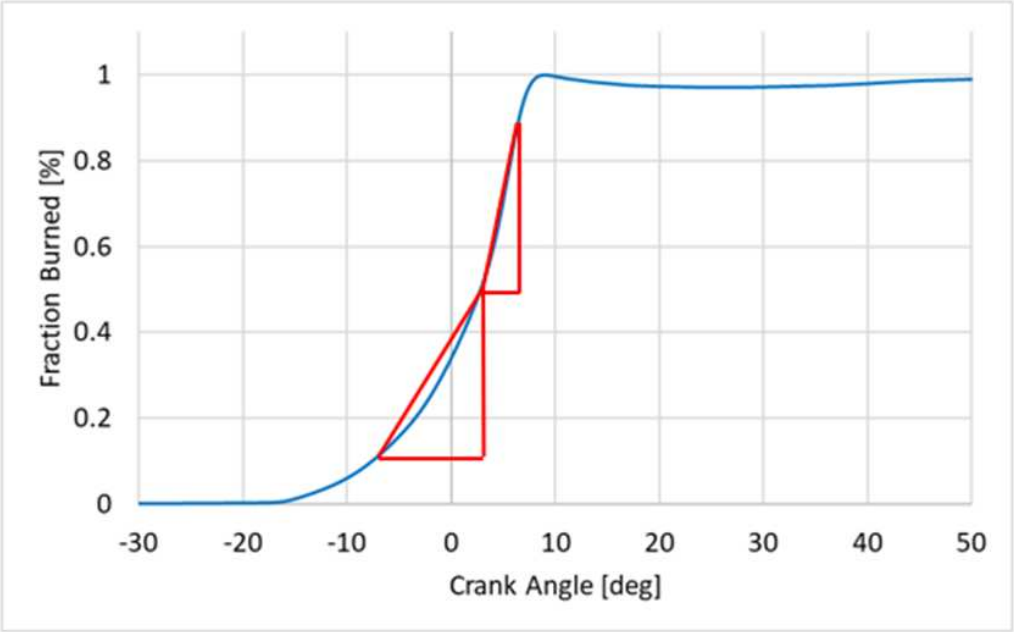

Figure 49: MFB Heat Release Acceleration Demonstration with Heavy Knock

On the MFB plot in Figure 49, the two red slope triangles isolate the burn durations from 10-50% MFB and 50-90% MFB. It is seen that the slope of the 50-90% MFB is steeper than the 10-50% MFB period. This factor is the fifth variable that inputs to the CIM and plays a large part in C-EGAI because the location and slope of the 50-90% MFB will determine how much heat release will be released during auto-ignition. The AHRR of the cycle from Figures 48 and 49 is shown in Figure 50. It can be calculated from this trace that over 55% of the heat release for this cycle is due to auto-ignition. It is theorized that these greater auto-ignition events can destabilize subsequent cycles, reducing the controllability of auto-ignition events.

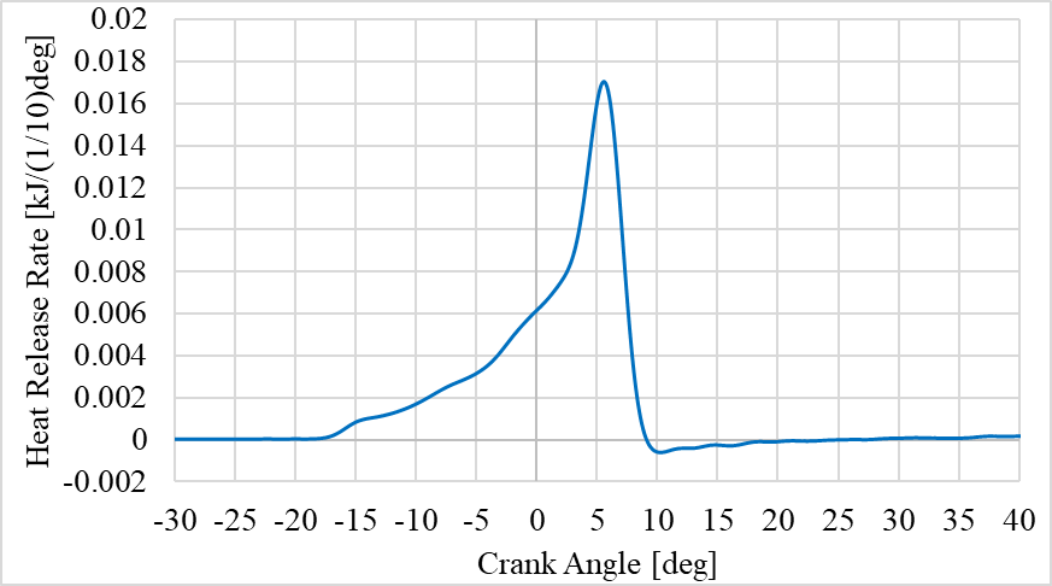

Figure 50: AHRR for Heavy Knocking CFR Engine Cycle

KOCA values for a CIM sweep on the CFR engine is shown in Figure 51. This plot exhibits a linear relationship between CIM and KOCA. However, there was no KOCA value detected for combustion intensities below 5% CIM without EGR and below 25% CIM with EGR. The lack of auto-ignition is likely because the combustion intensity was too low to instigate auto-ignition events at the given conditions of the CFR engine.

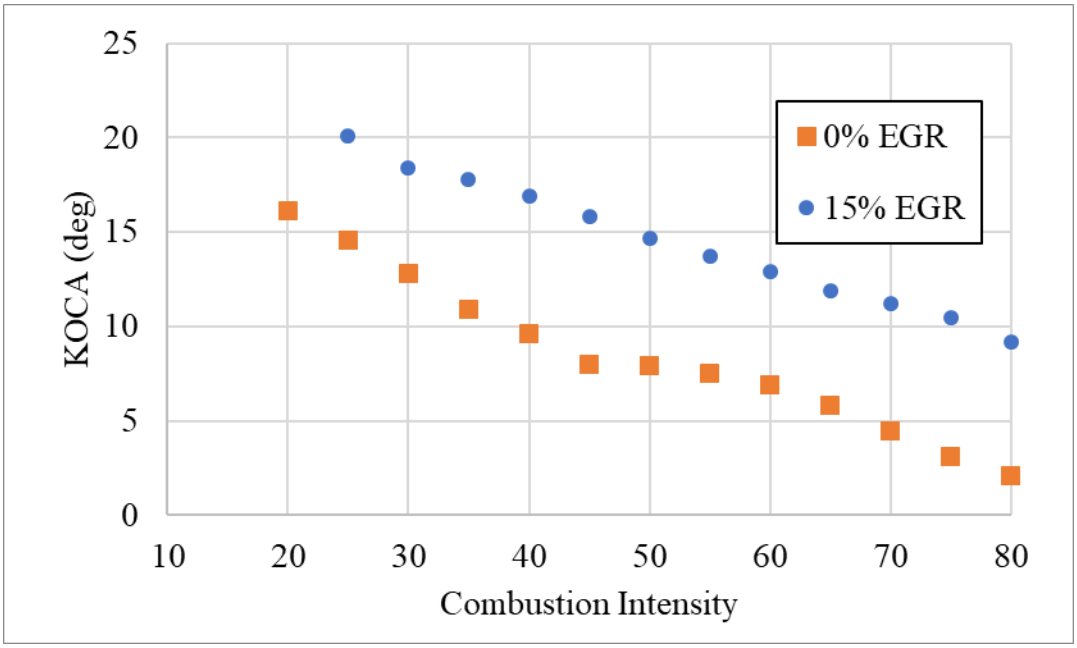

Figure 51: Combustion Intensity vs Knock Onset Crank Angle

5.2 EFFECT OF C-EGAI ON COMBUSTION PROCESS

With a functioning method of controlled end gas auto-ignition through CIM ignition control, the next step was an analysis of the effect C-EGAI. With the assumption that there is a direct relationship between f-EGAI and CIM, a CIM sweep was performed on the CFR engine. Figure 52 below shows the cylinder pressure traces from the C-EGAI sweep, where set values of f-EGAI were targeted at 15% EGR. Additionally, all other factors excluding ignition timing were set to Chapter 4 conditions that exhibited the greatest efficiency value. This led to greater peak pressures and auto-ignition introduction after a CIM value of 20%, with the slope of heat release increasing to greater values. The CIM value was unable to exceed 80% due to the knock intensity reaching the absolute knock limit of the engine, at an FFT knock intensity value of 3000 kPa*rms^2. The higher values of knock intensity were able to overcome the knock

suppression of the 15% EGR substitution and provide a consistent f-EGAI that controlled to a percent heat release4 due to auto-ignition within 1.5% of the target value. The final relation between CIM and f-EGAI determined from this sweep of C-EGAI can be found below in Table 4.

Table 4: Reference Values for CIM and f-EGAI Relationship for Specified Fuel Blend During this Study

Combustion Intensity	Average Fractional Heat Release
10%	0.00
20%	0.09
30%	0.17
40%	0.25
50%	0.34
60%	0.41
70%	0.49
80%	0.63

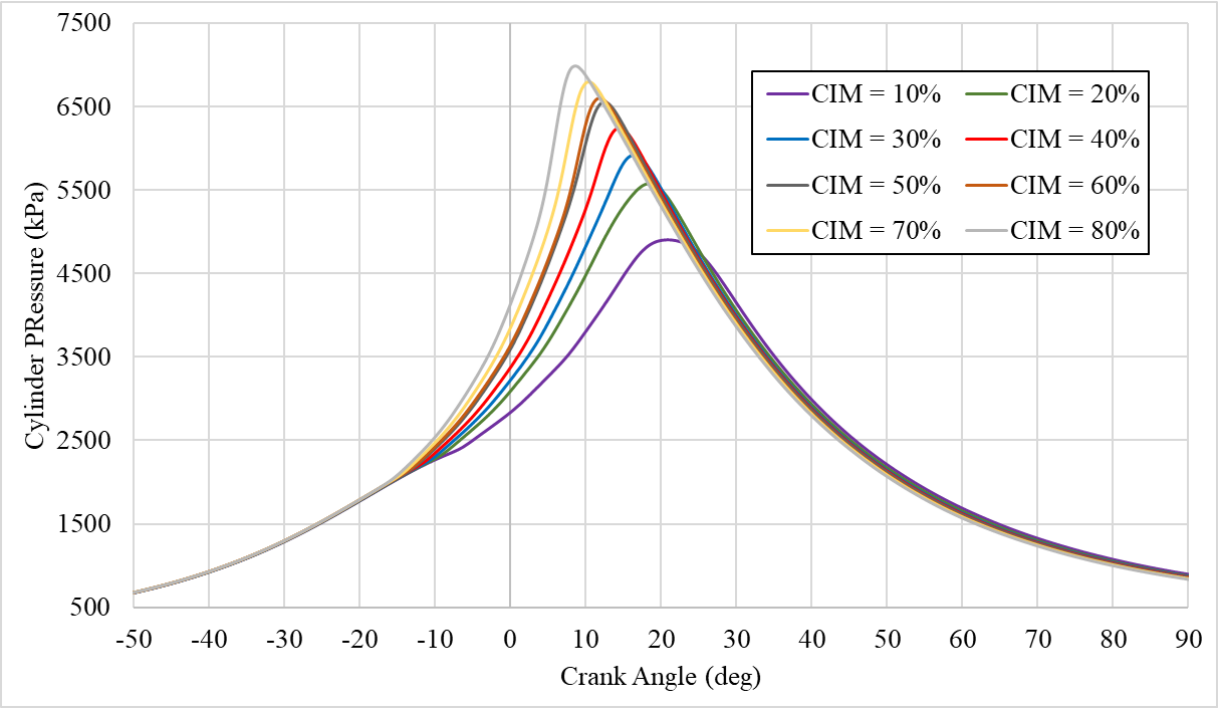

Figure 52: Cylinder Pressure Traces from C-EGAI Sweep of CIM

Figure 53 shows the plots for the AHRR for the same data set as in Figure 52. Once again, auto-ignition becomes visible above 20% CIM, and it can now be seen that over 50% CIM, a large portion of the total heat release occurs during the auto-ignition event. The increase in CIM to increase f-EGAI appeared to cause a larger advancement in ignition timing between lower levels of CIM, while there was a lower required change of ignition timing to instigate increases of CIM at higher levels.

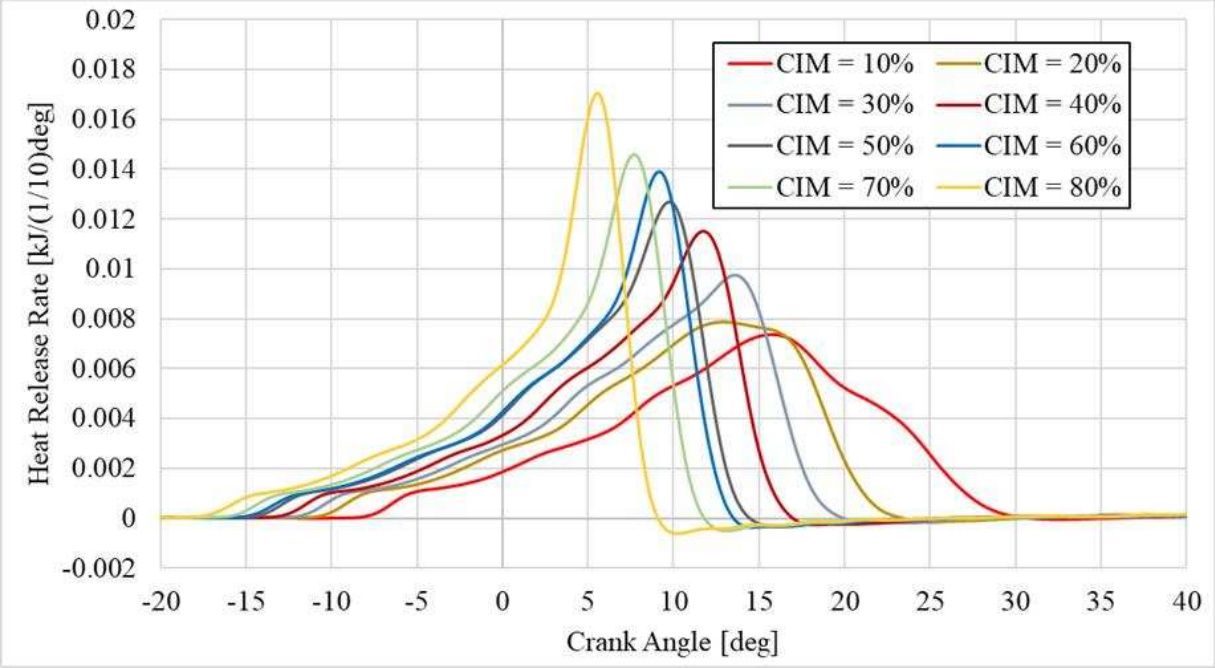

Figure 53: AHHR from C-EGAI Sweep of CIM

To determine the effect of C-EGAI on overall CFR engine performance, the efficiency and COV of Peak Pressure is plotted below in Figures 54 and 55. Both plots contain the data with 0% EGR from the initial CIM sweep, as well as 15% EGR to analyze C-EGAI. The sweep of CIM was done to demonstrate the improvements made through both EGR and C-EGAI

implementation. From the CIM sweep, the initial data set demonstrates a maximum efficiency at 46% CIM and a 0.31 end gas auto-ignition fraction. However, data set with EGR replacement demonstrates no peak efficiency value until the absolute knock limit is almost achieved at 74% CIM. This will be further investigated through the efficiency optimization of C-EGAI. Looking at Figure 55, there is no data point that crosses the COV of peak pressure value of 10 to indicate unstable combustion. While data set with 15% EGR replacement exhibited a higher COV of peak pressure, they both also exhibited minimal misfire rates maintaining values below 4%. With this data, it is likely that the optimal level of C-EGAI exists between fractional values of 0.25 and 0.45 heat release due to auto-ignition.

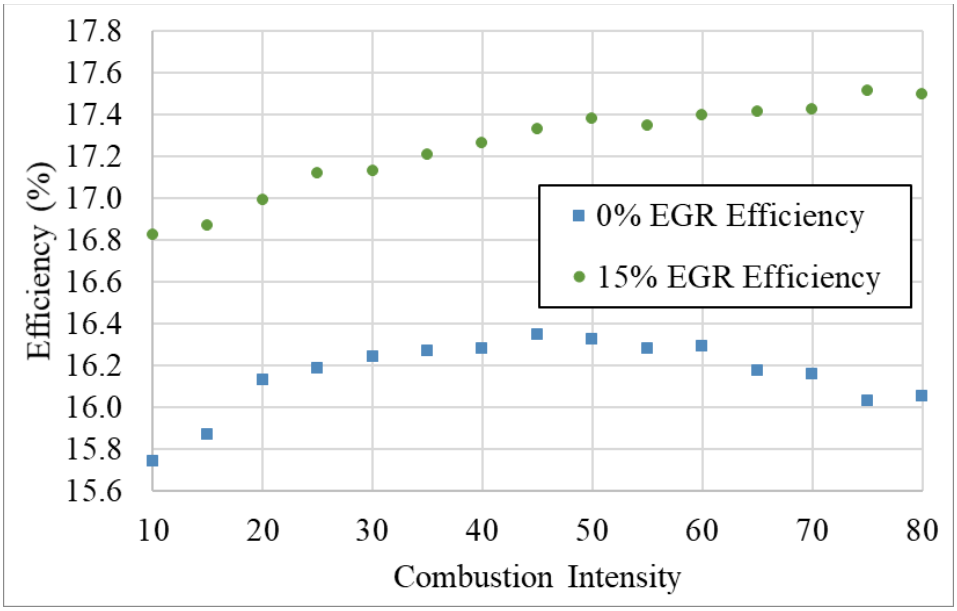

Figure 54: Efficiency Values from C-EGAI Sweep of CIM

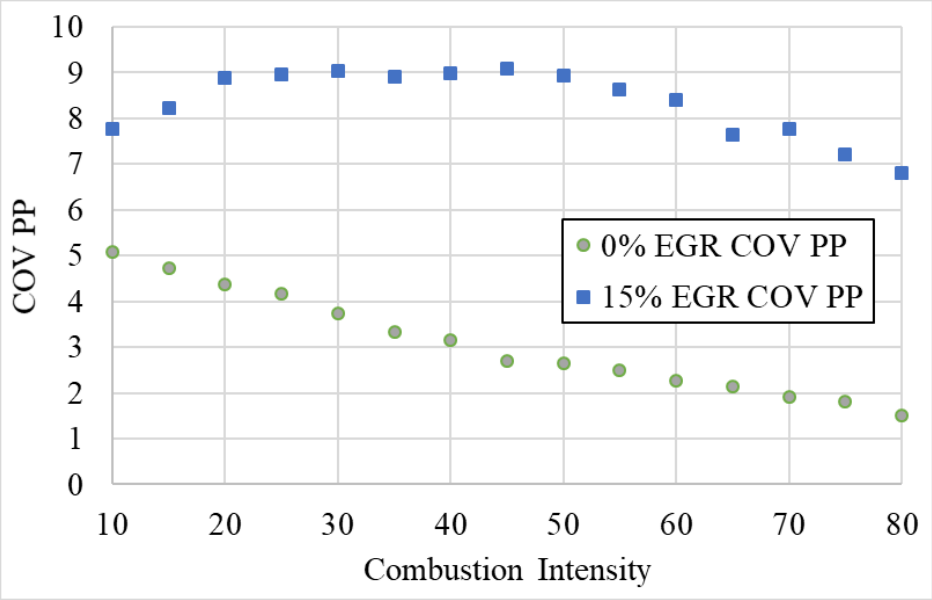

Figure 55: COV of Peak Pressure for Combustion Stability from C-EGAI Sweep of CIM

The final parameter largely effected by C-EGAI with CIM control was the combustion phasing. The location of CA10, CA50, and CA90 are key indicators in the performance of the EGR as well as combustion stability and auto-ignition prediction. Figure 56 shows a plot of CA10, CA50, and CA90 for the 0% EGR initial data set from Chapter 3, while Figure 57 shows a plot of the same variables for the 15% EGR C-EGAI sweep data set. With the period between CA10 to CA50 as well as the period from CA50 to CA90 closing as CIM increases, the acceleration in heat release due to higher levels of auto-ignition becomes even further evident. Another factor these plots show is that traditionally the most efficient engines perform the bulk of combustion immediately after 0° TDC. For this, the CA50 value should be located as near to 0° TDC as possible, without CA10 advancing beyond 4° bTDC. This factor lines up with the data shown in Figure 54, where the 0% EGR data had a peak efficiency of around 46% CIM and 15% EGR around 74% CIM.

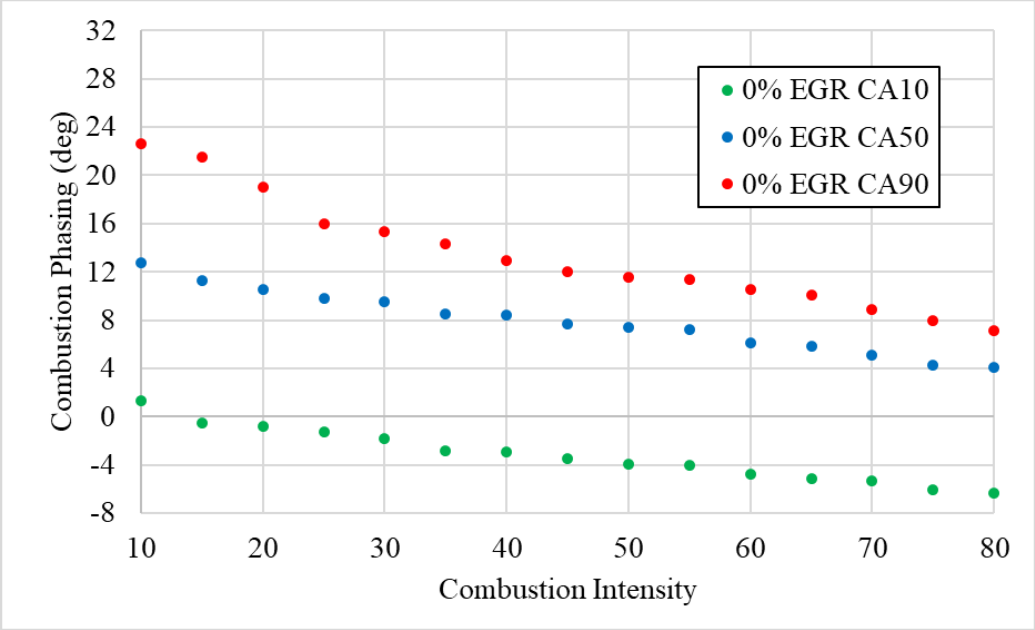

Figure 56: Combustion Phasing for 0% EGR from C-EGAI Sweep of CIM

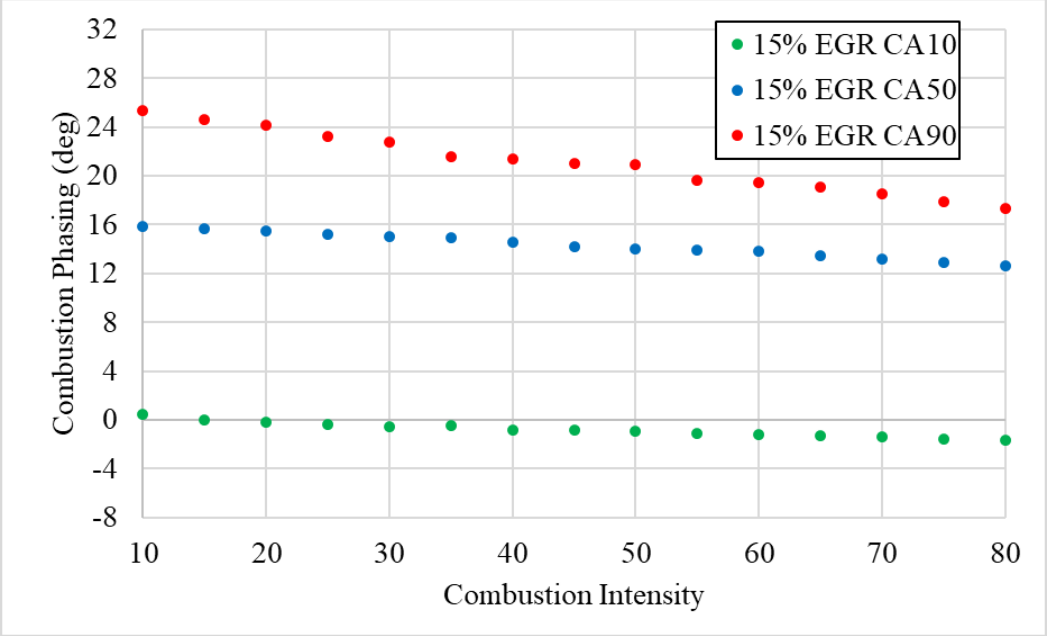

Figure 57: Combustion Phasing for 15% EGR from C-EGAI Sweep of CIM

5.3 EFFICIENCY OPTIMIZATION OF C-EGAI

To determine the effectiveness of C-EGAI on a stoichiometric, spark-ignited, natural gas engine, a system optimization was performed. Throughout this study, there have been five major variables that have been adjusted. A sweep of each of the five variables was performed while the other four were held to baseline values. A modified box-benken design variable optimization was run with efficiency as the merit function.

The five variables that were varied within this optimization were: Indicated Mean Effective Pressure (IMEP), Engine Speed, EGR Rate, Compression Ratio, and Combustion Intensity. Figure 58 demonstrates the sweeps of each of the five variables vs Efficiency. The other four variables were held at constant values equal to the baseline operating point of the efficiency optimization. These sweeps were necessary because the box benken design optimization technique requires an intuitive understanding of the direction the variables will want to move to be optimized, and these sweeps provide an understanding of how each will react during testing. It can be seen within this figure that engine speed and IMEP want to be maximized for the highest efficiency and reach their operational limits for the CFR engine. Furthermore, the compression ratio shows an optimal value around 10.5; optimal values for the other variables occur at an EGR rate of around 15%, a CIM around 42.5%, and a timing of 10.3° bTDC. The efficiency optimization will validate the location of these peak efficiency values and determine the optimal conditions for the CFR engine under stoichiometric, spark ignited, natural gas conditions with EGR and C-EGAI.

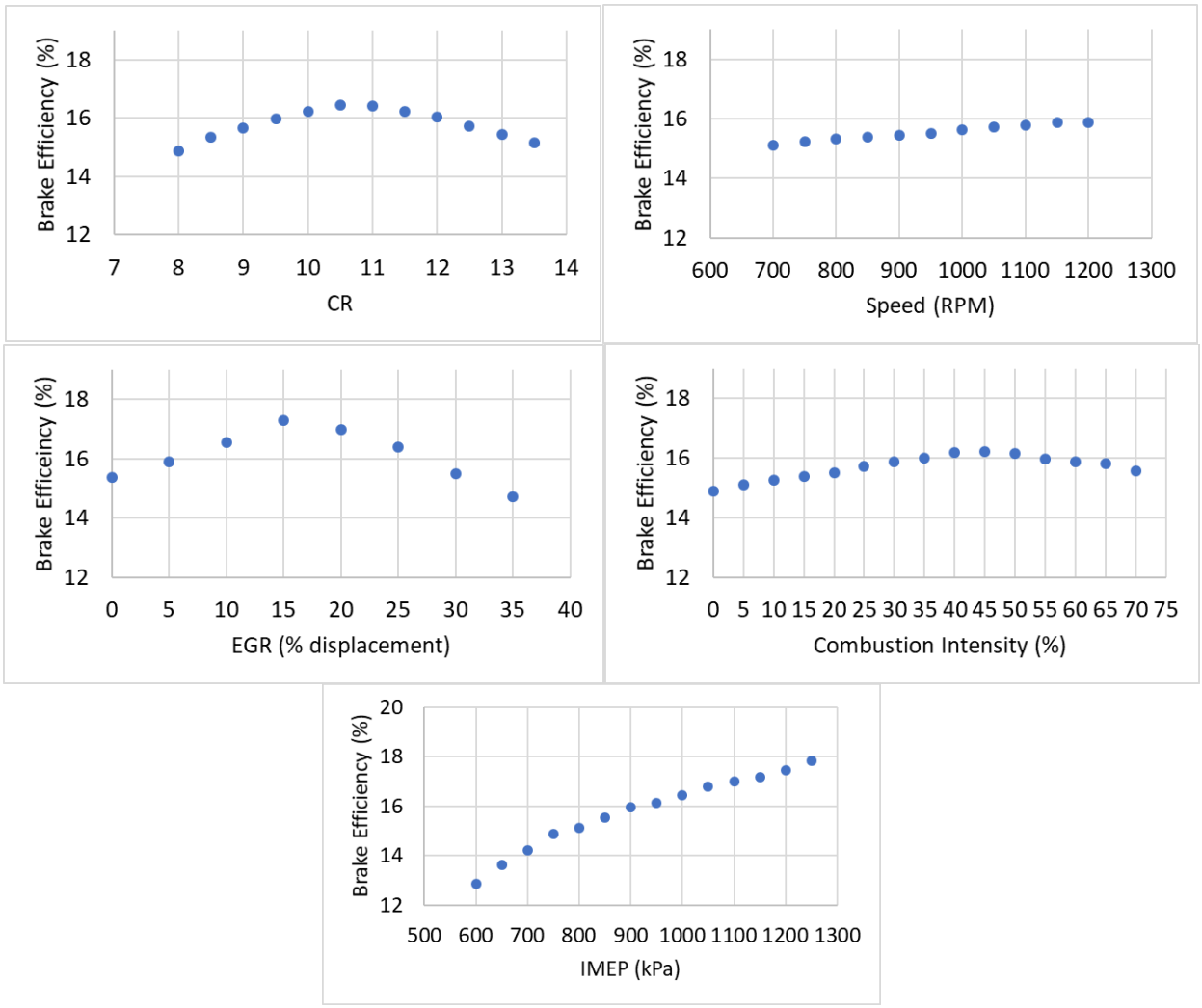

Figure 58: Optimization Variable vs Efficiency Sweeps for Five Main Variables

The efficiency optimization method selected was a type of Response Surface Method (RSM) that was determined suitable for this application. This method is deemed the Modified Box-Benken Design [36][37]. Figure 59 displays a graphic to help explain the RSM. To properly map the operational conditions of an engine, a multidimensional space of N dimensions, where N = number of variables to be optimized, is created and every data point within that space is evaluated to generate a complete surface map of performance. The modified Box-Benken design allows the operator to take a select origin point within the N-dimensional space and test every

point around the origin in predetermined step sizes and generate a vector equal to the merit function defined by the RSM. This RSM warrants the use of a merit function to calculate the vector of optimal performance and can be equal to as many dependent variables as the operator demands of the system, with specified weights of each dependent variable to affect the desired direction of the final vector. The vector is then followed until the merit function reaches a maximum value, and the process of generating the vector around the new maximum is repeated until the new vector travels only within the known noise of the system. In this case there are five variables, so thus a 5-dimensional space, and the merit function is only equal to the brake efficiency of the CFR engine.

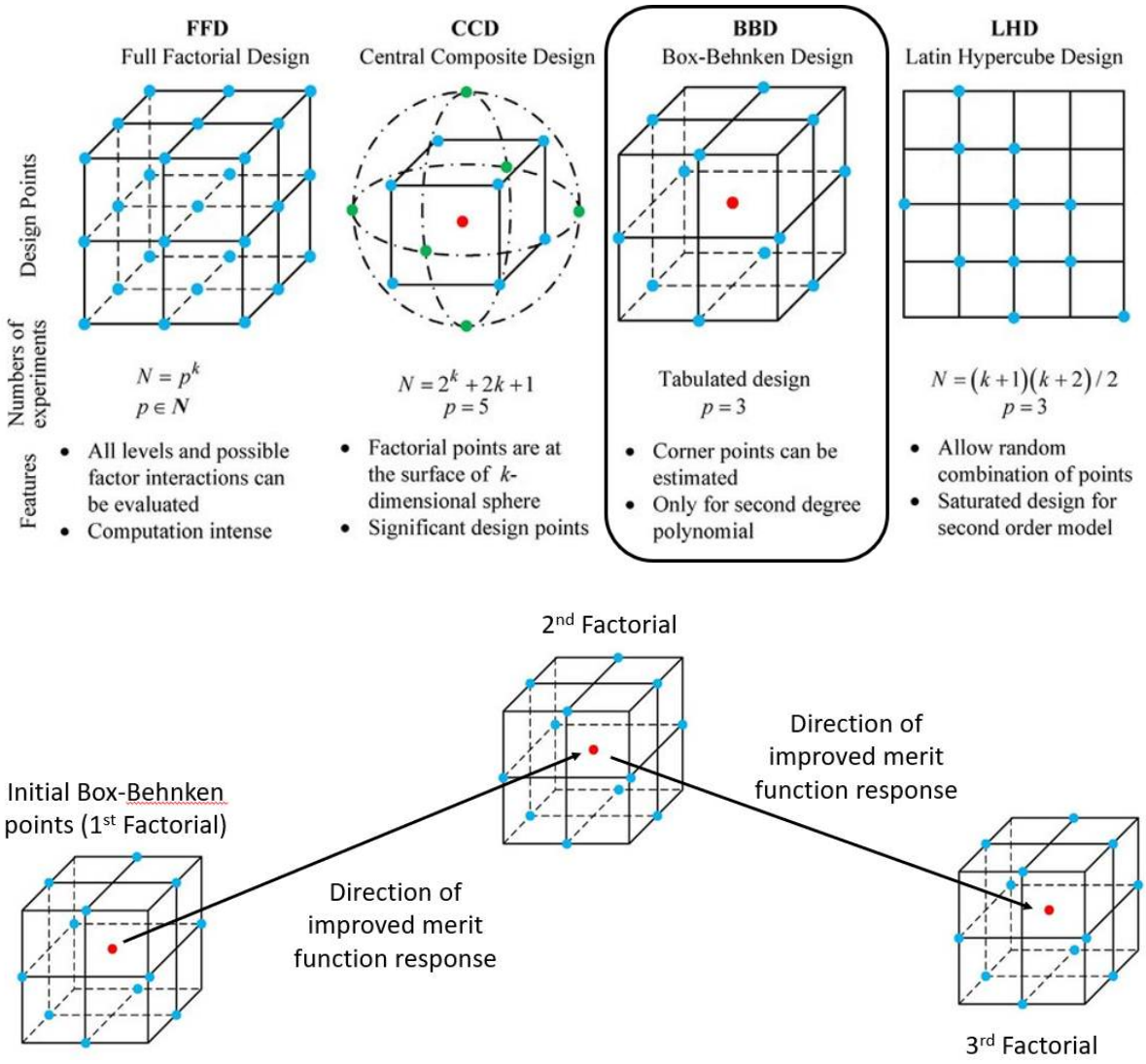

Figure 59: Demonstrational Graphic for Modified Box-Benken Design Response Surface Method [36]

The modified Box-Benken RSM simplified the optimization of the CFR engine. With the only desired dependent variable within the merit function of the RSM being brake efficiency, the system can move rapidly and require fewer iterations to find the optimal conditions. The baseline conditions from methane number testing on the CFR engine as well as the optimal conditions from the data in Chapter 4 were used to determine the initial origin for the RSM. Table 5 establishes the initial values for the five independent variables, their predetermined step sizes to

be used throughout the process, the operational limits of the CFR engine, and the sensitivity factor (smaller value equals larger steps of the efficiency optimization vector). These values were used for the initialization of the RSM analysis on the CFR engine. The result should determine the optimal level of C-EGAI operation with EGR beyond the original knock limited maximum efficiency. Equations 9, 10, and 11 demonstrate how the merit function is calculated from the vectors of the individual independent variables.

$$v_i = \frac{[F(xn) - q_{avg}]}{Z_{\pm 1}} \quad \text{Equation (9)}$$

$$v_f = AVG_{all} * AVG_i \quad \text{Equation (10)}$$

$$v_{n+1} = \frac{[v_{n-1} + v_f * x_i]}{a} \quad \text{Equation (11)}$$

Where:

v_i = Vector of one independent variable

F(xn) = Merit function (brake efficiency)

q_avg = Center point of RSM

Z_±1 = Step direction of idependent varibale

v_f = Final vector

AVG_all = Average of all vectors

AVG_i = Average of independent variable vectors

V_n+1 = Step size of next value I efficiency vector

v_n-1 = Previous efficiency vector value

x_i = Independent variable step size

a = Sensitivity factor

Table 5: Origin Parameters, Step Sizes, and Limits of Optimization for Independent Variables

Parameters at Center Point:		
Speed (RPM)	900	RPM
EGR	10	%
CR	10	
IMEP	1000	kPa
Comb. Int.	30	%
Increment Definition, Equivalent to +1 in Analysis:		
Speed	50	RPM
EGR	3	%
CR	0.5	
IMEP	50	kPa
Comb Int	5	%
Sensitivity Factor		
0.5		
Engine Operating Limits		
Knock	3000	kPa*rms^2
Exhaust Temps	700	°C
Engine Speed	1200	RPM
IMEP	1250	kPa
CR	18	
EGR Rate	40%	%

The full test procedure for the RSM efficiency optimization required four vectors to determine the point of peak performance. Figure 60 shows cylinder pressure trace plots from the first calculated vector. This plot is a good demonstration of the increase in compression ratio, IMEP, and CIM as the efficiency vector is followed. The remaining three efficiency vectors resulted in similar plots, slowly advancing the CFR engine towards peak performance.

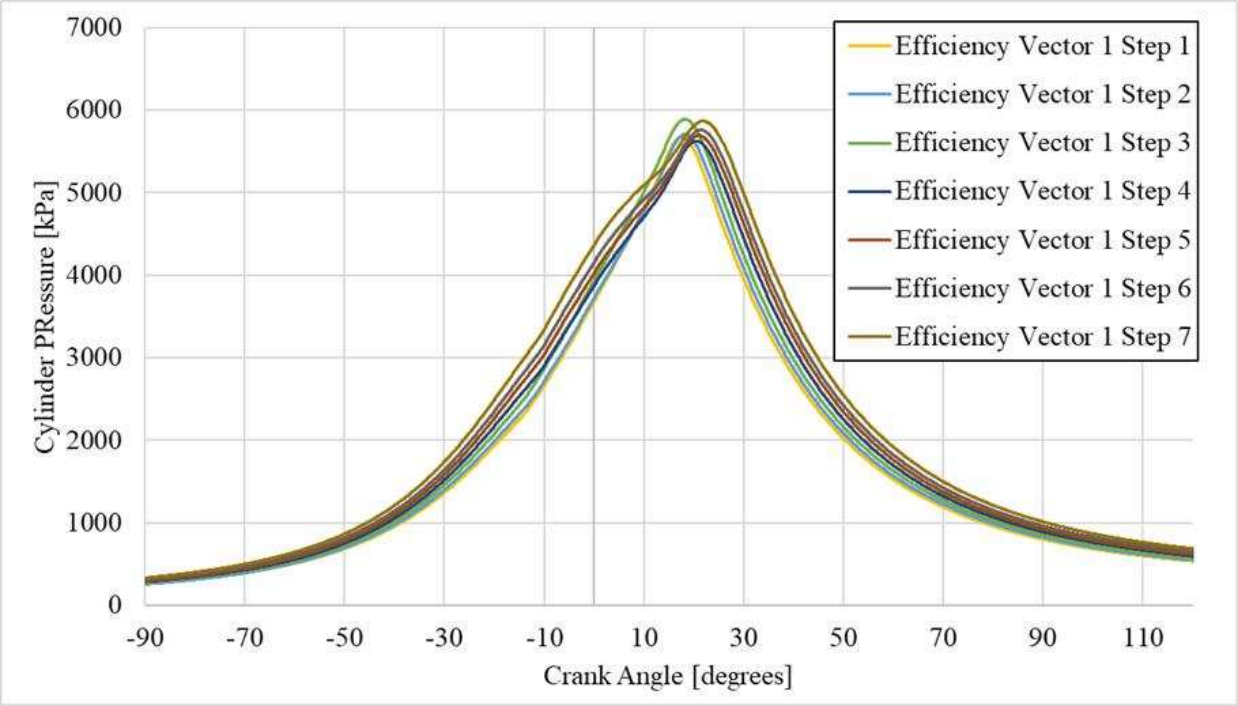

Figure 60: Cylinder Pressure Traces from CFR Engine for Vector 1 of Efficiency Optimization

Table 6 outlines the parameters at the origin of CFR performance, and the parameters of the five independent variables that were found after the completion of the fourth efficiency vector, and peak performance was achieved. The selected initial data point is an arbitrary point seeing how this method follows the direction of steepest ascent to benefit the merit function. Int his case picking a different initial data point should not change the final result. The stopping condition for the RSM is when the change measured by the corner change step sizes of the independent variables operate within the known noise of the system. Mathematically, this is represented by when the standard deviation of the origin repetitions exceeds the standard deviation of the corner step size data points. The rest of the data collection and vector generation calculations can be found in Appendix D.

Table 6: Initial and Final Parameters for Independent Variables of Efficiency Optimization

	Starting Data Point	Final Data Point
IMEP (kPa)	900	1150
Speed (RPM)	900	1080
EGR (% displacement)	12	17.8
CR	10	10.55
Comb. Int. (%)	30	39.5

To better demonstrate the effect each efficiency optimization vector had on the CFR engine, the cylinder pressure traces are plotted in Figure 61. This plot contains the initial pressure trace as well as the traces from the final operational point of each optimization vector. Then Table 7 yields the real values and step parameters from all four phases of the efficiency optimization vectors. This table in conjunction with Figure 58 show that the optimization began to near the point of peak performance by the end of the second vector and overshot the point of peak performance in the third vector with engine speed and IMEP. Except for IMEP, which was held 100 kPa just below the system maximum value, no variables reached the maximum system imits of the CFR engine.

Table 7: Definitions of Efficiency Optimization Variables by Phase

phase 1					
	Speed	EGR	CR	IMEP	Comb. Int.
center	900	12	10	1000	30
+1	950	15	10.5	1050	35
-1	850	9	9.5	950	25
phase 2					
	Speed	EGR	CR	IMEP	Comb. Int.
center	1150	15.4	10.3	1100	35.5
+1	1200	18.4	10.8	1150	40.5
-1	1100	12.4	9.8	1050	30.5
phase 3					
	Speed	EGR	CR	IMEP	Comb. Int.
center	1100	16.8	10.6	1150	37.5
+1	1150	19.8	11.1	1150	42.5
-1	1050	13.8	10.1	1150	32.5
phase 4					
	Speed	EGR	CR	IMEP	Comb. Int.
center	1080	17.5	10.55	1150	39.5
+1	1130	20.5	11.05	1150	44.5
-1	1030	14.5	10.05	1150	34.5

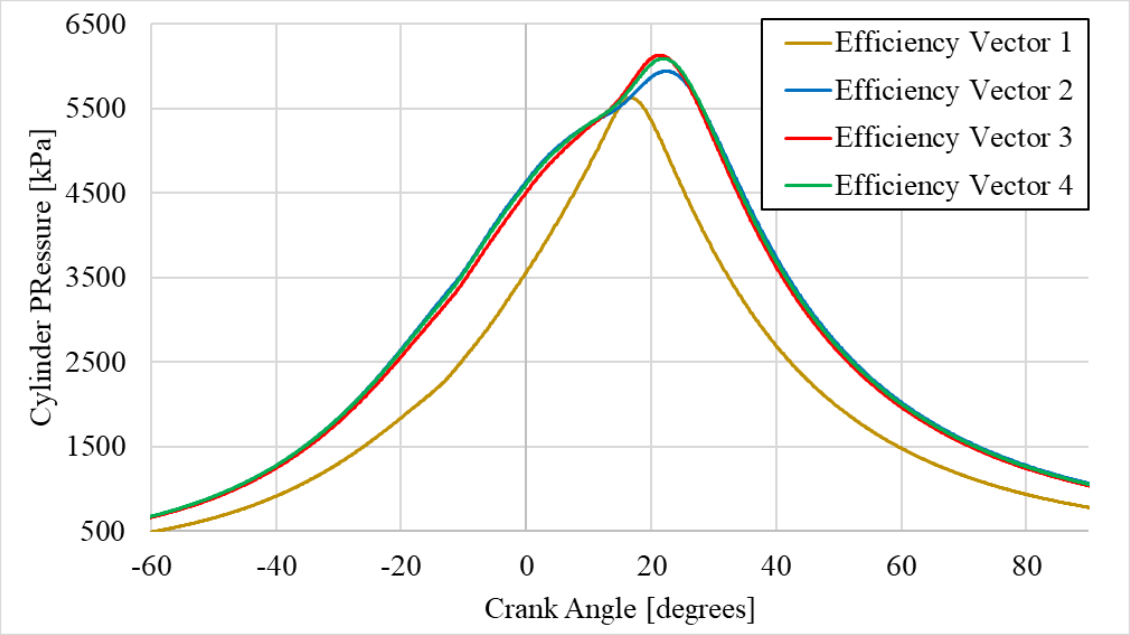

Figure 61: Cylinder Pressure Traces from Phases 1 through 4 of Efficiency Optimization

To demonstrate the effect the efficiency optimization had on the CFR engine Figure 62 plots every step of the efficiency optimization. This plot shows that the system began with a brake efficiency value of 17.7% and reached peak performance at a value of 21.3%. These values are low in comparison to larger engines, although these values are record highest efficiency values established by the CFR engine under stoichiometric, spark ignited, natural gas conditions.

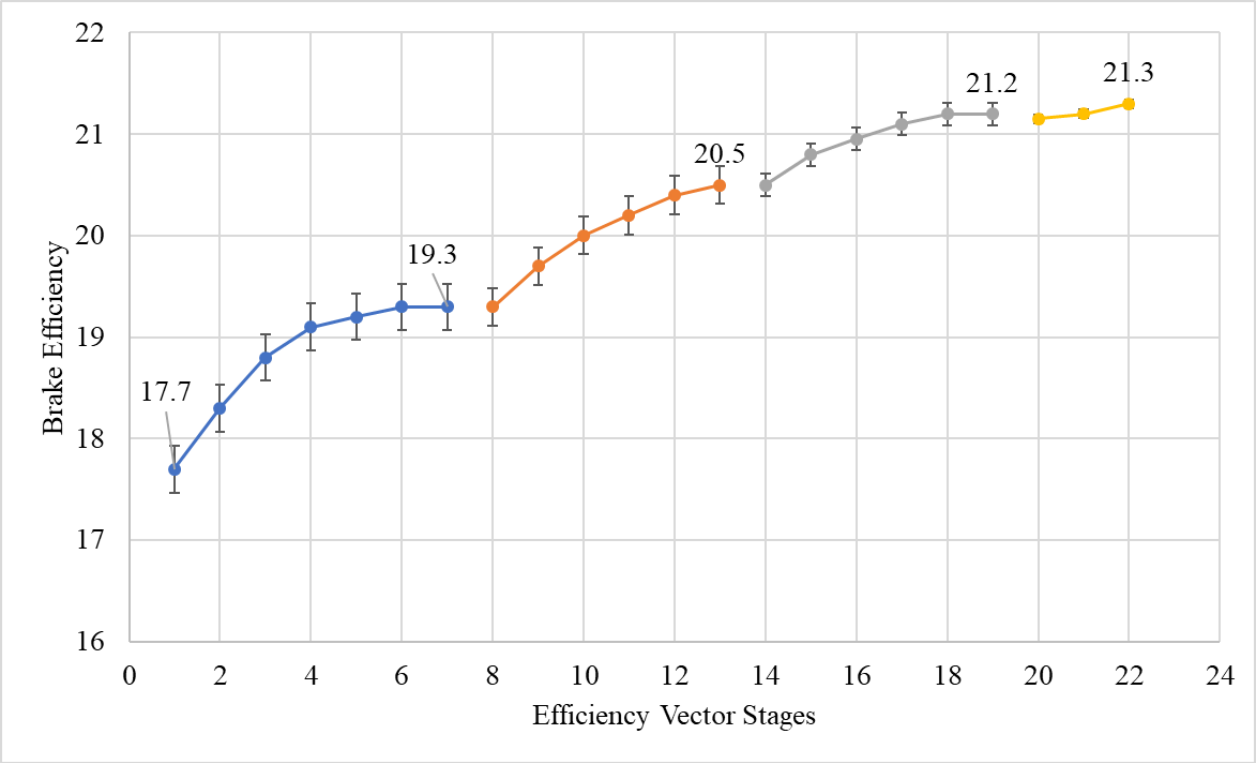

Figure 62: Efficiency Values from Every Step of Efficiency Optimization

To quantify the f-EGAI in the engine from the efficiency optimization, as well as the relationship between the CIM metric and the C-EGAI factor, Figure 63 presents the percent heat release due to auto-ignition vs the efficiency steps taken over the optimization's vectors. The peak performance level of C-EGAI established for the CFR engine was 33.9% heat release due to auto igniting. This value is specific to the CFR engine and may vary with the application.

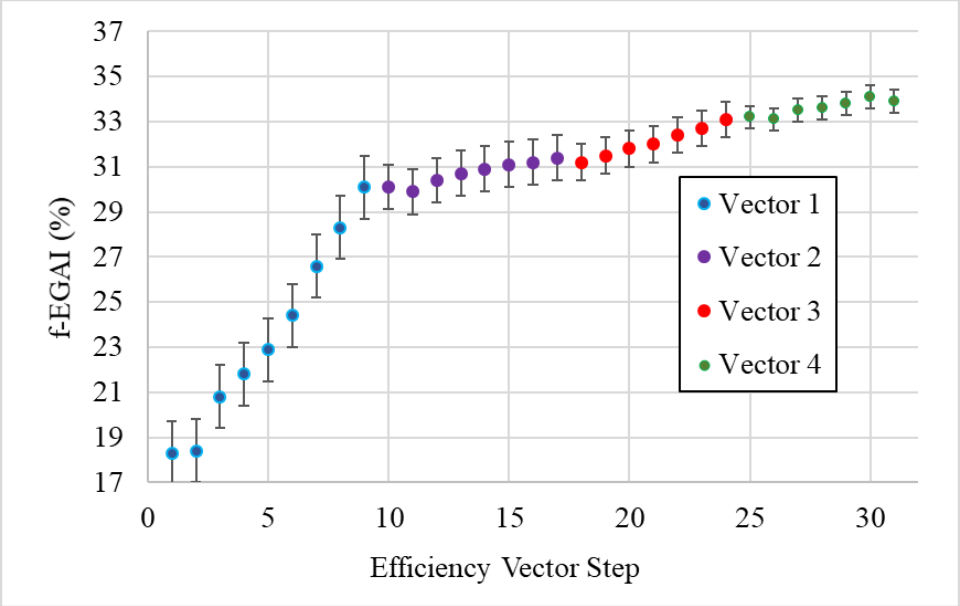

Figure 63: f-EGAI values from Every Step of Efficiency Optimization

CHAPTER 6: CONCLUSIONS AND FUTURE WORK

6.1 CONCLUSIONS

The purpose of this work was to evaluate the effect of exhaust gas recirculation and controlled end gas auto-ignition on a stoichiometric, spark ignited, natural gas engine. This evaluation was completed by implementing the desired technologies on a Cooperative Fuel Research engine and analyzing the effect on engine performance and brake efficiency. The effectiveness of EGR and C-EGAI on performance improvements was quantified by comparing the collected data from this study to previously acquired CFR engine data as well as commercially available natural gas engines. The noteworthy impacts of EGR and C-EGAI on the test engine were as follows:

1) The combustion intensity metric displays a linear correlation with fractional end gas auto-ignition. This correlation can be used to implement controlled end gas auto-ignition.
2) The maximum usable exhaust gas recirculation rate on the CFR engine is 23%, while the optimal rate is around 17% based on misfire percentage at stoichiometric conditions.
3) With the implementation of EGR on the CFR engine as a stoichiometric, natural gas, spark ignited engine, the maximum brake efficiency increased from 15.6% to 20.1%, due to the increase in knock limitation, with a 28% relative increase. This increase was likely due to the elevation of boost pressure to maintain the same mass air flow with the addition of increasing EGR rates.
4) Total emission concentrations of CO, THC, and NOx lowered at optimal EGR rates between 16% and 20%. On average: CO increased from 197 to 542 ppmd @ 15% O2,

THC increase from 423 to 569 ppmd @ 15% O2, and NOx lowered from 1212 to 413 ppmd @ 15% O2.

5) The implementation of C-EGAI on the CFR engine resulted in an additional efficiency gain from the 20.1% of EGR implementation to 21.3% maximum brake efficiency.
6) The optimization of CFR engine variables lead to the realization of peak efficiency on the CFR engine. The Modified Box-Benken RSM took the IMEP, speed, EGR rate, CIM, and compression ratio to their optimal values for CFR operation with EGR and C-EGAI.

6.2 FUTURE WORK

Future work in this research area should focus on the optimization of C-EGAI parameters specific to alternative and more practical engine formats. These include larger bore natural gas engines, as well as engines that experience more transient conditions such as on-road trucking engines. Ongoing work at CSU involves testing the C-EGAI control scheme on a single cylinder Cummins X15 natural gas trucking engine. It is predicted that the implementation of C-EGAI on such an engine should provide a large enough system efficiency gain to match that of an equivalently size diesel compression ignition engine. The control through the CIM with ignition variability will make the implementation of C-EGAI possible across the many different platforms due to the involvement of the five input variables for CIM. This could normalize CIM across multiple engines so that the CFR engine data can be utilized as a template for testing on additional platforms.

The ability to modify the input fuel blend on the CFR engine was available during this work, but time restrictions limited the amount of testing that could be performed. Additional future work should involve testing the full spectrum of industrially acceptable methane numbers for natural gas blends on the CFR engine. The results for maximum efficiency and optimal f-EGAI value may be adjusted with the input of varying natural gas blends. This is due to the low methane number of the natural gas blend tested within this study, so a higher methane number with less auto ignition tendencies should be able to operate at higher conditions without reaching the knock limitations found in this study.

The primary barrier that remains is the development of a live f-EGAI controller, rather than using a correlation between CIM and f-EGAI. The ability to calculate f-EGAI for every cycle without asymptotically being knock limited, would provide ease of implementation of future applications. Current methods of live knock quantification do not generate correlations to f-EGAI as easily as parametric ignition timing methods such as CIM. However, there may be additional technological advancements that would implement more practical high-speed pressure analysis.

REFERENCES

[1] Hockett, Andrew. Hampson, Greg. Marchese, Anthony. "Sensitivity Study on Natural Gas/Diesel RCCI CFD Simulations Using Multi-Component Fuel Surrogates." Int. J. Powertrains. 2016.

[2] Brecq, G., Bellettre, J. & Tazerout, M., 2003. A New Indicator for Knock Detection in Gas SI Engines. International Journal of Thermal Sciences (42), pp. 523-532.

[3] Hoepke, Bjoern, et al. "EGR Effects on Boosted SI Engine Operation and Knock Integral Correlation." SAE International Journal of Engines, vol. 5, no. 2, 2012, pp. 547–559. JSTOR.

[4] Millo, F. & Ferraro, C., 1998. Knock in SI Engines, A Comparison Between Different Technicques for Detection and Control. SAE Paper Number 982477 ed. Milan: SAE.

[5] Barton, R. K., Lestz, S. S. & Duke, L. C., 1970. Knock Intensity as a Function of Engine Rate of Pressure Change, New York: Society of Automotive Engineers.

[6] Amann, Manfred, et al. "The Effect of EGR on Low-Speed Pre-Ignition in Boosted SI Engines." SAE International Journal of Engines, vol. 4, no. 1, 2011, pp. 235–245. JSTOR.

[7] Fischer, M. Günther, M. Berger, C. Troeger, R. Pasternak, M. Mauss, F. "Suppressing Knocking by Using Clean EGR – Better Fuel Economy and Lower Raw Emissions Simultaneously." Knocking in Gasoline Engines. KNOCKING 2017. Springer, Cham. Pp. 363-384.

[8] Szybist, James P., et al. “The Reduced Effectiveness of EGR to Mitigate Knock at High Loads in Boosted SI Engines.” SAE International Journal of Engines, vol. 10, no. 5, 2017, pp. 2305–2318. JSTOR.

[9] Bayliff, Scott. Marchese, Anthony. Windom, Bret. Olsen, Daniel. “The effect of EGR on Knock Suppression, Efficiency, and Emissions in a Stoichiometric, Spark Ignited, Natural Gas Engine.” *Western States Combustion Institute Fall Meeting.* 2019.

[10] Grondin, Oskar. Moulin, Peter. Chauvin, James, "Control of a turbocharged Diesel engine fitted with high pressure and low-pressure exhaust gas recirculation systems." Proceedings of the 48h IEEE Conference on Decision and Control (CDC) held jointly with 2009 28th Chinese Control Conference, Shanghai, 2009, pp. 6582-6589.

[11] Tutak, Wojciech. “Numerical Analysis of the Impact of EGR on the Knock Limit in SI Test Engine.” *Institute of Internal Combustion Engines.* Vol. 21. 2011. Pp 397-406.

[12] Cengel, Y. A. & Boles, M. A., 2011. Thermodynamics: An Engineering Approach. 7th ed. New York (New York): McGraw-Hill.

[13] Pulkrabek, W. W., 2004. Engineering Fundamentals of the Internal Combustion Engine. 2nd ed. Upper Saddle River (New Jersey): Pearson Prentice Hall.

[14] Li, Hailong. Haugen, Geir. Ditaranto, Mario. Berstad, David. And Jordal, Kristin. “Impacts of Exhaust Gas Recirculation (EGR) on the Natural Gas Combined Cycle Integrated with chemical Absorption CO2 Capture Technology.” *Energy Procedia.* Vol. 4, 2011, pp. 1411 – 1418. 24

[15] Kumano, Kengo. Yamaoka, Shiro. “Analysis of Knocking Suppression Effect of Cooled EGR in Turbo-Charged Gasoline Engine." SAE Technical Paper 2014-01-1217, 2014,

[16] Grandin, Borje. Angstrom, Hans-Erik. “Knock Suppression in a Turbocharged SI Engine by Using Cooled EGR.” *International Fall Fuels and Lubricants.* SI Engines: Combustion and Emission Formation. (SP-1393), 1998.

[17] Cha, Jinyoung. Kwon, Junhong. Cho, Youngjin. Park, Simsoo. “The Effect of Exhaust Gas Recirculation (EGR) on Combustion Stability, Engine Performance and Exhaust Emissions in a Gasoline Engine.” *KSME International Journal.* Vol. 15, 2001. issue 10, pp. 1442-1450.

[18] Soylu, S. & Van Gerpen, J., 2003. Development of an Autoignition Submodel for Natural Gas Engines. Fuel 82, pp. 1699-1707.

[19] Watanabe, Eiichi, and Itaru Fukutani. “Knock Reduction of Spark-Ignition Engines by EGR.” *SAE Transactions*, vol. 95, 1986, pp. 240–246. *JSTOR*,

[20] Shen, Xianqing. Shen, Kai. Zhang, Zhendong. “Experimental Study on the Effect of High-Pressure and Low-Pressure Exhaust Gas Recirculation on Gasoline Engine and Turbocharger.” *Sage Journals.* Vol. 10, 2018.

[21] Schmillen, Karl. Rechs, Manfred. “Different Methods of Knock Detection and Knock control.” *SAE International.* vol. 225. 1991. Pp. 242-246.

[22] Waukesha Engine Division, Dresser Industries, 2003. Waukesha CFR F-1 & F-2 Research Method (F-1) Motor Method (F-2) Octane Rating Units Operation and Maintenance. Second ed. Waukesha(Wisconsin): Dresser Waukesha.

[23] Wise, Daniel. Olsen, Daniel. Caille, Gary. “Investigation into Producer Gas Utilization in High Performance Natural Gas Engines.” *Colorado State University, Mechanical Engineering; Dissertation.* 2013.

[24] Waukesha Engine Division, Dresser Industries, 1980. The Waukesha CFR Fuel Research Engine. Waukesha(Wisconsin): Waukesha.

[25] American Gas Association. “AGA 3.1: Orifice Metering of Natural Gas and Other Related Hydrocarbon Fluids.”

[26] Burgdorf, Klaas. Denbratt, Ingemar. “Comparison of Cylinder Pressure Based Knock Detection Methods.” *SAE: Combustion and Emission Formation in SI Engines.* 1997.

[27] Schmillen, Karl. Rechs, Manfred. “Different Methods of Knock Detection and Knock Control.” *SAE: Sensors and Actuators.* 1991.

[28] Barton, R. Lestz, S. Duke, L. “Knock Intensity as a Function of Engine Rate of Pressure Change.” *Society of Automotive Engineers.* 1970

[29] Xu, Hui. “CMI Knock Index Determination Method.” *Cummins Inc.* 2018.

[30] Brunt, M. Pond, C. Biundo, J. “Gasoline Engine Knock Analysis Using Cylinder Pressure Data.” *SAE International.* 980896. 1998 pp. 118.

[31] Elmqvist, C. et al., 2003. Optimizing Engine Concerpts by Using a Simple Model for Knock Prediction, s.l.: SAE International.

[32] Nair, Suraj. Hampson, Gregory. Carlson, Jeffrey. “Controlled Multi-staged Combustion Strategy for Overcoming Load Limitations of Fuel Flexible Gas / Diesel Egines.” *New Engine Developments – Gas & Dual Fuel.* CIMAC Congress. 2019.

[33] Chiera, Domenico. Carlson, Jeff. Nair, Suraj. McCreery, Sam. Hampson, Gregory. “High Efficiency Natural Gas Engine Combustion Using Controlled Auto-Ignition.” *ASMA Internal Combustion Technical Conference.* 2019.

[34] Amador Diaz, German. Gomez Montoya, Juan. Corredor Martinez, Lesme. Olsen, Daniel. Salazar Navarrow, Adalberto. “Influence of Engine Operating Conditions on

Combustion Parameters in a Spark Ignited Internal Combustion Engine Fueled with Fuel Blends of Methane and Hydrogen." *Elsevier Editorial System for Energy Conversion and Management.* Manuscript. 2016.

[35] Elgohary, Mohamed. Seddiek, Ibrahim. Salem, Ahmed. "Overview of Alternative Fuels with Emphasis on the Potential of Liquefied Natural Gas as Future Marine Fuel." *Institute of Mechanical Engineers.* Sage journals. 2014.

[36] Lian, Binbin. Sun, Tao. Song, Yimin. "Parameter Sensitivity Analysis of a 5-Dof Parallel Manipulator." *Tianjin University: China.* Robotics and Computer-Integrated Manufacturing. 46. 2017.

[37] NIST, SEMATECH. "Engineering Handbook of Statistical Methods." *US Department of Commerce.* 2013.

APPENDIX A: TEST PROCEDURES

The following are operating procedures developed for this project in an effort to ensure safe, reliable, and repeatable test cell and engine operation. They are provided here to allow the reader to review the processes followed in conducting this work and collecting the data reflected.

CFR START-UP CHECKLIST

Engine prep to be performed after VI is started and ready to control the engine:

< > Turn on CFR main power

< > Verify engine oil is at a minimum is 100°F

< > Verify that the fuel manifold vent valve is shut

< > Verify exhaust backpressure valve fully open

< > Open valve to GC sample line {if operating}

< > Power up 5-Gas Analyzer pump and heater {if operating}

< > Open combustion air valves

< > Verify compression ratio setting {typical start-up rc ≈ 10:1, Dial Indicator = 0.235”}

< > Position cooling water valves for engine operation. Drain valve is opened first, then inlet

< > Verify cooling water flow through the cylinder pressure transducer

< > Verify cooling water level in sight glass

< > Verify engine lube oil at ½ sight glass

Starting the engine with VI controls:

At "Operational Parameters" tab:

< > Verify "Inlet Air Manual [%]" is set to 20

< > Verify "Inlet Air Control" is off

< > Click Intake Air Vent to enable (icon should be green)

< > Start CFR engine from Main CFR control panel on engine skid then click "Air Enable" button

< > With engine running set "Air Set point" to the desired inlet air pressure in kPa absolute

< > Select "Inlet Air Control" button to enable closed loop pressure control of the inlet air

< > Shut intake air vent valve

< > Switch on charge amplifier (hit reset button until "operate" is indicated)

< > Switch oil heater off

< > Ensure crankcase condensate drain and exhaust condensate drain valves are shut

< > Set compression ratio to desired level

< > Take a motoring data set (50 cycles) to enable later determination of dynamic TDC at CR

< > Verify manifold isolation valves positioned as necessary for intended fuel blend

< > Verify low flow manifold valves positioned as necessary for low flow fuel line-up

< > Open gas regulators for desired fuel blend

< > Verify downstream fuel isolation valve is open

At "Fuel Blending Control" tab:

< > Set the "Desired Fuel make up[%]" to the desired levels

< > Set the "Desired AF ratio" – based on CR and anticipated knock onset point

< > Set "AFR Range" to 40

< > Set the "Maximum Duty Cycle" (usually to 55)

< > Push the "Fuel System Enable" button

< > Set the "Fuel Manual Control" to 25

< > Verify "AFR Sample to Avg." is greater than zero (default is 20)

< > Switch ignition system on

< > Verify Altronic software is enabled, set ignition time to desired point

< > Push the "PWM Enable" to start the injection

< > Select desired "AFR control" mode – "AFR Recorder"

< > After air fuel ratio stabilizes (approx. 15 sec.) push "Auto Fuel Control" to enable closed loop air fuel ratio control.

< > Switch air heater on at operating console; set VI intake air heater control to 45°C and Pulse Period to 6, enable intake air heater

CFR SHUT-DOWN CHECKLIST

Normal Shutdown:

< > {Operational Parameters: Air Setpoint} Set boost pressure to 101kPa

< > Open exhaust backpressure valve

< > Isolate fuel system at the downstream fuel isolation valve

< > Open the fuel manifold vent valve

< > Shut all fuel regulators

< > {Fuel Blending Control: Auto Fuel Control} Turn off “Auto Fuel Control”

< > After fuel pressure drops to zero gage turn off “PWM Enable” to stop fuel injection

< > Click the “Fuel System Enable” button to disable the fuel system

< > Bleed off any residual fuel line pressure through the low flow fuel system

< > Turn off power strip to 5 gas analyzer sample line

< > Shut GC sample line valve

< > Switch off air-fuel heater

< > Open drain valve from crankcase vent line

< > Open drain valve from exhaust piping in the overhead

< > Allow engine to cool for approximately 5 minutes {~90°C Engine Coolant Temperature}

< > Stop the Combustion Logger

< > Switch off the charge amplifier

< > {Operational Parameters: Inlet Air Control} Turn off “Inlet Air Control”

< > Shut down engine from main CFR Control Panel

< > {Operational Parameters: Air Enable} Turn off “Air Enable”

< > Open intake air vent in VI using Shut-Down Feature

< > Isolate supply to engine cooling water, inlet first

< > Isolate combustion air supply

< > Switch off engine ignition

< > Switch off charge amplifier

< > Stop Host VI, close

< > Stop EECL-CFRIO, close

< > Collapse CFRIO in menu, disconnect

< > Close out LabView Main Menu

< > Switch off 480VAC power to 24VDC power supply

< > Switch off 208VAC power to CFR engine

Emergency Shutdown:

< > Depress ESD on Main CFR Control Panel

< > Shut all compressed gas regulators

< > Open 208VAC disconnect

< > Switch off 480VAC power switch

< > Open fuel manifold vent

< > Open intake air vent

< > Shut Cooling Water Supply valve

< > Shut Cooling Water Drain Valve

< > Shut Compressed Air Supply Valves

CFR CLEARANCE VOLUME AND PISTON CLEARANCE

The compression ratio of the CFR engine is determined by measuring the vertical position of the cylinder relative to an indexed position of known compression ratio. For this test cell a dial indicator is positioned to read “Zero” at the point of compression ratio set to 18:1. The cylinder will travel vertically as compression ratio is decreased to a minimum value of 4:1. The dial indicator reading corresponds to compression ratio as described below:

Engine compression ratio, rc, is given by the relationship

$$r_c = \frac{V_D + V_c}{V_c}$$

where:

rc = Compression Ratio

VD = Displacement Volume

Vc = Clearance Volume

Rearranging terms and solving for clearance volume,

$$V_c = \frac{V_d}{1 - r_c}$$

The height of the cylinder head above the piston face at top dead center is given by:

$$DI = \frac{V_c}{\pi \left(\frac{b}{2}\right)^2}$$

Where:

DI = Dial Indicator Reading

b = cylinder bore

A calculations reference sheet is prepared in Microsoft Excel© to translate dial indicator readings to compression ratio, shown in Figure A-1.

CFR Compression Ratio (r_c) Worksheet:

V_{DISP}	37.331 in^3	=	611.74 cm^3
R	37.330 in	=	94.82 cm
Bore	3.250 in	=	8.26 cm
Stroke	4.500 in	=	11.43 cm

$V_{clearance} = V_{displacement}/(r_c-1)$ and Cylinder Height = $V_c/\pi\cdot(b/2)^2$

At r_c = 18:1

V_c(18:1)= 2.196 in^3

Cyl Ht = 0.265 in

Calculator (indexed to 0= 18:1)

Dial Indicator Reading: 0.225

Calculated Compression Ratio: 10.19 :1

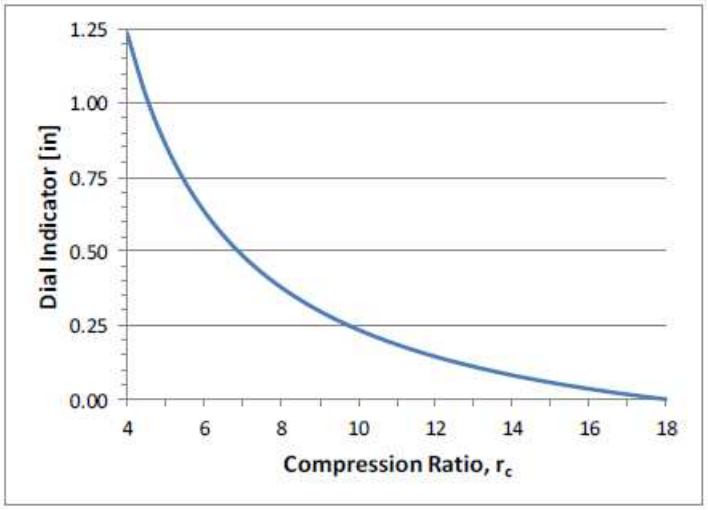

Compression Ratio	Dial Indicator Position [in]
4 :1	1.235
4.5 :1	1.021
5 :1	0.860
5.5 :1	0.735
6 :1	0.635
6.5 :1	0.553
7 :1	0.485
7.5 :1	0.428
8 :1	0.378
8.5 :1	0.335
9 :1	0.298
9.5 :1	0.265
10 :1	0.235
10.5 :1	0.209
11 :1	0.185
11.5 :1	0.164
12 :1	0.144
12.5 :1	0.127
13 :1	0.110
13.5 :1	0.095
14 :1	0.081
14.5 :1	0.069
15 :1	0.057
15.5 :1	0.046
16 :1	0.035
16.5 :1	0.026
17 :1	0.017
17.5 :1	0.008
18 :1	0.000

Figure A-1: Compression ratio worksheet

TEST PLAN CFR-1

Objectives:

Impact of EGR on CFR engine performance

- Determine EGR limit of CFR engine
- Determine critical compression ratios of CFR engine with various EGR rates
- Determine maximum boost pressure at critical compression ratio for CFR engine with EGR
- Evaluate maximum efficiency and optimal operation conditions for CFR engine with EGR and basic C-EGAI
- Analyze effect of various fuel blends on CFR engine with EGR and basic C-EGAI at optimal operational conditions

Operational Conditions:

- Fuel blend: building natural gas
- A/F ratio: stoichiometric as determined by O2 sensor
- Jacket water temperature: 95 degrees C
- Engine speed: 900 RPM or determined by 60 Hz
- Timing, compression ratio, intake boost pressure, EGR rate and as specified in procedure

Phase 1: Define critical compression ratio and the associated EGR limit

- With no EGR, the ignition timing will be varied to find the optimal spark timing at a compression ratio of 8

- Then the compression ratio will be increased until a definite level of knock occurrence is induced (Defined by a knock index value of 100)
- The optimal compression ratio will be established 1 CR unit below the critical CR.
- EGR rate will be increased by 5% per data point until the EGR limit is found (EGR limit defined by COV PP being greater than 10%)
    - Boost pressure will be increased with increasing EGR rate to hold CFR engine at 2 kW of electrical power
- Theoretical prime EGR rate will be defined at a COV PP ~ 6%, but is subject to further evaluation in post processing
-

Phase 2: Find new critical compression ratio of CFR engine with EGR.

- At each data point defined in phase 1, hold all variables constant except for compression ratio
- Increase compression ratio at each data point until knock limit is reached
- Prime compression ratio is one CR unit below critical CR
-

Phase 3: Increase IMEP and power density

- At each data point defined in phase 2, hold all variables constant except for boost pressure (and technically fuel to maintain stoichiometry)
- Utilize the original prime CR defined at the beginning of phase 1
- Increase boost pressure while maintaining stoichiometry until knock limit is reached
- Take note of the effect on power level and efficiency with increasing boost pressure and EGR rate

Phase 4: With the data from phase 2 and 3, sweep variables to maximize efficiency at defined optimal EGR rates

- Using data processed from phases 2 and 3, define a window of optimal CFR engine efficiency with EGR
- Within this window, repeat data points while sweeping alternative variables:
    - Boost pressure near knock limit
    - Compression ratio near knock limit
    - Retarding ignition timing until knock limit is reached
        - Intervals of 3 degrees from -9 to knock limit
    - EGR rate of 15% below EGR limit to the limit
- This data will be compiled to establish a set of optimal operational conditions for the CFR engine with EGR
- This phase will fulfill the goal of demonstrating the efficiency gain caused by EGR and basic C-EGAI

Phase 5: Within the window of maximum efficiency, repeat data points with various fuel blends

- The optimal operational conditions for the CFR engine with EGR and basic C-EGAI defined in phase 4 will be utilized in this phase
- The data points will be repeated for the designated fuel blends
    - Wet gas: MN ~ 68
    - Dry gas: MN ~ 97
    - 100% Methane: MN ~ 100
    - Average pipeline natural gas from around the US: MN ~ 68, 72, 77, 82, 86, 88

- The data gathered in phase 5 will be useful for the definition of the effect of EGR and C-EGAI on a stoichiometric natural gas engine.

Procedure (Part 1)

1-I. Prepare the engine for operation in accordance with the general CFR operating procedure:

A. Start the engine with presets as follows:

1. Compression Ratio: 6:1
2. Intake Boost Pressure 1.0 bar
3. Ignition Timing 13˚ bTDC

B. Operate until steady operating conditions are achieved

VI Start-Up Checklist

1. **Opening CFR Real Time VI**
   - **a.** Open CFR LabVIEW Project
     - **i.** Start > National Instruments LabVIEW > CFR Project
   - **b.** Connect EECL-CFRIO (129.82.106.164)
     - **i.** Right click > Connect
   - **c.** Open and run CFR RT2.vi
     - **i.** Will be located in the drop-down selection of the EECL-CFRIO
     - **ii.** Right click > Open > Load with Selected > White run arrow
   - **d.** Minimize CFR RT.vi window

2. **Opening CFR mixing and control VI**
    a. CFR main UC R4. Vi
        i. Right click CFR Main R4 > Run
3. **Combustion Logger v. 4_0**
    a. Open Combustion Logger v.4_0
        i. Start > National Instruments Lab View > Combustion Logger v.4_0
        ii. Click white run arrow (not the green one yet)
        iii. Under Engine Configuration, click "load"
            1. Load CFR Engine
        iv. Change pegging pressure, ignition timing, and compression ratio to match testing conditions
        v. Change encoder offset to 638.2
        vi. Click green run button

CFR Start-Up Checklist

Engine prep to be performed after VI is started and ready to control the engine:

- Make sure to perform VI start up list first
- Turn "Oil Heater" indicator to "high" until engine oil is at a minimum of 110°F
- Verify gas bottle heaters are plugged in, if using CO2
- Verify that the fuel manifold vent valve is shut
- Verify exhaust backpressure valve fully open
- Open Valve to GC sample line (only if operating GC)
- Power up 5-gas analyzer pump and heater (only if operating 5-gas)
- Open Combustion air valves

- Verify compression ratio setting (typical start-up CR = 8:1, Dial Indicator = 0.378")
- Position cooling water valves for engine operation. Drain valve is opened first, then inlet
- Verify cooling water flow through the cylinder pressure transducer
- Verify cooling water level in sight glass
- Verify engine lube oil at ½ sight glass
- Flip switch to connect 480 VAC (panel east of engine) and 208 V (brick wall north of engine)

Starting the engine with VI controls:

At "Operational Parameters" tab:

- Verify "Auto A/F Control" is off
- Verify "Inlet Air Manual [%] is set to 25
- Verify "Inlet Air Control" is off
- Click "Intake Air Vent" to enable (icon should be green)
- Start CFR Engine from Main CFR control panel on engine skid, allow engine to come up to operating rpm, then click "Air Enable" button
- With engine running set "Air Set Point" to the desired inlet air pressure in kPa absolute
- Select "Inlet Air Control" button to enable closed loop pressure control of the inlet air
- Verify manual intake air vent valve is shut
- Switch on charge amplifier (hit reset button until "operate" is indicated.) (Check for pressure curve.) Check max pressure reading to be around TDC. Hit reset butting until it is)
- Switch oil heater off

- Ensure crankcase condensate drain and exhaust condensate drain valve are shut
- Set compression ratio to desired level
- Verify manifold isolation valves positioned as necessary for intended fuel blend
- Verify low flow manifold valves positioned as necessary for low flow fuel line-up
- Open gas regulators for desired fuel blend
- Verify downstream fuel isolation valve is open

At “Fuel Blending Control”

- Set the “Desired Fuel Make up [%]” to the desired levels
- Set the “Desired AF Ratio” – based on CR and Anticipated knock onset point
- Set “AFR Range” to 30

- Verify “air PID Gains” set to correct value
    - Fuel: P = -1.400 I = 0.160 D = 0.250
    - A/F: P = 0.250 I = 0.350 D = 0.500
    - Heater: P = 1.000 I = 0.010 D = 0.000
    - Air: P = 0.080 I = 0.040 D = 0.000

(The PID values can change. A Change will cause instability in firing)

- Set the “Maximum Duty Cycle” (usually around 55, if AFR *stoich* of fuel is low (=5) this will be much higher (90-100))
- Push the “Fuel System Enable” button
- Ensure “Auto Fuel Control is OFF

- Set the “Fuel Manual Control” to 25
- Verify “AFR Sample to Avg.” is greater than zero (default is 30)
- Push the “PWM Enable” to start the injection
- See “CPU 95 – Ignition System” below for ignition start up
- Select desired “AFR control” mode – “AFR Recorder” (If measuring off exhaust constituents)
- After air fuel ratio stabilizes, push “Auto Fuel Control” to enable closed loop air fuel ratio control
- Switch air heater on at operating console; set VI intake air heater control to 45°C and Pulse period to 6, enable intake air heater in VI.
- Wait for engine coolant temp to reach 90°C AND exhaust temp to reach 210°C
- *After exhaust reaches 200°C, Turn on NOx sensor #1*

CPU 95 – Ignition System:

- After the engine is motoring, flip ignition switch on CFR front panel to “ON”
- Select “SETUP” on the CPU 95 Control Module. Use “UP and DOWN arrows” to change value/setting.

Select “Next” to move through menu

  - Multi Strike – OFF
  - Output Energy – E3
  - Adjust Over speed – 1050 RPM
  - Reset Pin – 38.8°bTDC
  - Value Protection – OFF (Has to be OFF in order to change Ignition Timing)

    - Press ESC to go to Main Menu
- Select “TIMING” on the CPU 95 Control Module
    - Hit “UP” to select “GLOBAL”
    - Hit “UP” to select “ADJUST RETARD” (This is the ignition retard from the reset pin)
        - Hit “UP” to advance ignition timing
        - Hit “DOWN” to retard ignition timing
            - The global ignition timing is shown as the bottom number on the control pas and is given in °bTDC
        - Hit “ESC” to save changes

CFR Shut-Down Checklist

Normal Shutdown:

- Switch off engine ignition
- (Operation Parameters: Air Setpoint) Set boost pressure to 101 kPa
- Turn off “PWM Enable” to stop fuel flow
- Isolate fuel system at the downstream fuel isolation valve
- Shut all fuel regulators
- Open the fuel manifold vent valve
- Click “PWM Enable to depressurize NG (Make sure to return “Desired Fuel” to 0). Click again to close
- Depressurize CH4, C2H6, CO, CO2, N2, & H2 through the low flow vent line

- Unplug CO2 and CH4 regulator heaters
- (Fuel Blending Control: Auto Fuel Control) Turn off “Auto Fuel Control”
- Click the “Fuel System Enable” button to disable the fuel system
- Turn off power strip to 5 gas analyzer sample line (if using)
- Shut GC sample line valve (if using)
- Open exhaust backpressure valve
- Verify Air-fuel heater is switched off
- Open drain valve from crankcase vent line
- Open drain valve from exhaust piping in the overhead
- Allow engine to cool for approximately 5 minutes (= 90°C coolant temperature)
- (Operational Parameters: Inlet Air Control) Turn off “Inlet Air Control”
- Shut down engine from main CFR Control Panel
- (Operation Parameters: Air Enable) Turn off “Air Enable”
- Open “Intake Air Vent” in VI using Shut-Down Feature
- Close supply o engine cooling water, inlet first
- Shut combustion air valves
- Switch off charge amplifier

Flip switch to disconnect 480 VAC (Panel east of engine) Line and 208 V Line (Brick wall north of engine)

- Stop Host VI, close
- Stop EECL-CFRIO, close
- Collapse CFRIO in menu, disconnect
- Close out LabVIEW Main Menu

APPENDIX B: ENGINE CONTROL AND LOGGING OVERVIEW

ENGINE TEST CELL CONTROLS

This project is conducted using two specific programs developed at the Colorado State University Engines and Energy Conversion Laboratory by the Engineering Manager, Mr. Kirk Evans. Both programs are written in LabVIEW© in support of ongoing research projects at the University. The first program, Combustion Analyzer, is a general internal combustion engine operation monitoring and performance logging program accepting operating parameter input from sensors on the engine and translating that information to combustion characterization of the operating engine. The program is adaptive to a number of different engines and has a module developed specifically for the CFR F2 engine used in this work. The second program, CFR Host VI, is specifically developed for operational control of the CFR F2 engine test cell to include fuel blending, engine operation, and exhaust systems.

COMBUSTION ANALYZER

The combustion logger configuration page is shown in Figure B-1. Inputs are accepted for pegging pressure and location, ignition timing, compression ratio, encoder resolution and offset, bore, stroke, connecting rod length, clearance volume polytropic coefficient and modeled heat release method. Once enabled the program provides active sensor input displayed in real time.

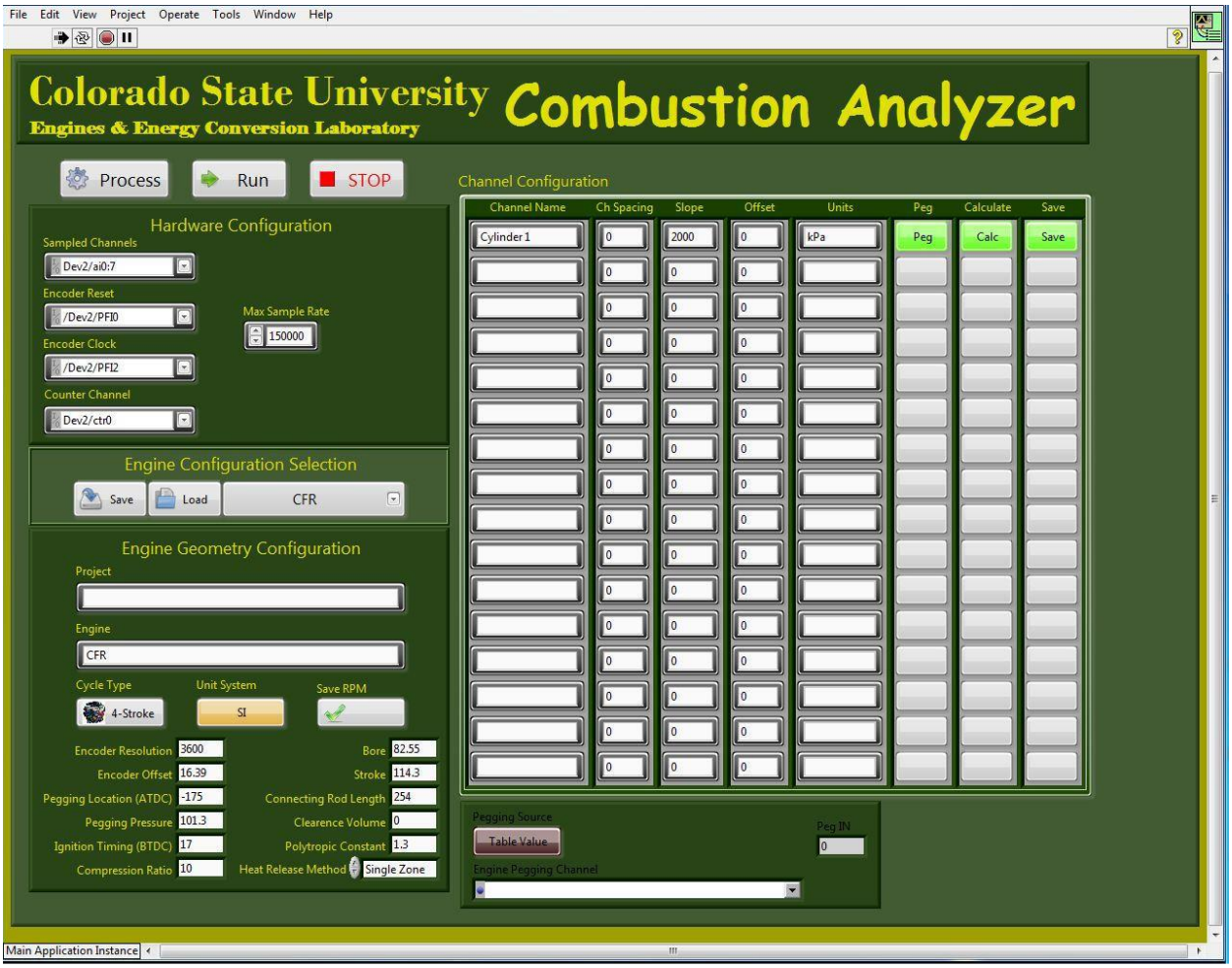

Figure B-1: Combustion Analyzer Configuration Input Opening Screen.

Figure B-2 shows the engine monitoring page, specifically the cylinder pressure display showing real time pressure [kPa] vs. crank angle, θ [0° = TDC]. For this particular image a plot is shown with the engine motoring. Calculated values for peak pressure, location of peak pressure, IMEP, NMEP, PMEP, ignition delay, and burn duration are provided in real time as well as the Coefficient of Variance for those parameters as indicated.

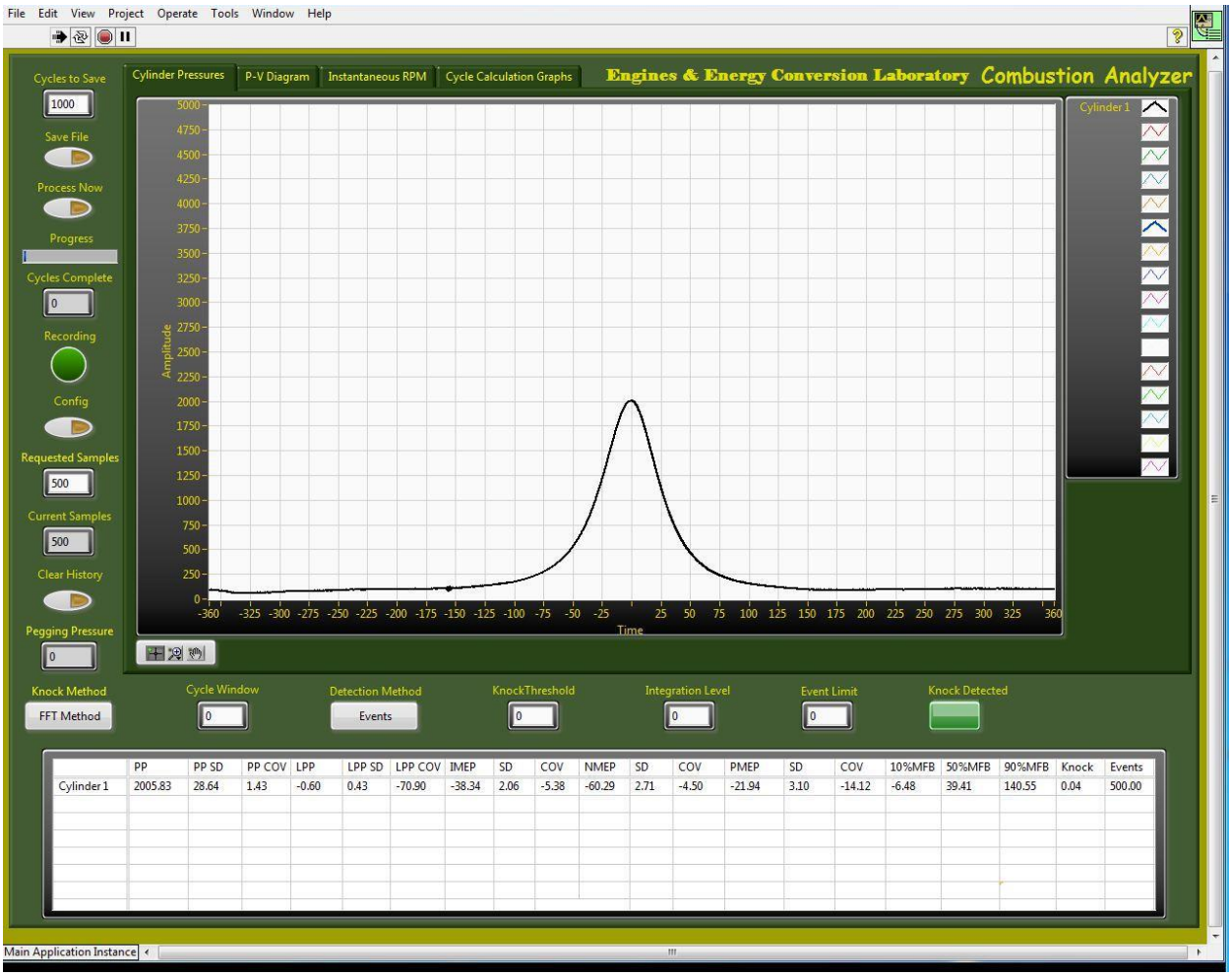

	PP	PP SD	PP COV	LPP	LPP SD	LPP COV	IMEP	SD	COV	NMEP	SD	COV	PMEP	SD	COV	10%MFB	50%MFB	90%MFB	Knock	Events
Cylinder 1	2005.83	28.64	1.43	-0.60	0.43	-70.90	-38.34	2.06	-5.38	-60.29	2.71	-4.50	-21.94	3.10	-14.12	-6.48	39.41	140.55	0.04	500.00

Figure B-2: Engine Operations Monitoring Page, Cylinder Pressure Display.

Figure B-3 also shows an in-cylinder pressure vs. crank angle plot for the engine operating at a compression ratio of 10:1, ignition timing of 17°bTDC, burning natural gas. Note that NMEP is shown as 895 kPa with location of peak pressure at 16°aTDC and other parameters as indicated.

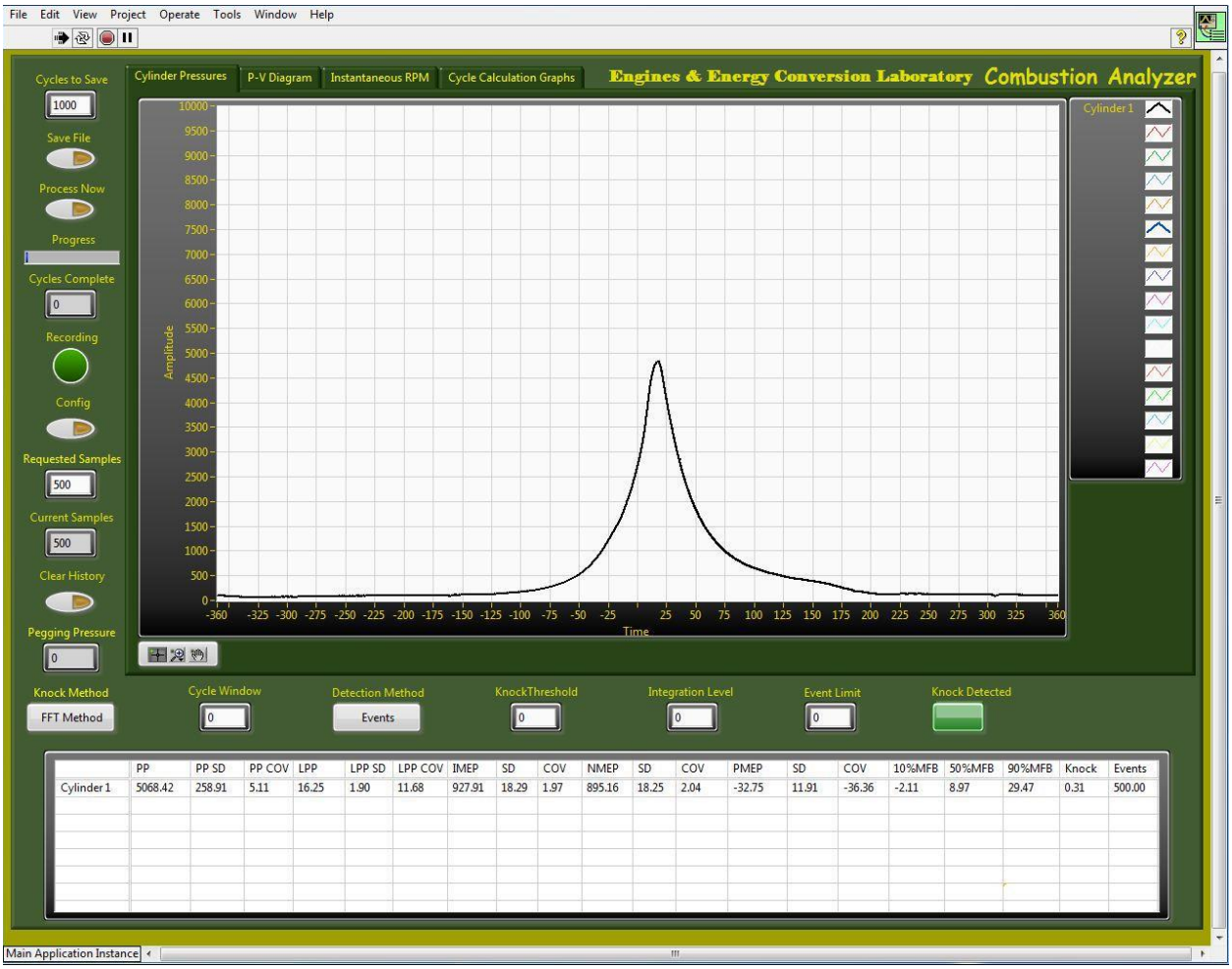

Figure B-3: Engine Operations Monitoring Page, Cylinder Pressure Display.

Figure B-4 shows the pressure vs. volume curve for the operating engine. Scaling may be altered as necessary and is frequently desired to be shown in logarithmic scale for this particular plot.

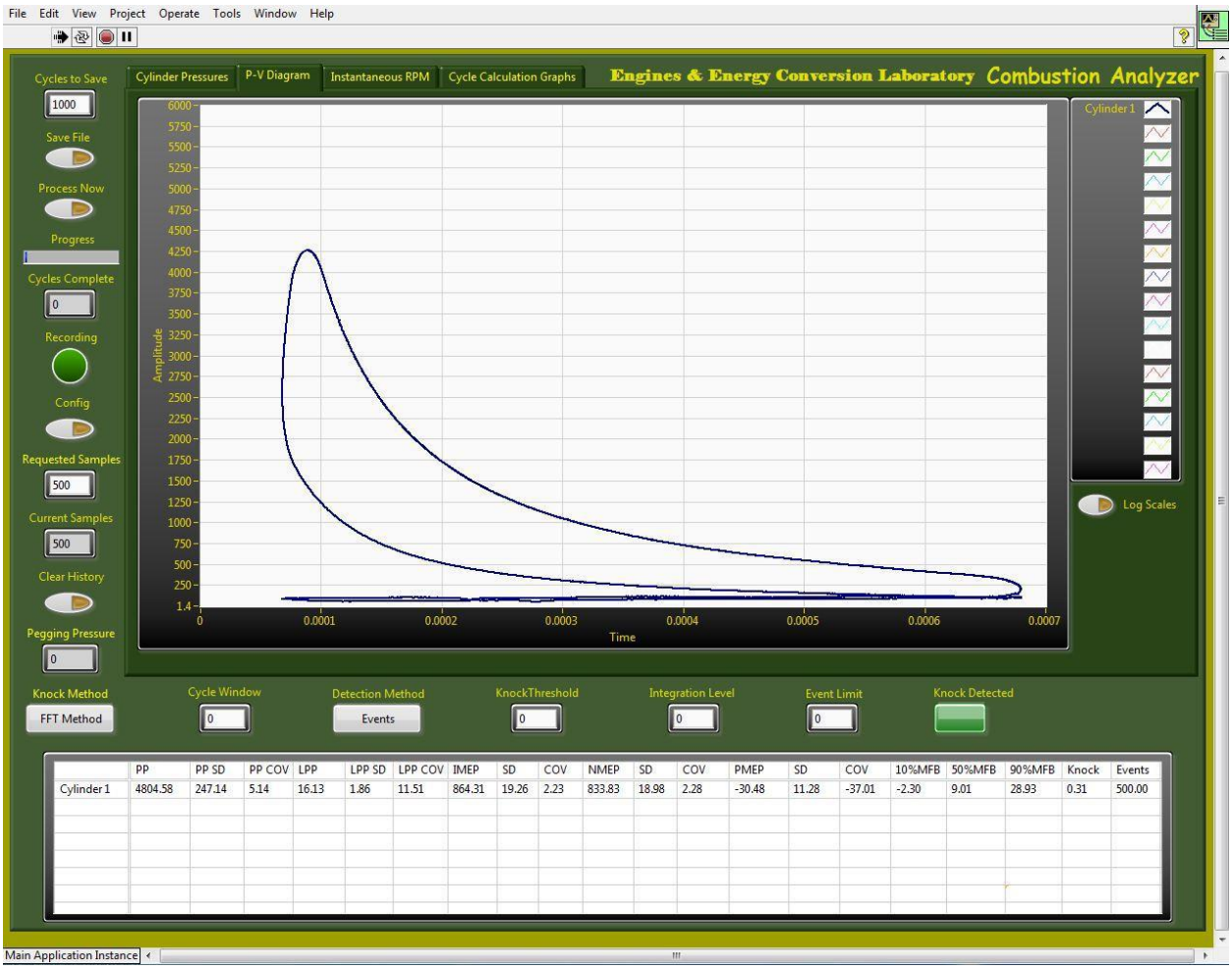

	PP	PP SD	PP COV	LPP	LPP SD	LPP COV	IMEP	SD	COV	NMEP	SD	COV	PMEP	SD	COV	10%MFB	50%MFB	90%MFB	Knock	Events
Cylinder 1	4804.58	247.14	5.14	16.13	1.86	11.51	864.31	19.26	2.23	833.83	18.98	2.28	-30.48	11.28	-37.01	-2.30	9.01	28.93	0.31	500.00

Figure B-4: Engine Operations Monitoring Page, P-V Plot Displayed (operating)

Figure B-5 shows the instantaneous RPM plot for the operating engine. For the CFR engine, a nominally constant speed device, the oscillation of actual engine speed as a function of crank can be observed in this plot.

Figure B-5: Engine Operations Monitoring Page, Instantaneous RPM Plot Displayed.

Figure B-6 knock detection screen for the analyzer. The plot is of the Fast Fourier Transform amplitude at 6 kHz (±200 Hz) for each engine cycle, shown in real time. This plot is illustrative of function only, no threshold values for amplitude level, integration level and event recurrence have been entered.

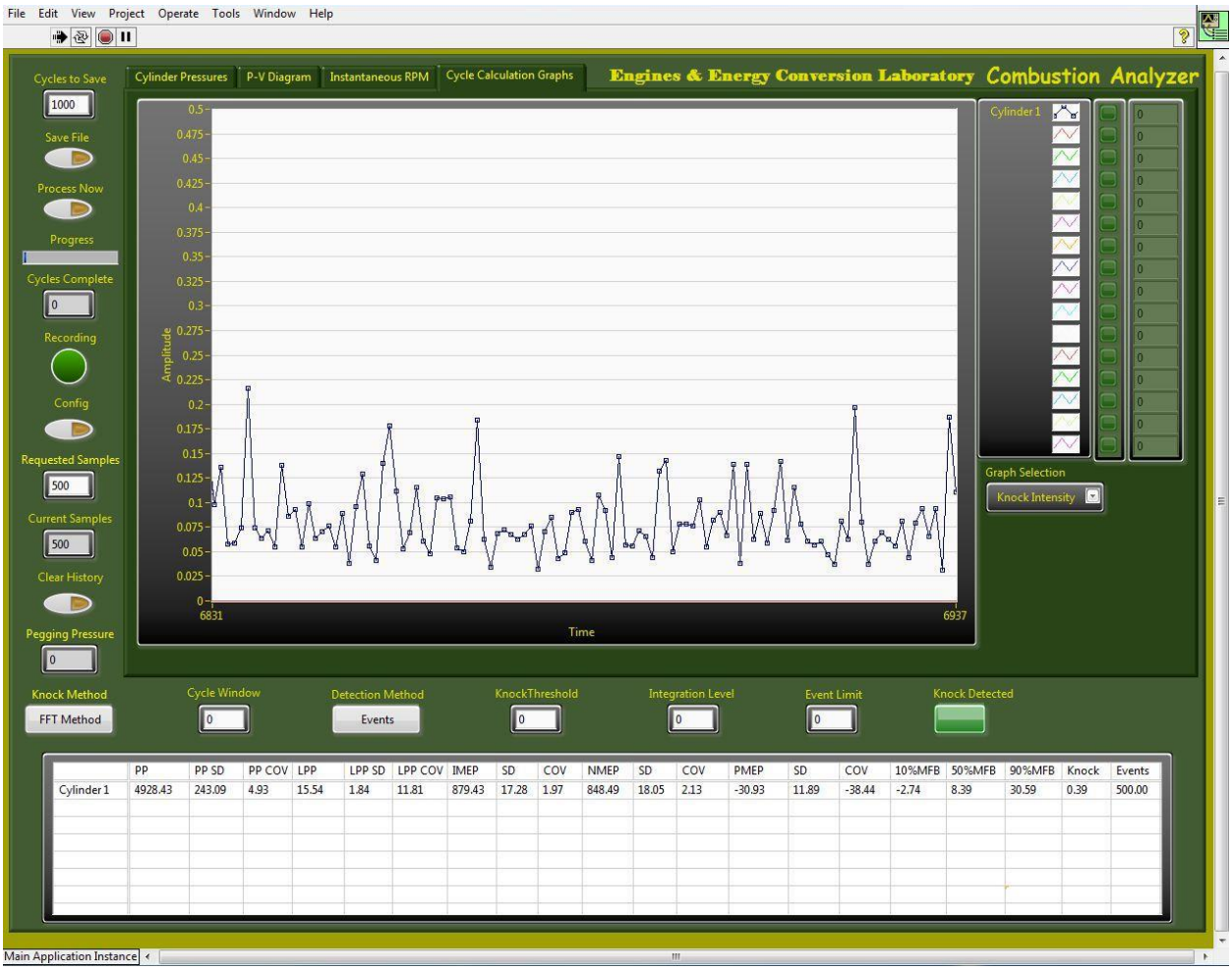

Figure B-6: Engine Operations Monitoring Page, FFT Amplitude Displayed.

Figure B-7 is a block diagram excerpt showing the combustion loop module of the combustion analyzer program.

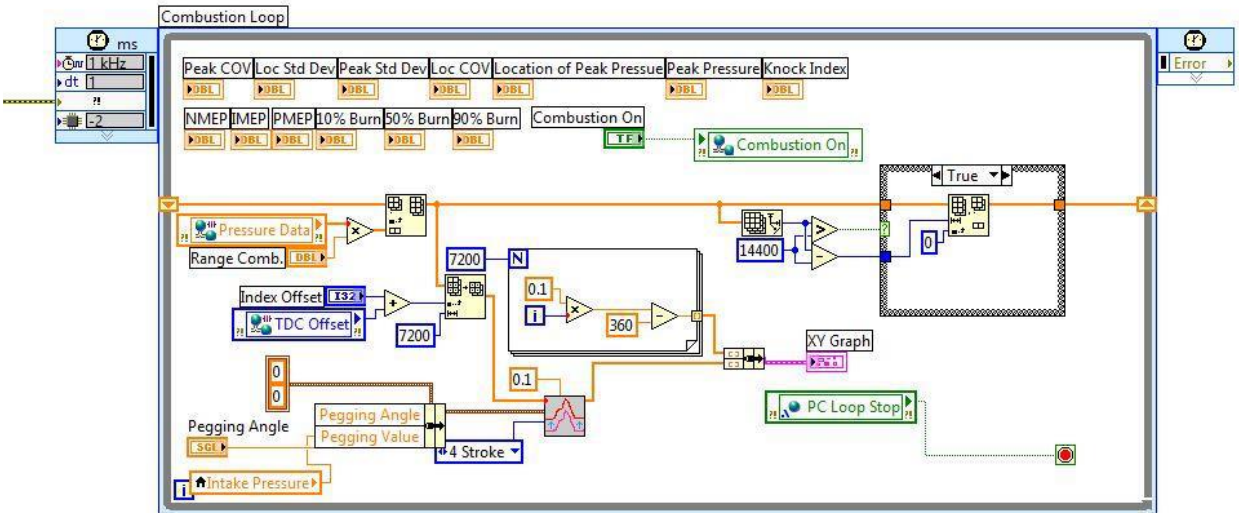

Figure B-7: Combustion Loop Module of Combustion Analyzer Block Diagram.

B-1 CFR TEST CELL VI

The LabVIEW© program CFR Host VI is developed for operation of the test cell to include the fuel blending system, control of engine operations and emissions monitoring and logging. Figure B-8 shows the Operational Parameters screen of program. From this screen the operator can monitor key temperatures (inlet air, exhaust, engine coolant), exhaust and intake pressure, engine RPM and output power. Additionally, intake boost pressure is controlled by enabling remote air control and setting air setpoint (intake air boost pressure) to desire levels to elevate or reduce engine nmep. The intake air vent icon is a safety shutdown feature that allows the operator to isolate fuel and combustion air (removing power from fail shut isolation solenoid valves for fuel and air) while venting the intake manifold to atmosphere (removing power from the fail open intake ventilation solenoid valve). When activated the icon changes from green to red.

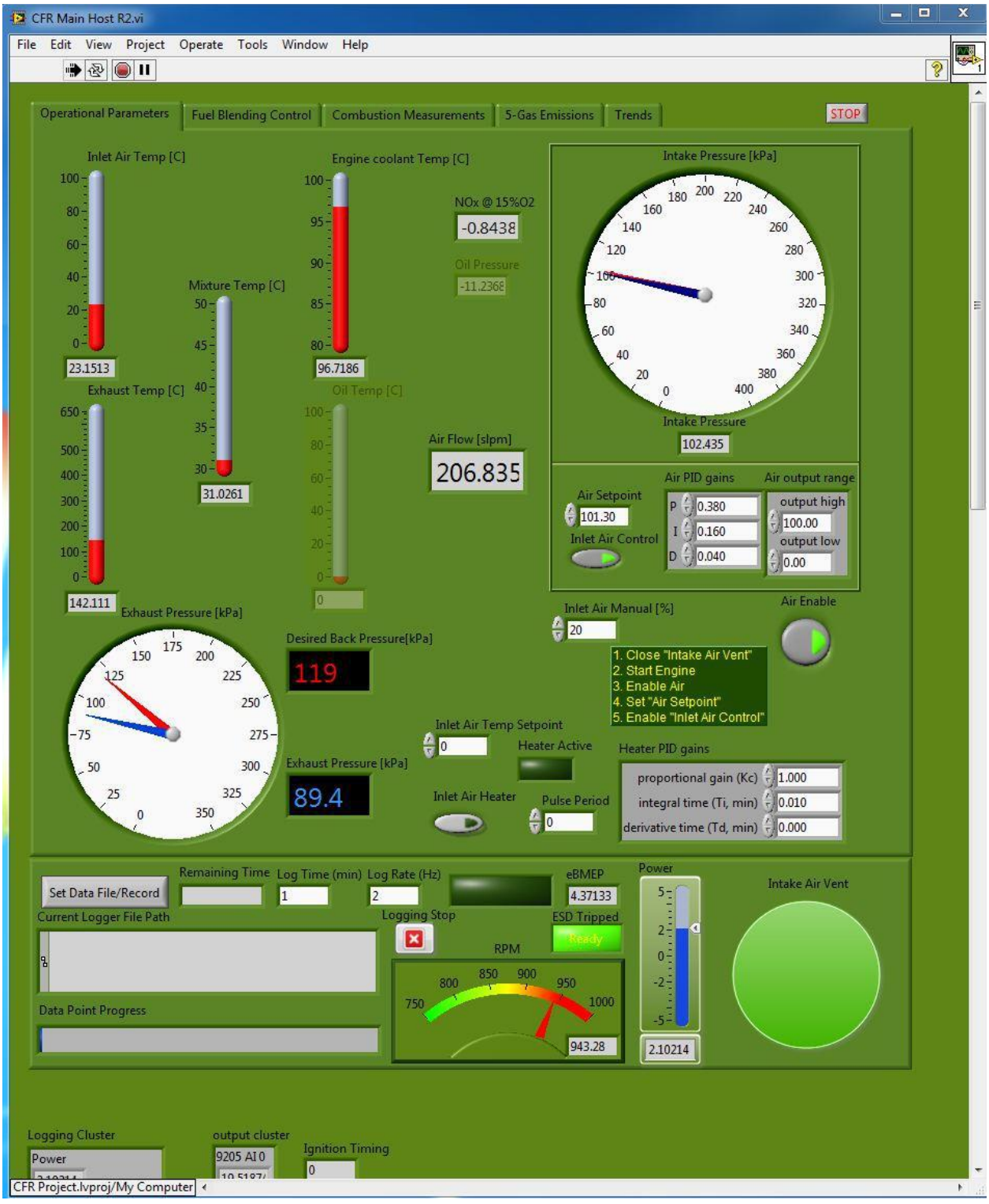

Figure B-8: CFR Host VI Operational Parameters Screen.

Figure B-9 shows the Fuel Blending Control screen for the CFR Host VI. This screen allows the operator to set operating characteristics of the fuel blending system and monitor performance of the system is real time. Fuel injector maximum duty cycle, desired air-fuel ratio, Air-Fuel Recorder range presets are entered. Stoichiometric conditions are controlled with air-fuel control selected from a choice of broad-band O2 sensor input (Air-Fuel Recorder) control or mass flow control (combustion air mass flow meter output to summed fuel component mass flow output). Either system will compare air-fuel ratio with desired and adjust accordingly. The fuel system is enabled from this screen physically operating the fuel injectors which send proportioned fuel to the engine.

Figure B-9: Fuel Blending Control Display of the CFR Host VI Program.

Figure B-10 shows the 5-Gas Emissions display of the CFR Host VI. The display provides real time broadcast of the data output from the 5-Gas Analyzer monitoring engine exhaust for the CFR. The data set enabled consists of value for total hydrocarbons (THC), oxygen (O2), nitrogen oxides or NOx (NO and NO2), carbon dioxide (CO2), and carbon monoxide (CO). It is noted that all of the displays for the CFR Host VI allow the operator to monitor RPM, bmep, and output power as well as to observe/active intake air ventilation in the event of an emergency shutdown of the engine.

Figure B-11 shows a block diagram excerpt of the fuel blending module of the CFR Host VI and is included to give the reader an organization frame of reference for the program.

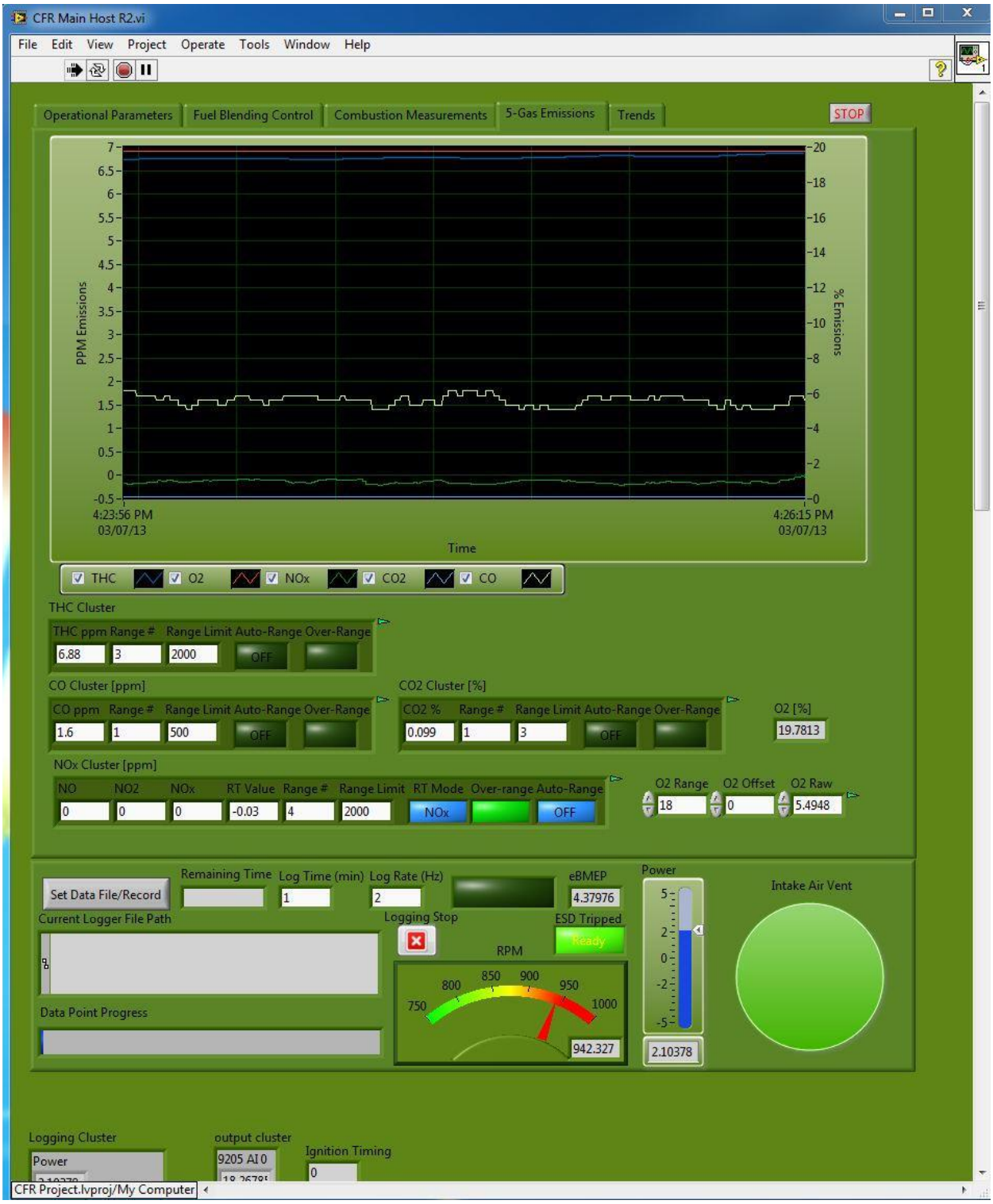

Figure B-10: 5-Gas Emissions Display for the CFR Host VI.

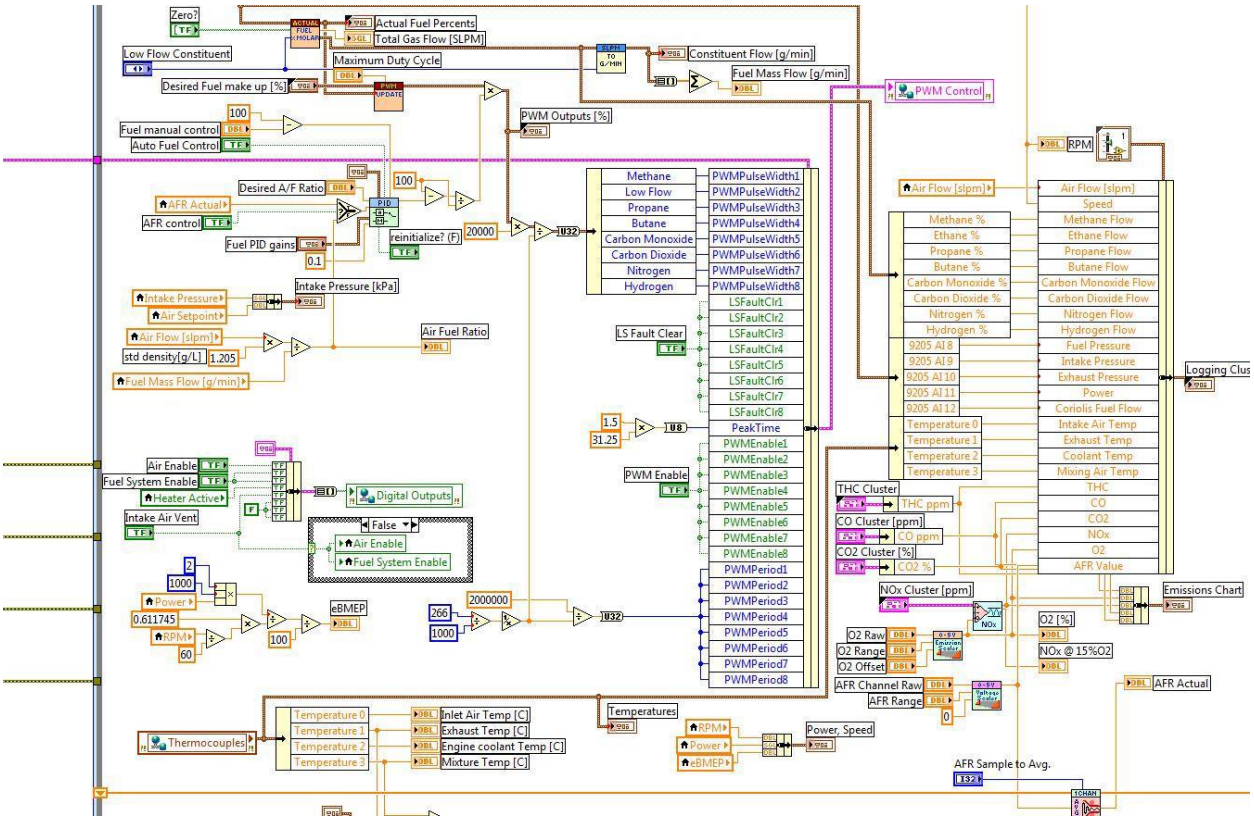

Figure B-11: Block Diagram of CFR Host VI Fuel Blending Module

B-2 ELECTRONIC IGNITION

A third system enabling automated operation and control of the CFR engine is the electronic ignition system installed in the test cell. The Woodward Large Engine Control Module (LECM) allows the operator to monitor and adjust ignition timing during engine operation without any mechanical interface to the engine. Figure B-11 shows the program terminal display while the engine is operating with ignition timing set at 17.0°bTDC.

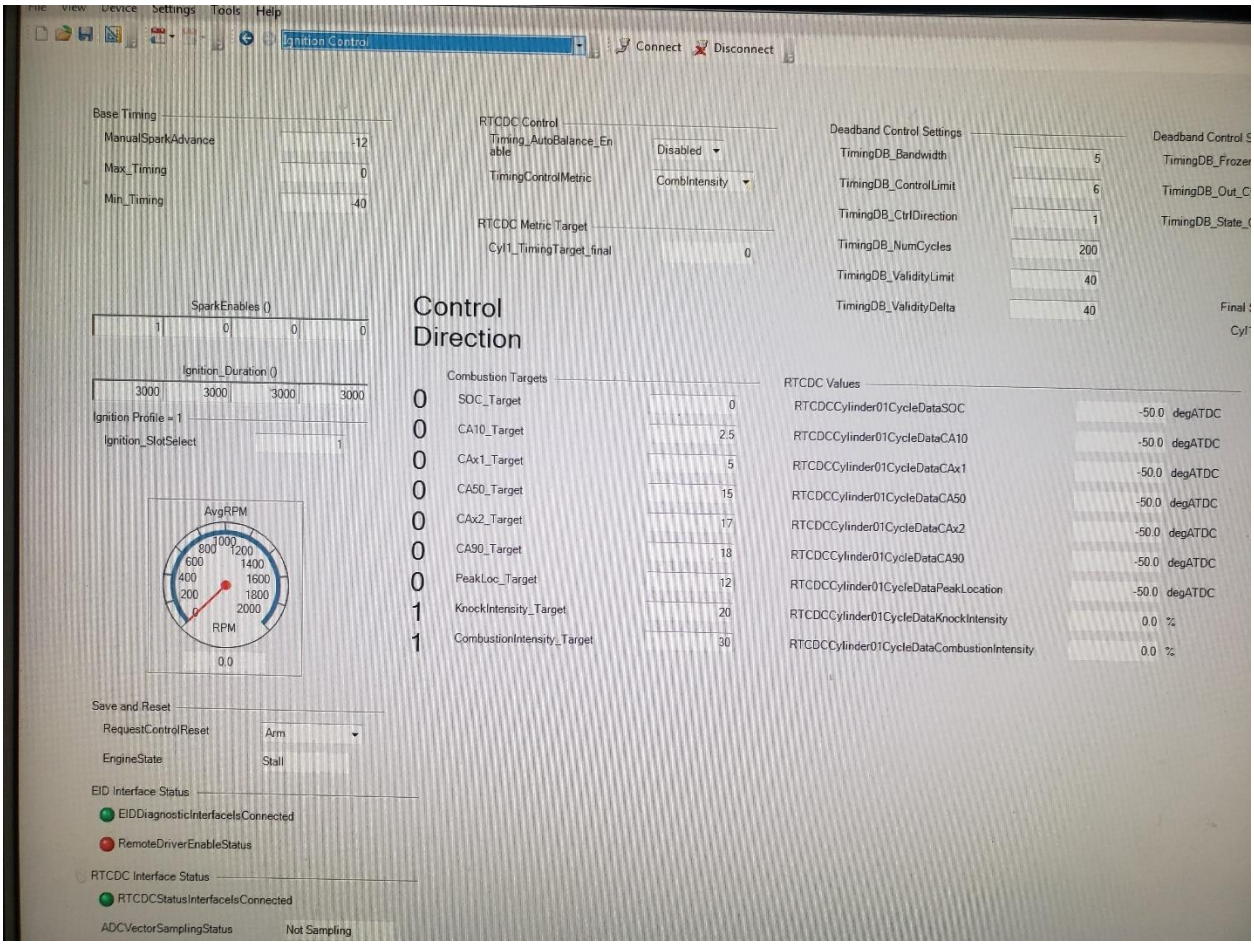

Figure B- 12: Electronic Ignition Terminal Program Display

APPENDIX C: TEST CELL REPAIR AND EGR CART CONSTRUCTION

The CFR engine required numerous upgrades and repairs to ensure proper operation and adequate data collection throughout the study. The updated CFR engine can be seen in figure C-1, and the list of repairs include:

- Compression ratio verification
- Gasket sealing
- Exhaust system rebuild
- Intake system rebuild
- Wiring cabinet rebuild
- Mass flow meter calibrations
- Exhaust sampling verification
- LabVIEW coding rewire
- Oil system reroute
- Cylinder pressure sensor calibration
- Intake and exhaust dynamic pressure sensor installation
- Fuel flow meter calibrations

Figure C-1: Updated CFR Engine

Additionally, on top of the repairs, a few upgrades were issued to the CFR engine. The first of which were the inclusion of dynamic intake and exhaust pressure sensors to allow for three pressure analysis of 1D models as well as more accurate pegging pressures and fluid temperatures. These sensors can be seen in Figure C-2.

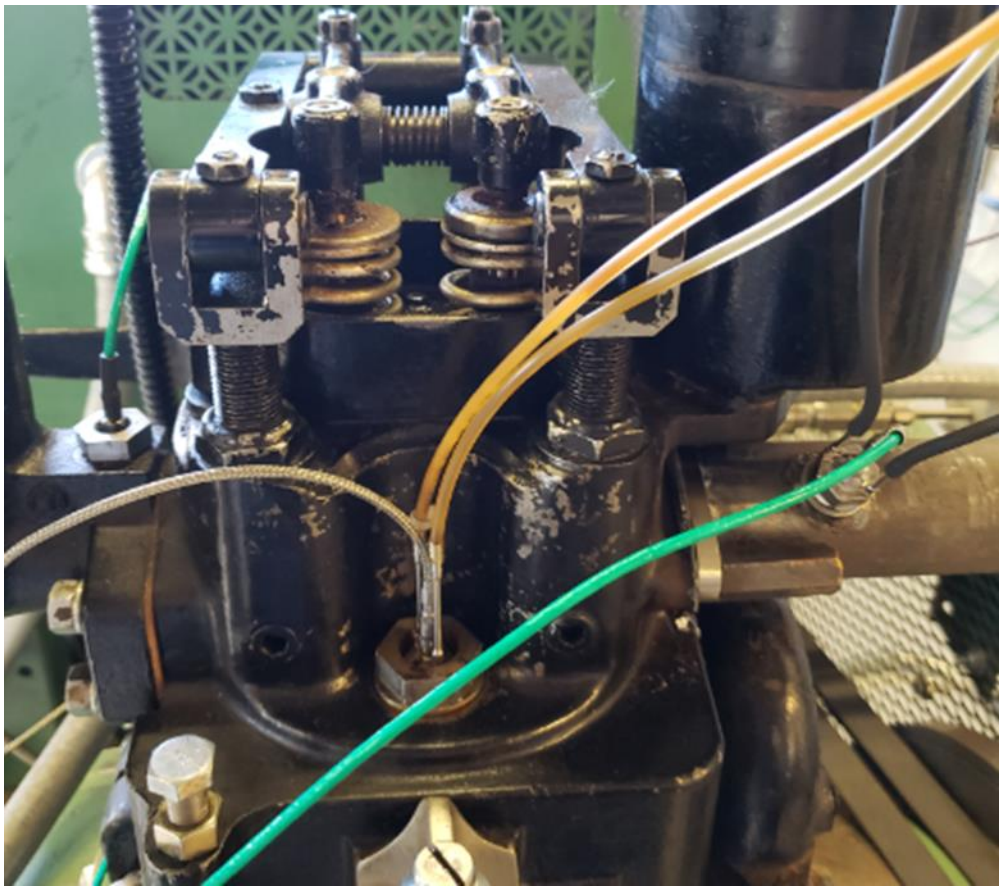

Figure C-2: Dynamic Intake and Exhaust Pressure Sensors on CFR Engine

The CFR engine is designed to have testing conducted at a nominal engine speed of 900 RPM. However, this CFR engine utilized an induction motor rather than the standard synchronous motor, which caused average operation to exist between 935 and 945 RPM. To fix this, a regenerative VFD was introduced to the system to allow for control of engine speeds between 600 and 1200 RPM, while controlling within 0.5 RPM of the target value. The regenerative VFD is visible in figure C-3.

Figure C-3: Yaskawa Regenerative VFD on CFR Engine

To ensure proper flow rates are recorded throughout the variable pipeline natural gas testing was conducted with, a secondary mass flow measurement system was required. Rather than relying on a second set of species-specific mass flow meters, a Coriolis mass flow meter to measure the total fuel flow was installed and used for all mass flow measurements. The Coriolis mass flow meter can be seen in figure C-4.

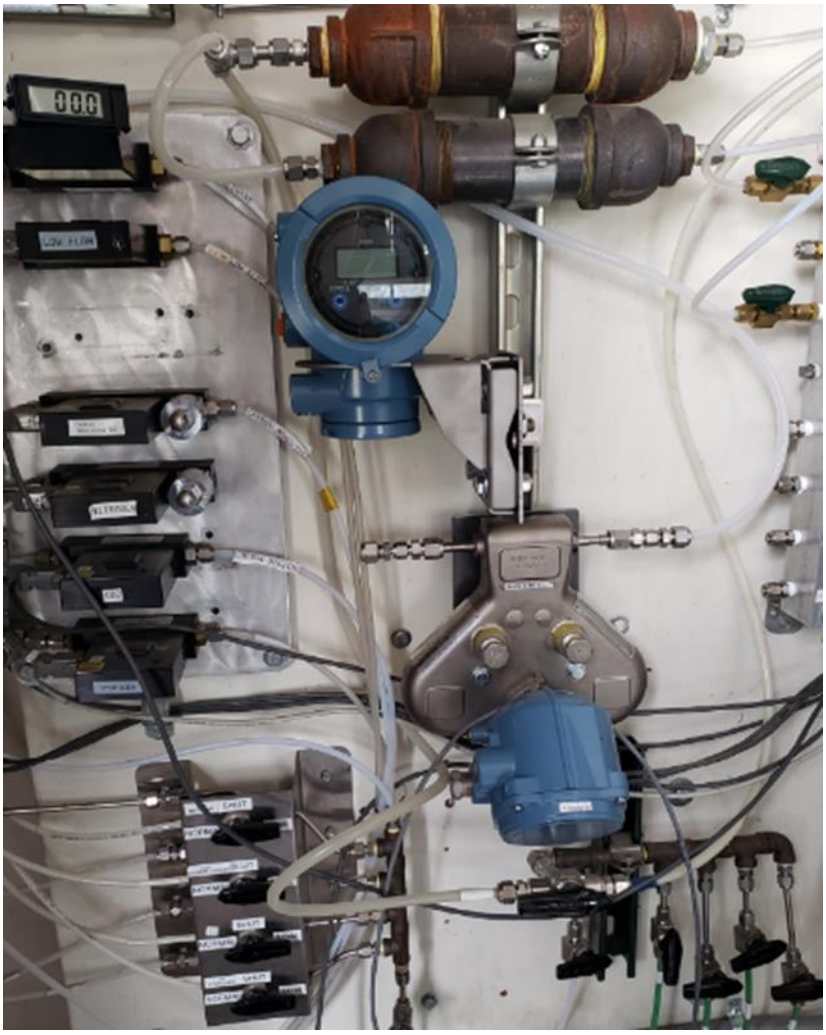

Figure C-4: Coriolis Flow Meter for CFR Engine

To make advanced ignition control possible for C-EGAI an advanced ignition system was required. The Woodward LECM fulfilled this request and can be seen installed on the CFR engine in figure C-5.

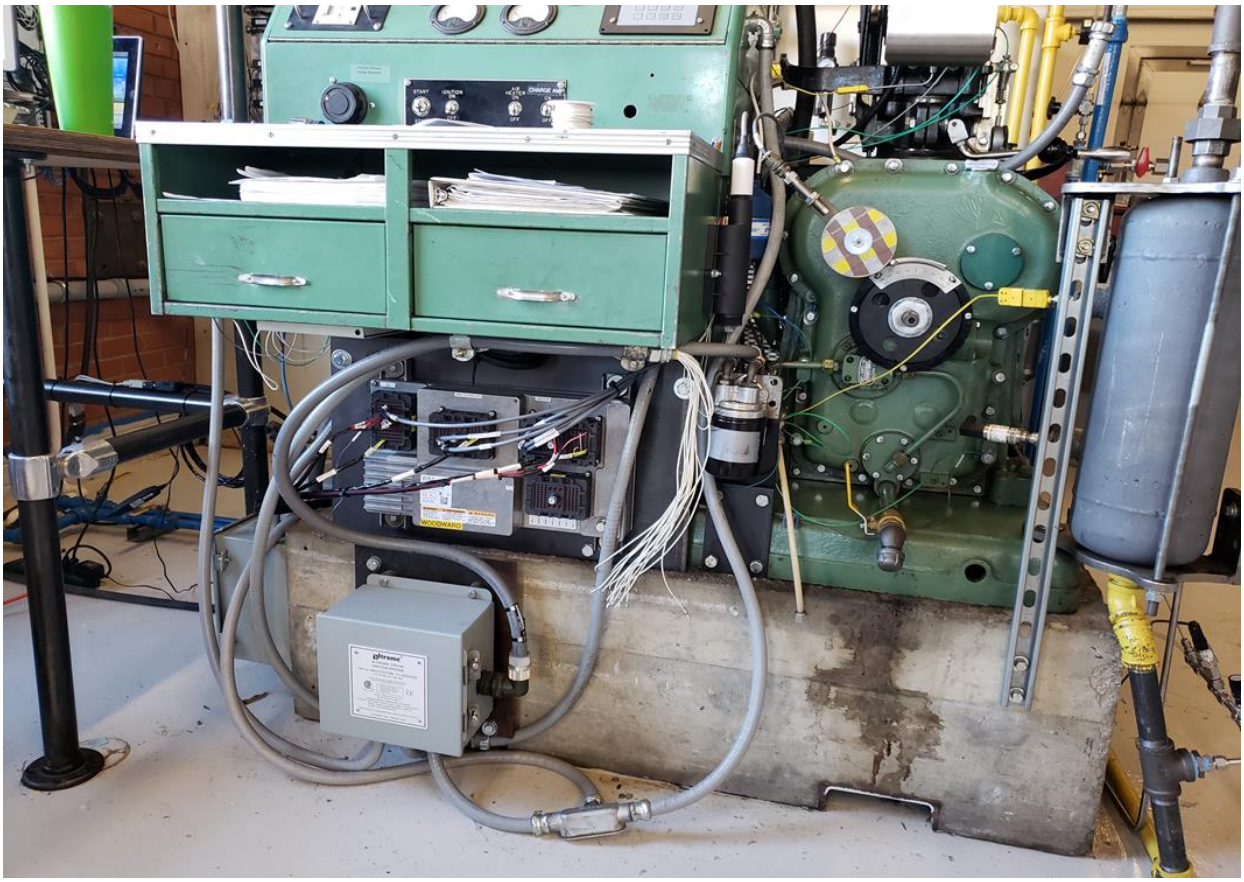

Figure C-5: Woodward LECM Front Mounted on CFR Engine

Furthermore, with new systems on the CFR engine, the EGR test cart was developed for the CFR engine specifically for this study. The EGR cart requirements included simulating a high-pressure loop EGR systems while being able to provide up to 40% EGR rate by displacement of the intake charge at all power levels. The finished EGR cart can be seen in Figure C-6.

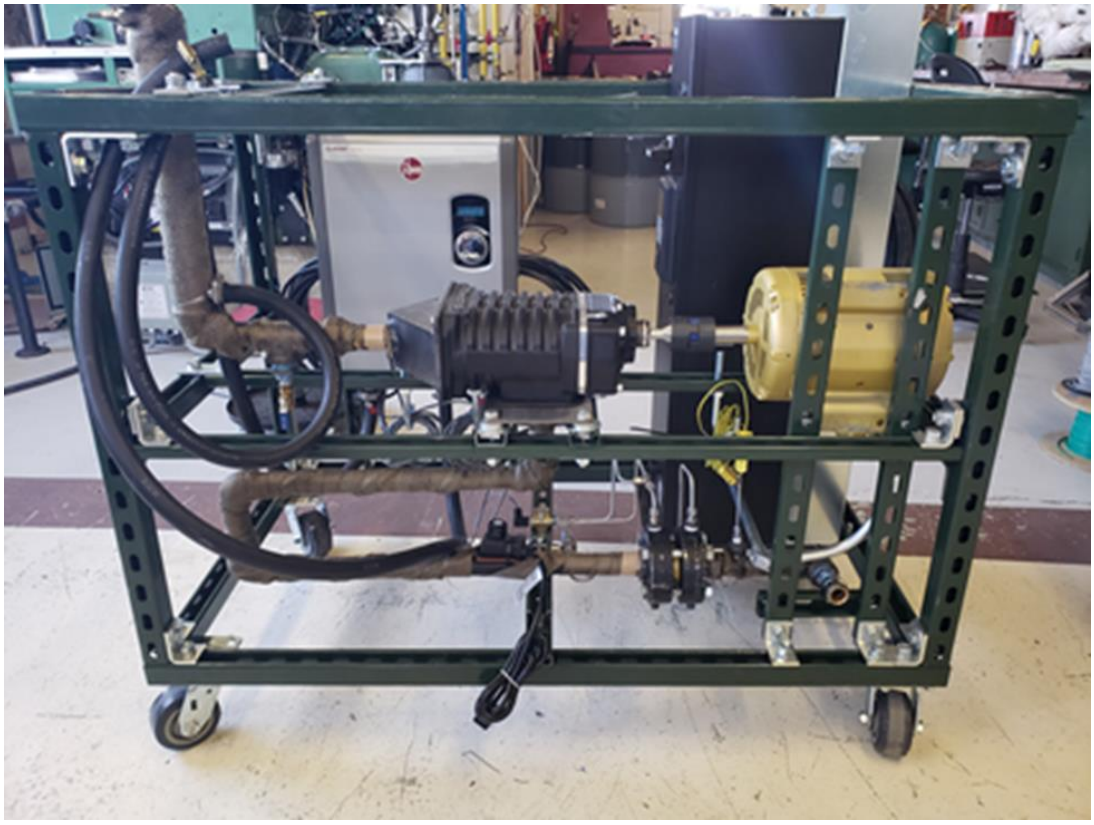

Figure C-6: Full EGR Test Cart System for CFR Engine

The EGR cart required specific systems to fulfill the requirements. These are outlined in the list below:

- EGR cooler for 1.8L Volkswagen diesel engine.
- 75 Amp, 208 V tankless water heater to ensure exhaust gas fluid is not cooled below condensation point in EGR cooler, and maintain average intercooler temperatures of 140°F.
- 1.2 L displacement Whipple twin screw positive displacement blower to regulate EGR flow in CFR engine.

- 5 horsepower, 208 V electric motor to drive positive displacement blower at all flow range requirements.
- Eaton VFD for controlling electric motor to specific speeds for EGR displacement rates.
- AGA report #3 standard orifice mass flow meter

APPENDIX D: DATA TABLES

Table D- 1: Baseline Data Acquisition for CFR Engine

Test #	Description	Control Parameters					Nominal Values			Actual CR	EGR Temp	Recorded BMEP	Recorded IMEP	Electric Power [kW]	AFR Actual [O2]	Ignition timing
		Fuel Blend	CA 50	EGR	BMEP	CR	Intake Temperature	Phi								
1	try match flow rates I had in the CFR	Building NG	10		6	8	60° c	1		7.43414	X	6.08	1056.03	2.79	0.991	-15.15
2	Best case (furthest from knock)	Building NG	15		6	8	60° c	1		743414	X	5.991	1040.88	2.77	1.005	-11.34
3	There should be knock	Building NG	10		6	10	60° c	1		9.08785	X	5.996	1013.53	2.75	0.999	-13.64
4	There should be knock onset	Building NG	15		6	10	60° c	1		9.08785	X	6.051	1014.59	2.81	1.009	-9.36
5		Building NG	20		6	10	60° c	1		9.08785	X	6.041	1033.95	2.79	0.996	-8.99
6		Building NG	5	10%	4	10	60° c	1		9.08785	54.3	4.24	858.92	1.95	1.011	-18.08
7		Building NG	5	15%	4	10	60° c	1		9.08785	55.7	4.036	830.25	1.82	1.082	-19.48
8		Building NG	5	20%	4	10	60° c	1		9.08785	57.9	3.89	810.22	1.79	1.07	-21.01
9		Building NG	5	30%	4	10	60° c	1		9.08785	59.7	4.07	829.35	1.89	1.04	-21.01
6.1	retest	Building NG	10	10%	4	10	60° c	1		9.08785	58.7	4.15	804.04	1.89	0.995	-18.62
7.1	retest	Building NG	10	15%	4	10	60° c	1		9.08785	59.4	4.22	810.44	1.94	0.997	-20.27
8.1	retest	Building NG	10	20%	4	10	60° c	1		9.08785	60.2	4.26	807.43	1.95	1.007	-21.01
9.1	retest	Building NG	10	30%	4	10	60° c	1		9.08785	60.8	3.78	739.43	1.76	0.996	-21.01
10		Building NG	15		6	12	60° c	1		10.6694	X	5.958	1036.19	2.73	1.009	-8.99
11		Building NG	20		6	13	60° c	1		11.4315	X	5.941	1041.77	2.73	1.009	-8.99
12	Knocking case	Building NG	Sweep to light knock [12.5] (60)		4	12	60° c	1		10.6694	X	3.981	790.54	1.83	0.999	-11.57
13	Knocking case	Building NG	Sweep to medium knock [9.75] (350)		4	12	60° c	1		10.6694	X	4.031	797.81	1.86	0.997	-13.87
14	Knocking case	Building NG	Sweep to heavy knock [7.75] (1000)		4	12	60° c	1		10.6694	X	4.035	799.21	1.84	1.008	-15.59
15	Fix CA50 on #9 and add EGR	Building NG	10	10%	4	12	60° c	1		10.6694	58.3	4.242	838.92	1.96	0.989	-13.63
16	Fix CA50 on #9 and add EGR	Building NG	10	20%	4	12	60° c	1		10.6694	59.9	3.978	793.39	1.81	0.994	-18.87
17	Fix CA50 on #9 and add EGR	Building NG	10	30%	4	12	60° c	1		10.6694	59.2	4.04	809.07	1.82	1.009	-21.01
18	Fix CA50 on #10 and add EGR	Building NG	15	10%	4	12	60° c	1		10.6694	59.1	4.331	849.52	2.02	1.011	-9.71
19	Fix CA50 on #10 and add EGR	Building NG	15	20%	4	12	60° c	1		10.6694	60.1	4.001	799.11	1.84	1.003	-15.21
20	Fix CA50 on #10 and add EGR	Building NG	15	30%	4	12	60° c	1		10.6694	60.4	4.024	808.91	1.88	0.998	-21.01
21	Fix CA50 on #11 and add EGR	Building NG	20	10%	4	12	60° c	1		10.6694	60.2	4.301	842.66	1.99	1.021	-8.99
22	Fix CA50 on #11 and add EGR	Building NG	20	20%	4	12	60° c	1		10.6694	59.7	3.887	784.33	1.79	1.008	-12.98
23	Fix CA50 on #11 and add EGR	Building NG	20	30%	4	12	60° c	1		10.6694	61.2	4.031	802.23	1.79	0.995	-21.01
24	Knocking case	Building NG	Sweep to light knock [15]		4	14	60° c	1		12.1833	X	4.074	801.39	1.86	1.007	-9.81
25	Knocking case	Building NG	Sweep to medium knock [13.1]		4	14	60° c	1		12.1833	X	4.002	798.58	1.83	1.008	-11.09
26	Knocking case	Building NG	Sweep to heavy knock [11.25]		4	14	60° c	1		12.1833	X	4.024	796.49	1.84	1.009	-12.16
27	Fix CA50 on #22 and add EGR	Building NG	10	10%	4	14	60° c	1		12.1833	60.1	3.99	805.91	1.81	0.986	-14.19
28	Fix CA50 on #22 and add EGR	Building NG	10	20%	4	14	60° c	1		12.1833	60.4	4.12	829.15	1.91	1.009	-17.48
29	Fix CA50 on #22 and add EGR	Building NG	10	30%	4	14	60° c	1		12.1833	61.2	3.68	751.15	1.69	0.996	-21.01
30	Fix CA50 on #23 and add EGR	Building NG	15	10%	4	14	60° c	1		12.1833	61.8	4.242	834.12	1.93	0.994	-10.26
31	Fix CA50 on #23 and add EGR	Building NG	15	20%	4	14	60° c	1		12.1833	61.9	4.258	830.27	1.97	0.999	-16.89
32	Fix CA50 on #23 and add EGR	Building NG	15	30%	4	14	60° c	1		12.1833	60.8	3.73	758.42	1.63	1.011	-21.01
33	Fix CA50 on #24 and add EGR	Building NG	20	10%	4	14	60° c	1		12.1833	60.9	4.345	841.9	2.01	1.008	-8.99
34	Fix CA50 on #24 and add EGR	Building NG	20	20%	4	14	60° c	1		12.1833	62.1	4.121	814.12	1.93	0.998	-13.81
35	Fix CA50 on #24 and add EGR	Building NG	20	30%	4	14	60° c	1		12.1833	60.5	3.654	755.94	1.61	1.011	-21.01

Table D- 2: Model Validation of 1D and #d Models of CFR Engine

Phase	Test #	Description	EGR % targe	Phi	ntake Temp. [C	Spark Timind	Desired IMEP	ngine Speed [RPI	Actual CR	COV PP	EGR Temp. [C	Recorded IMEP	Power [kW]	Actual phi	Fuel MN	gnition Timing [aTDC	take press set point [kP	take Pressure [kP	haust backpressure [kP	EGR Cart VFD [Hz	EGR mass flow [g/min	uel Flow [SLPM	uel Flow [g/min
1: EGR limit	1	at critical CR	0%	1	60	CA50 = 13.8	800	60 Hz = 941.9	X	X	N/a	816.14	X	X	70	-9.893	101.3	103.61	X	X	N/a	20.57	13.63
	1.1	at optimal CR	0%	1	60	CA50 = 13.8	800	942.1	X	X	N/a	797.58	X	X	70	-12.287	101.3	102.34	X	X	N/a	19.81	13.36
	2		5%	1	60	CA50 = 13.8	800	941.7	X	X	49.7	809.98	X		70	-11.954	102	103.41	X	X	2.45	18.57	12.12
	3		10%	1	60	CA50 = 13.8	800	943.3	X	X	50.3	822.19	X		70	-12.116	101	102.98	X	X	6.45	19.24	13.07
	4		15%	1	60	CA50 = 13.8	800	942.2	X	X	51.7	799.94	X		70	-12.494	100	102.49	X	X	21.57	18.16	12.18
	5		20%	1	60	CA50 = 13.8	800	942.8	X	X	51.8	803.71	X		70	-12.511	102	104.02	X	X	33.62	18.09	12.11
	6	PP COV^6.9	25%	1	60	CA50 = 13.8	800	942.4	X	X	52.1	805.6	X		70	-12.732	102	103.96	X	X	45.78	17.95	12.03
	7	PP COV^8.7	30%	1	60	CA50 = 13.8	800	949.2	X	X	53.6	798.52	X		70	-13.052	106	106.53	X	X	51.73	17.68	11.91
	8	PP COV^9	35%	1	60	CA50 = 13.8	800	942.8	X	X	55.7	804.33	X		70	-12.767	111	112.42	X	X	64.81	18.12	12.15
	9	PP COV^11.2	40%	1	60	CA50 = 13.8	800	942.7	X	X	56.2	805.3	X		70	-12.833	113	113.7	X	X	72.48	18.21	12.12
1.1 retest	1	Find opt. CA50 (max IMEP)	0%	1	60	CA50 = 10.3	800	57.5 Hz = 899.5	9.08785	X	X	805.2	1.78	0.998	Pipeline (GC	-14.98	105	103.38	X	X	X	20.66	13.81
	2	Find Crit. CR	0%	1	60	CA50 = 10.3	800	57.5 = 899.7	10.5261 = 0.15	X	X	824.51	1.93	1.006	Pipeline (GC	-13.36	105	106.23	X	X	X	20.64	13.76
	3	No EGR at CR opt	0%	1	60	CA50 = 10.3	800	57.5 = 899.6	.54881 = 0.20	X	X	810.05	1.81	1.004	Pipeline (GC	-14.11	105	104.82	X	X	X	20.63	13.78
	4		5%	1	60	CA50 = 10.3	800	57.5 = 899.9	9.54881	4.72 - 5.37	57.8	811.15	1.87	1.008	Pipeline (GC	-15.05	106.5	107.12	101 (static buffer)	4	10.2	20.64	13.78
	5		10%	1	60	CA50 = 10.3	800	57.5 = 900.2	9.54881	5.17 - 6.23	58.6	812.52	1.88	1.012	Pipeline (GC	-15.68	109	109.96	105	8	22.4	20.61	13.75
	6		15%	1	60	CA50 = 10.3	800	57.5 = 900.9	9.54881	5.65 - 6.15	59.3	817.65	1.91	1.011	Pipeline (GC	-18.89	116	117.72	109	11	36.2	20.54	13.72
	7		20%	1	60	CA50 = 10.3	800	57.5 = 900.8	9.54881	5.11 - 5.78	59.5	819.73	1.94	0.999	Pipeline (GC	-21.01	122	123.41	116	16	52.8	20.51	13.71
	8		25%	1	60	CA50 = 10.3	800	57.5 = 900.4	9.54881	5.96 - 6.46	64.04	805.34	1.92	0.999	Pipeline (GC	-21.01	128	127.86	124	19	68.7	20.47	13.67
	9	Practical EGR limit hit	30%	1	60	CA50 = 10.3	800	57.5 = 899.9	9.54881	4.16 - 5.24	62.03	730.07	1.71	1.008	Pipeline (GC	-21.01	134	133.56	127	24	88.63	20.44	13.64
	10		35%	1	60	CA50 = 10.3	800	57.5 = 895.3	9.54881	3.81 - 4.12	61.14	597.89	0.99	1.006	Pipeline (GC	-21.01	144	143.34	135	28	104.56	20.39	13.63
	11	Max COV PP	23%	1	60	CA50 = 10.3	800	57.5 = 900.2	9.54881	6.93 - 7.82	60.08	799.58	1.84	0.998	Pipeline (GC	-21.01	128	127.25	120	16	62.1	20.39	13.62
2: critical CR	12	Start: CR = 0.205 & IMEP = 800	0%	1	60	CA50 = 10.3	800	57.6 = 900.3	9.54881	4.61	X	816.86	1.73	0.996	Pipeline (GC	-13.46	105	106.77	101	X	X	20.77	13.87
	13	CR crit: KI > 80	5%	1	60	CA50 = 10.3	800	57.6 = 900.8	10.1391	4.93	57.5	813.52	1.82	0.997	Pipeline (GC	-14.21	105.5	104.56	103	5	11.8	20.47	13.67
	14		10%	1	60	CA50 = 10.3	800	57.6 = 900.9	10.1952	5.68	58.9	813.02	1.85	0.999	Pipeline (GC	-16.12	109.5	108.36	105	9	24.3	20.36	13.59
	15		15%	1	60	CA50 = 10.3	800	57.5 = 900.5	10.387	6.39	59.3	824.46	1.93	1.001	Pipeline (GC	-19.51	116.5	117.33	111	13	36.8	20.36	13.57
	16		20%	1	60	CA50 = 10.3	800	57.5 = 900.6	11.3594	8.94	60.2	831.64	1.95	1.002	Pipeline (GC	-21.01	123	122.25	118	16	51.7	20.31	13.57
	17	IMEP decreased past this CR	25%	1	60	CA50 = 10.3	800	57.5 = 900.4	11.5291	5.38-6.31	60.8	795.67	1.9	0.998	Pipeline (GC	-21.01	129	128.64	125	20	67.9	20.21	13.51
	18	Pushed CR further	25%	1	60	CA50 = 10.3	800	57.5 = 899.7	14.1048	3.48	61.3	785.15	1.81	1.007	Pipeline (GC	-21.01	129	130.36	122	20	68.1	20.21	13.5
	19	Pushed EGR rate furthere	30%	1	60	CA50 = 10.3	800	57.5 = 897.3	11.8073	3.17	62.2	663.86	1.28	1.01	Pipeline (GC	-21.01	137	136.89	130	25	87.7	20.15	13.47
3: Critical power	20	Start: CR = 0.205 & IMEP = 800	0%	1	60	CA50 = 10.3	X	57.5 = 899.8	9.54881	5.24	X	777.24	1.81	0.999	Pipeline (GC	-14.57	101	102.91	96.7	X	X	20.07	13.41
	21	CR crit > 80	5%	1	60	CA50 = 10.3	X	57.5 = 902.1	9.54881	4.59	59.7	866.85	2.15	0.999	Pipeline (GC	-14.32	111	111.18	106	6	12.5	21.98	14.69
	22		10%	1	60	CA50 = 10.3	X	57.4 = 901.4	9.54881	5.74	60.5	892.31	2.21	1.006	Pipeline (GC	-16.79	120.5	119.15	115	11	25.4	22.49	15.01
	23		15%	1	60	CA50 = 10.3	X	57.3 = 900.7	9.54881	7.17	61.2	921.98	2.36	1.006	Pipeline (GC	-18.98	129.5	129.88	124	16	39.5	23.03	15.38
	24		20%	1	60	CA50 = 10.3	X	56.8 = 900.3	9.54881	8.39	65.1	1162.83	3.24	1.001	Pipeline (GC	-21.01	172	171.82	165	20	75.8	27.97	18.69
	25	Only knock onset was reached	25%	1	60	CA50 = 10.3	X	56.4 = 899.1	9.54881	6.12	70.02	1285.18	3.61	1.003	Pipeline (GC	-21.01	202	202.96	192	25	108.7	31.26	20.91
	26	trying to reach better knock	25%	1	60	CA50 = 10.3	X	57.2 = 907.6	11.8333	7.76	71.1	1185.49	3.24	1.008	Pipeline (GC	-21.01	192	191.34	184	24	101.6		
	27	Unable to push engine further	30%	1	60	CA50 = 10.3	X	X	X	X	X	X	X	X	Pipeline (GC	X	X	X	X	X	X	X	X
4: efiiciency opt.	28	Baseline test for the day	0%	1	60	CA50 = 10.3	800	57.6 = 899.4	9.54881	4.49	X	801.93	1.67	0.989	Pipeline (GC	-13.67	102	101.98	100	X	X	20.27	13.54
	29	Sweep CA50 to determine best	15%	1	60	CA50 = 6	800	57.6 = 901.3	9.54881	6.44	57.8	818.59	1.85	0.998	Pipeline (GC	-21.01	116.5	117.41	112	11	35.8	20.29	13.56
	30	efficiency point.	15%	1	60	CA50 = 9	800	57.5 = 899.6	9.54881	6.51	59.8	818.92	1.82	1.002	Pipeline (GC	-20.86	116.5	116.58	112	11	36.2	20.31	13.55
	31		15%	1	60	CA50 = 12	800	57.5 = 899.5	9.54881	5.61	59.6	816.54	1.87	1.001	Pipeline (GC	-18.64	116.5	116.74	112	11	35.9	20.27	13.54
	32		15%	1	60	CA50 = 15	800	57.5 = 899.6	9.54881	5.13	59.9	804.06	1.84	0.996	Pipeline (GC	-16.47	116.5	115.16	111	11	36.6	20.31	13.53
	33		15%	1	60	CA50 = 18	800	57.5 = 899.7	9.54881	5.52	60.3	788.48	1.81	0.997	Pipeline (GC	-14.78	116	116.54	111	11	36.1	20.13	13.46
	34		15%	1	60	CA50 = 21	800	57.5 = 899.4	9.54881	6.69	60.2	776.42	1.75	0.989	Pipeline (GC	-12.08	116	116.72	111	11	35.6	20.1	13.47
	35	Do these last, may not be needed	15%	1	60	CA50 = 6	800	57.5 = 900.6	10.5463	6.53	58.9	814.82	1.93	1.003	Pipeline (GC	-21.01	116	116.92	110	11	36.2	20.24	13.52
	36		15%	1	60	CA50 = 9	800	57.5 = 900.8	10.5463	6.51	59.6	814.54	1.93	1.007	Pipeline (GC	-21.01	116	117.08	110	11	35.7	20.24	13.49
	37		15%	1	60	CA50 = 12	800	57.5 = 900.8	10.5463	9.62	60.1	816.67	1.95	1.002	Pipeline (GC	-18.89	116	117.59	110	11	36.3	20.23	13.5
	38		15%	1	60	CA50 = 15	800	57.5 = 900.8	10.5463	5.56	60.3	808.86	1.94	0.999	Pipeline (GC	-16.46	116	115.31	110	11	35.8	20.23	13.52
	39		15%	1	60	CA50 = 18	800	57.5 = 900.5	10.5463	5.62	60.6	793.92	1.83	1.001	Pipeline (GC	-14.75	116	114.82	110	11	35.4	20.21	13.51
	40		15%	1	60	CA50 = 21	800	57.5 = 900.2	10.5463	5.34	60.7	780.96	1.82	1.001	Pipeline (GC	-13.27	116	117.33	110	11	36.1	20.19	13.48
	41		20%	1	60	CA50 = 6	800	57.5 = 900.3	9.54881	5.63	61.7	801.58	1.89	0.999	Pipeline (GC	-21.01	119	120.12	114	16	50.1	21.13	13.44
	42		20%	1	60	CA50 = 9	800	57.5 = 900.3	9.54881	5.54	61.8	802.63	1.91	0.998	Pipeline (GC	-21.01	121	119.37	115	16	50.4	20.06	13.41
	43		20%	1	60	CA50 = 12	800	57.5 = 900.2	9.54881	5.35	61.7	801.49	1.89	0.998	Pipeline (GC	-20.93	121	122.28	116	16	51.1	21.11	13.43
	44		20%	1	60	CA50 = 15	800	57.5 = 900.2	9.54881	5.76	61.9	795.45	1.87	0.996	Pipeline (GC	-20.01	121	122.86	115	16	50.8	20.07	13.39
	45		20%	1	60	CA50 = 18	800	57.5 = 900	9.54881	5.58	61.5	789.29	1.84	1.005	Pipeline (GC	-17.93	121	121.21	115	16	50.9	20.19	13.49
	46		20%	1	60	CA50 = 21	800	57.5 = 899.9	9.54881	6.14	62.1	775.08	1.78	0.997	Pipeline (GC	-16.28	121	119.64	115	16	50.8	20.18	13.49
	47		20%	1	60	CA50 = 6	800	57.5 = 900.4	10.5463	5.05	61.4	804.24	1.9	1.004	Pipeline (GC	-21.01	121	119.57	115	16	51.1	19.98	13.34
	48		20%	1	60	CA50 = 9	800	57.5 = 900.5	10.5463	5.38	61.5	804.15	1.9	1.008	Pipeline (GC	-21.01	121	121.19	115	16	51.2	19.96	13.32
	49		20%	1	60	CA50 = 12	800	57.5 = 900.5	10.5463	5.41	60.9	801.65	1.89	1.002	Pipeline (GC	-20.98	121	120.65	115	16	50.9	19.95	13.29
	50		20%	1	60	CA50 = 15	800	57.5 = 900.3	10.5463	5.52	60.7	800.91	1.88	1.004	Pipeline (GC	-19.24	121	123.26	115	16	50.4	20.12	13.38
	51		20%	1	60	CA50 = 18	800	57.5 = 899.9	10.5463	6.01	61.6	788.28	1.86	1.004	Pipeline (GC	-18.37	121	120.73	115	16	50.3	20.02	13.36
	52		20%	1	60	CA50 = 21	800	57.5 = 899.7	10.5463	5.72	62.1	773.03	1.82	1.009	Pipeline (GC	-16.45	121	120.67	115	16	51.2	19.99	13.34

Table D- 3: Baseline C-EGAI Testing on CFR Engine

Phase	Test #	Description	Phi	Intake Temp. [C]	CA50 Timing	Desired IMEP	Engine Speed [RPM]	Desired CR (new)	EGR set point	intake press set point [kPa]	Recorded Comb. Intensity	Knock Ripple KI	FFT KI	CA50	Recorded IMEP	Ignition Timing	Actual phi	efficiency	Intake Pressure [kPa]
CR sweep	1	cr sweep 8 - 15	1	65	12	800	900	8	0	109	1	2.4	7.4	11.8	801	-13.3	0.991	16.6	108.7
	2		1	65	12	800	900	8.5	0	106	2	2.6	9.3	11.6	798	-12.7	0.995	16.9	106.2
	3		1	65	12	800	900	9	0	106	8.1	4.9	10.9	11.5	802	-12.2	0.989	17.1	105.1
	4		1	65	12	800	900	9.5	0	104	13	5.1	14.2	11.7	805	-11.6	1.01	17.3	104.5
	5		1	65	12	800	900	10	0	104	14.9	5.7	20.8	12.2	804	-11.3	1.013	17.4	103.3
	6		1	65	12	800	900	10.5	0	103	15.7	7	28.3	12	805	-10.8	0.987	17.9	104.9
	7		1	65	12	800	900	11	0	103	16.4	9.4	42.1	11.8	801	-10.6	0.993	18	102.9
	8		1	65	12	800	900	11.5	0	103	32.5	15	52.1	12.1	796	-10.6	0.989	18.1	102.5
	9		1	65	12	800	900	12	0	103	62.2	33.3	102	11.9	806	-10.3	0.997	18.2	104.2
	10		1	65	12	800	900	12.5	0	102	100	63	276.4	12	808	-9.9	1.001	18	101.8
Speed sweep	16	sweep sweep 700 - 1200	1	65	12	800	800	10	0	104	6.4	4.6	10.5	11.8	794	-11.8	0.991	16.6	102.2
	17		1	65	12	800	850	10	0	103	16.2	5.4	12.3	11.6	803	-11.3	1.001	17.7	102.8
	18		1	65	12	800	900	10	0	103	11.5	6	22.6	12.1	808	-11.5	0.993	18.1	103.4
	19		1	65	12	800	950	10	0	103	16.7	7.9	29.2	11.7	808	-11.7	1.002	18.5	102.3
	20		1	65	12	800	1000	10	0	104	17.2	8	43.5	12	801	-12.1	1.006	17.7	104.6
	21		1	65	12	800	1050	10	0	106	18.6	8.6	68.9	12.2	809	-12.4	1.009	18	106.6
	22		1	65	12	800	1100	10	0	106	16.3	6.3	108	11.8	802	-12.7	1.01	17.9	105.8
IMEP sweep	27	imep sweep 600 - 1150	1	65	12	600	900	10	0	80	10.6	0	8.1	11.8	606	-12.4	1.008	13.2	81.3
	28		1	65	12	650	900	10	0	86	13.2	1.2	8.5	11.6	657	-11.9	1.011	14	86.1
	29		1	65	12	700	900	10	0	91	13.4	3.6	9.5	12.3	711.5	-11.6	1.009	15.4	92.1
	30		1	65	12	750	900	10	0	96	14.2	4.6	11.6	12	751.5	-11.5	1.004	16.8	97.1
	31		1	65	12	800	900	10	0	103	18.1	7.6	21.7	11.8	802	-11.5	0.992	17.7	102.7
	32		1	65	12	850	900	10	0	109	19.5	11.6	31.4	12	859	-11.3	1.006	18.1	110.3
	33		1	65	12	900	900	10	0	113.5	23.1	15.2	41.8	11.6	899	-11	1.009	19.1	114.3
	34		1	65	12	950	900	10	0	120.5	25	20.3	94.8	12	954	-11.1	1.002	18.9	121.8
	35		1	65	12	1000	900	10	0	127	28.5	30.4	123	12.3	999	-10.9	0.999	20.1	128.9
	36		1	65	12	1050	900	10	0	134	51.4	47.5	295	12.2	1054	-10.8	1.006	19.5	134.2
	37		1	65	12	1100	900	10	0	140	69.2	53.7	386	12	1111	-10.7	0.008	21.3	141.3

Table D- 4: Modified Box-Benken RSM Example Calculation Tables for Vector Generation

Design Of Experiments Method of Steepest Ascents Optimization Technique

Objective Function Q(f(xn)):
Goal is to maximize efficiency.

Parameters at Center Point:

Speed (RPM)	900	RPM
EGR	10	%
CR	10	
IMEP	1000	kPa
Comb. Int.	30	%

Increment Definition, Equivalent to +1 in Analysis:

Speed	50	RPM
EGR	3	%
CR	0.5	
IMEP	50	kPa
Comb Int	5	%
Sensitivity Factor=	1	

Data:	Speed RPM	EGR	CR	IMEP	Combustion Intesntiy	Speed RPM	EGR	CR	IMEP	Combustion Intesntiy	F(xn) efficiency	Speed	EGR	CR	IMEP	Combustion Intensity
Center 1	0	0	0	0	0	900	10	10	1000	30	17.7					
Center 2	0	0	0	0	0	900	10	10	1000	30	17.8					
Corner 1	1	1	1	1	1	950	13	10.5	1050	35	18.5	0.75	0.75	0.75	0.75	-0.017894737
Corner 2	1	1	1	1	-1	950	13	10.5	1050	25	18.4	0.65	0.65	0.65	-0.65	-0.018
Corner 3	1	1	1	-1	1	950	13	10.5	950	35	17.4	-0.35	-0.35	0.35	-0.35	-0.019052632
Corner 4	1	1	1	-1	-1	950	13	10.5	950	25	18.2	0.45	0.45	-0.45	-0.45	-0.018210526
Corner 5	1	1	-1	1	1	950	13	9.5	1050	35	18	0.25	-0.25	0.25	0.25	-0.018421053
Corner 6	1	1	-1	1	-1	950	13	9.5	1050	25	17.9	0.15	-0.15	0.15	-0.15	-0.018526316
Corner 7	1	1	-1	-1	1	950	13	9.5	950	35	18	0.25	-0.25	-0.25	0.25	-0.018421053
Corner 8	1	1	-1	-1	-1	950	13	9.5	950	25	17.7	-0.05	0.05	0.05	0.05	-0.018736842
Corner 9	1	-1	1	1	1	950	7	10.5	1050	35	17.6	0.15	-0.15	-0.15	-0.15	-0.018526316
Corner 10	1	-1	1	1	-1	950	7	10.5	1050	25	17.5	0.25	-0.25	-0.25	0.25	-0.018421053
Corner 11	1	-1	1	-1	1	950	7	10.5	950	35	17.9	-0.15	0.15	-0.15	0.15	-0.018842105
Corner 12	1	-1	1	-1	-1	950	7	10.5	950	25	17.6	0.15	-0.15	0.15	0.15	-0.018526316
Corner 13	1	-1	-1	1	1	950	7	9.5	1050	35	17.3	0.45	0.45	-0.45	-0.45	-0.018210526
Corner 14	1	-1	-1	1	-1	950	7	9.5	1050	25	17.9	-0.15	-0.15	0.15	-0.15	-0.018842105
Corner 15	1	-1	-1	-1	1	950	7	9.5	950	35	17.9	-0.15	-0.15	-0.15	0.15	-0.018842105
Corner 16	1	-1	-1	-1	-1	950	7	9.5	950	25	18	-0.25	-0.25	-0.25	-0.25	-0.018947368
Corner 17	-1	1	1	1	1	850	13	10.5	1050	35	17.2	-0.55	-0.55	-0.55	-0.55	-0.021523412
Corner 18	-1	1	1	1	-1	850	13	10.5	1050	25	17.1	-0.65	-0.65	-0.65	0.65	-0.021647059
Corner 19	-1	1	1	-1	1	850	13	10.5	950	35	17.5	-0.25	-0.25	0.25	-0.25	-0.021176471
Corner 20	-1	1	1	-1	-1	850	13	10.5	950	25	17.6	-0.15	-0.15	0.15	0.15	-0.021058824
Corner 21	-1	1	-1	1	1	850	13	9.5	1050	35	17.4	-0.35	0.35	-0.35	-0.35	-0.021294118
Corner 22	-1	1	-1	1	-1	850	13	9.5	1050	25	17.9	0.15	-0.15	0.15	-0.15	-0.020705882
Corner 23	-1	1	-1	-1	1	850	13	9.5	950	35	17.2	-0.55	0.55	0.55	-0.55	-0.021523412
Corner 24	-1	1	-1	-1	-1	850	13	9.5	950	25	17.6	-0.15	0.15	0.15	0.15	-0.021058824
Corner 25	-1	-1	1	1	1	850	7	10.5	1050	35	17.5	0.25	-0.25	-0.25	-0.25	-0.020588235
Corner 26	-1	-1	1	1	-1	850	7	10.5	1050	25	17.7	0.05	-0.05	-0.05	0.05	-0.020823529
Corner 27	-1	-1	1	-1	1	850	7	10.5	950	35	17.4	0.35	-0.35	0.35	-0.35	-0.020470588
Corner 28	-1	-1	1	-1	-1	850	7	10.5	950	25	17.3	0.45	-0.45	0.45	0.45	-0.020352941
Corner 29	-1	-1	-1	1	1	850	7	9.5	1050	35	17	0.75	0.75	-0.75	-0.75	-0.02
Corner 30	-1	-1	-1	1	-1	850	7	9.5	1050	25	16.9	0.85	0.85	-0.85	0.85	-0.019882353
Corner 31	-1	-1	-1	-1	1	850	7	9.5	950	35	16.5	1.25	1.25	1.25	-1.25	-0.019411765
Corner 32	-1	-1	-1	-1	-1	850	7	9.5	950	25	16.4	1.35	1.35	1.35	1.35	-0.019294118
Center 3	0	0	0	0	0						17.8					
Center 4	0	0	0	0	0						17.6					
											Averages-->	0.15	0.025	0.025	-0.0375	-0.018526316
											Absolute Values-->	0.15	0.025	0.025	0.0375	0.018526316
											Average of All =	0.059375	Multiplier =	16.84211		
											Final Vector-->	0.45284	0.298367	0.244865	0.568731	0.26942

Procedure
1. Select centerpoint parameters.
2. Select appropriate increments.
3. Take data to complete cube.
4. Enter reference values.
5. Check "stop" criterion.
6. Follow optimization vector until q reaches minimum.
7. Repeat process.

Average Center q = 17.75
Stand. Dev. Of Center = 0.05

Average Corner q = 17.5625

Stand. Dev. Of Corners = 0.471533

If	**0.05**	**is > than**	**0.4715**	**stop**

Optimum region has has been located.

Optimization Vector

	RPM	EGR	CR	IMEP	Comb Int.
Point 1	900	10	10	1000	30
Point 2	922.64	10.90	10.12	1028.44	31.35
Point 3	945.28	11.79	10.24	1056.87	32.69
Point 4	967.93	12.69	10.37	1085.31	34.04
Point 5	990.57	13.58	10.49	1113.75	35.39
Point 6	1013.21	14.48	10.61	1142.18	36.74
Point 7	1035.85	15.37	10.73	1170.62	38.08
Point 8	1058.49	16.27	10.86	1199.06	39.43
Point 9	1081.14	17.16	10.98	1227.49	40.78

Table D- 5: C-EGAI Sweeps of CIM on CFR Engine

Phase	Test #	Description	Phi	Intake Temp. [C]	Spark Timing	Desired IMEP	Engine Speed [RPM	Desired CR	Combustion intensity goal	EGR set point	Intake press set point [kPa]	Recorded Comb. Intensity	Knock Ripple KI	FFT KI	CA50	CA10	CA2x	CA90	Recorded IMEP	Ignition Timing	Power [kW]	Actual phi
	1	CA50 sweep to knock onse	1	60	CA50	1000	900	0.235 = 9.087	X	0	132	5.4	3.6	16.23	15	2.8	19.3	23.5	1018.3	-9.6	2.49	1.009
	2		1	60	Comb Int	1000	900	0.235 = 9.087	10	0	132	9.1	8.3	37.8	12.8	1.3	19.3	22.6	1014.1	-10.7	2.54	1.01
	3		1	60	Comb Int	1000	900	0.235 = 9.087	15	0	132	15.6	18.9	125	11.3	-0.5	16.3	12.5	1032.3	-12.3	2.57	1.006
	4		1	60	Comb Int	1000	900	0.235 = 9.087	20	0	132	20.3	29.4	188	10.5	-0.8	15	19	1021.4	-12.6	2.55	0.996
	5		1	60	Comb Int	1000	900	0.235 = 9.087	25	0	132	26.1	36.7	262	9.8	-1.3	13.5	16	1015.5	-13.3	2.54	0.993
	6		1	60	Comb Int	1000	900	0.235 = 9.087	30	0	132	31.3	42	372	9.5	-1.8	12.8	15.3	1014.2	-14.1	2.59	1.008
	7		1	60	Comb Int	1000	900	0.235 = 9.087	35	0	132	36.5	44.6	505	8.5	-2.8	12.5	14.3	1018.1	-14.5	2.57	1.003
	8		1	60	Comb Int	1000	900	0.235 = 9.087	40	0	132	40.4	47.4	764	8.4	-2.9	12.1	12.9	1023.5	-15.3	2.58	1.006
0 EGR C-EGAI	9		1	60	Comb Int	1000	900	0.235 = 9.087	45	0	132	46.1	50.8	1020	7.7	-3.5	11	12	1018.7	-16.3	2.55	1.009
	10	comb intensity sweep	1	60	Comb Int	1000	900	0.235 = 9.087	50	0	132	50.2	61.1	1235	7.4	-3.9	10.6	11.6	1013.2	-16.6	2.57	1.005
	11		1	60	Comb Int	1000	900	0.235 = 9.087	55	0	132	55.5	63.2	1443	7.2	-4	10.3	11.4	1003.4	-16.9	2.53	1.004
	12		1	60	Comb Int	1000	900	0.235 = 9.087	60	0	132	61.1	73.5	1750	6.1	-4.8	9.4	10.5	1005.7	-17.2	2.53	1.005
	13		1	60	Comb Int	1000	900	0.235 = 9.087	65	0	132	66.3	78.1	2150	5.8	-5.1	8.9	10.1	1005.2	-17.6	2.51	0.997
	14		1	60	Comb Int	1000	900	0.235 = 9.087	70	0	132	70.2	89.8	2590	5.1	-5.3	8.7	8.9	1002.4	-18.2	2.51	1.003
	15		1	60	Comb Int	1000	900	0.235 = 9.087	75	0	132	74.8	93.4	2910	4.3	-6.1	7.3	8	991.3	-18.6	2.49	0.996
	16		1	60	Comb Int	1000	900	0.235 = 9.087	80	0	132	80.6	96.1	3120	4.1	-6.3	6.3	7.1	990.2	-19.3	2.52	1.003
	17		1	60	Comb Int	1000	900	0.235 = 9.087	85	0	132											
	18		1	60	Comb Int	1000	900	0.235 = 9.087	90	0	132											
	19	CA50 sweep to knock onse	1	60	Comb Int	1000	900	0.144 = 10.669	X	15	147.5	3.6	4.6	16.2	16	1	22.1	24.9	1039.76	-13.4	2.59	1.006
	20		1	60	Comb Int	1000	900	0.144 = 10.669	10	15	147.5	10.6	5.2	13.3	15.9	0.5	21.9	25.4	1037.1	-13.1	2.62	1.001
	21		1	60	Comb Int	1000	900	0.144 = 10.669	15	15	147.5	14.7	8.8	17.6	15.7	0	21.1	24.6	1039.8	-13.5	2.64	1.005
	22		1	60	Comb Int	1000	900	0.144 = 10.669	20	15	147.5	19.6	9.4	18.2	15.5	-0.2	20.9	24.2	1043.1	-13.8	2.69	1.007
	23		1	60	Comb Int	1000	900	0.144 = 10.669	25	15	147.5	25.4	12.1	24.1	15.2	-0.4	20.5	23.2	1045.2	-14	2.69	1.003
	24		1	60	Comb Int	1000	900	0.144 = 10.669	30	15	147.5	30.3	15.7	27.4	15	-0.6	19.9	22.8	1044.9	-14.1	2.71	1.004
	25		1	60	Comb Int	1000	900	0.144 = 10.669	35	15	147.5	35.8	17.6	40.6	14.9	-0.5	19.5	21.6	1039.1	-14.2	2.63	1.007
	26		1	60	Comb Int	1000	900	0.144 = 10.669	40	15	147.5	40.1	21.1	47.1	14.6	-0.8	19.4	21.4	1045.6	-14.4	2.71	1.001
15 EGR C-EGAI	27	comb intensity sweep	1	60	Comb Int	1000	900	0.144 = 10.669	45	15	147.5	45.8	23.3	58.9	14.2	-0.8	18.8	21	1043.8	-14.6	2.74	1.001
	28		1	60	Comb Int	1000	900	0.144 = 10.669	50	15	147.5	49.9	27.1	82.3	14	-0.9	18.7	20.9	1045.3	-14.7	2.72	1.001
	29		1	60	Comb Int	1000	900	0.144 = 10.669	55	15	147.5	55.6	31.9	97.1	13.9	-1.1	17.4	19.6	1042.7	-15	2.75	0.999
	30		1	60	Comb Int	1000	900	0.144 = 10.669	60	15	147.5	59.9	36.8	108	13.8	-1.2	17.3	19.5	1042.3	-15.2	2.69	1.004
	31		1	60	Comb Int	1000	900	0.144 = 10.669	65	15	147.5	65.2	38.2	130	13.5	-1.3	16.9	19.1	1042.2	-15.3	2.71	1.001
	32		1	60	Comb Int	1000	900	0.144 = 10.669	70	15	147.5	70.3	48.4	175	13.2	-1.4	16.8	18.5	1039.8	-15.5	2.72	0.998
	33		1	60	Comb Int	1000	900	0.144 = 10.669	75	15	147.5	75.4	49.7	189	12.9	-1.6	16.5	17.9	1038.1	-15.7	2.69	0.999
	34		1	60	Comb Int	1000	900	0.144 = 10.669	80	15	147.5	80.4	55.2	295	12.6	-1.7	15.9	17.3	1036.5	-15.9	2.71	0.999

Table D- 6: Full C-EGAI Optimization Data on CFR Engine

																					raw	raw	raw	norm 15%	norm 15%	norm 15%
data point	MN fuel	Phi Value	Air Flow [slpm	EGR Flow [g/min	EGR rate	Fuel Flow [g/min]	Fuel Coriolis [g/mi	eBMEP	e. Power	Brake Efficeinc	Avg. Peak Press	Max PP	Min PP	COV PP	IMEP	Exhaust Temp	Ignition Delay	Burn Duration	O2 %	CO2 %	CO [ppm]	THC [ppm]	Nox [ppm]	CO [ppm]	THC [ppm]	Nox [ppm]
1	69	1.003	186.142	0	0	13.822	14.788	3.8201	1.7517	14.64480073	4393.996	4925.78	3911.41	4.0801	804.533	539.147	12.635	19.909	0.62	10.1619	837.389	1553.142	3620.34	243.619	451.851	1053.25
2	69	1.006	185.503	0	0	13.783	14.779	4.0272	1.8475	15.48942572	5374.834	6091.13	4379.91	4.9203	823.917	523.951	11.028	17.994	0.62	10.1474	1049.6	2011.422	3698.07	305.358	585.177	1075.87
3	69	1.0002	186.681	0	0	13.781	14.762	3.9673	1.8204	15.26443449	4632.994	5215.75	3979.19	4.4515	809.945	535.441	13.105	22.416	0.62	10.149	722.827	1777.54	3766.32	210.29	517.1344	1095.72
4	69	1.008	184.431	12.3127	5.887	13.774	14.723	4.081	1.8722	15.70676651	4684.165	5426.89	3980.05	5.0534	809.929	520.168	12.466	19.656	0.62	10.228	1181.55	1428.532	3384.87	343.745	415.5986	984.75
5	69	1.007	184.6498	20.7596	9.161	13.758	14.771	4.1139	1.8889	15.86529993	4698.909	5554.01	3969.99	5.2382	811.896	514.383	12.814	20.143	0.62	10.2567	1043.78	1363.073	3147.34	303.665	396.5547	915.646
6	69	1.007	184.128	36.9315	15.331	13.727	14.7129	4.1728	1.9161	16.13010382	4657.975	5408.35	3979.22	5.684	817.791	501.555	15.001	22.439	0.62	10.3018	911.31	1373.399	2210.48	265.125	399.5589	643.089
7	69	0.997	185.469	51.0567	19.931	13.706	14.667	4.2511	1.9522	16.45918044	4412.211	5143.65	3715.81	4.9622	820.192	493.332	17.752	25.581	0.62	10.2339	546.987	1335.386	1442.91	159.133	388.4999	419.782
8	69	0.996	184.776	66.8261	24.626	13.6786	14.667	4.1612	1.9095	16.13142147	3675.335	4506.78	3019.36	6.2488	804.418	499.753	21.668	32.603	0.62	10.2068	539.535	1462.11	384.82	156.965	425.3674	111.955
9	69	1.009	182.149	86.2013	29.949	13.6555	14.6507	3.6398	1.6681	14.11591716	3007.962	3815.13	2718.98	3.9499	731.873	520.051	28.234	46.269	0.62	10.2409	1166.52	2200.067	68.2851	339.372	640.0588	19.866
10	69	1.015	183.441	103.6289	33.8108	13.6504	14.6067	2.3696	1.0853	9.187535932	2973.132	3536.85	2746.61	3.396	591.681	514.375	35.401	64.333	1.2	9.40872	2173.55	8765.636	27.7163	650.962	2625.241	8.30082
11	69	0.998	183.654	64.2109	24.019	13.6211	14.5739	4.0714	1.8681	15.84829565	3492.853	4237.64	2906.73	6.7694	795.491	507.571	22.952	34.732	0.62	10.2112	616.747	1535.769	277.823	179.428	446.7968	80.8262
12	69	0.994	189.376	0	0	13.859	14.862	3.7936	1.7409	14.51565227	4679.7861	5298	3994.78	4.689	816.305	541.509	11.461	19.124	0.7225	10.0587	565.422	1268.259	3838.32	165.332	370.8452	1122.34
13	69	0.997	186.949	11.793	5.299	13.678	14.691	3.9382	1.8087	15.28053516	5158.306	5873.12	4312.6	4.816	813.419	511.41	11.0207	18.581	0.6221	10.1425	565.488	1345.541	3824.55	164.533	391.4946	1112.78
14	69	1.004	184.356	22.7745	9.9923	13.62	14.614	3.9973	1.8363	15.57977395	5254.985	6190.77	4232.88	5.741	812.509	500.869	12.634	19.118	0.4816	10.2158	874.405	1428.871	3240.08	252.664	412.8795	936.237
15	69	0.999	184.844	36.7359	15.2178	13.584	14.565	4.1534	1.9071	16.22334555	5611.342	6575.06	4283.23	6.422	824.581	493.157	15.124	19.712	0.6485	10.1358	620.965	1598.992	2751.03	180.91	465.8446	801.474
16	69	1.003	183.898	53.5532	20.8091	13.576	14.591	4.2637	1.9585	16.67041348	5429.612	6933.73	4177.54	9.454	831.547	485.526	17.857	23.365	0.6202	10.1397	962.329	2124.728	1485.74	279.97	618.1468	432.246
17	69	1.001	182.244	70.8679	26.0099	13.5102	14.526	4.0834	1.8739	16.02799722	4187.715	5209.6	3727.98	5.483	795.514	480.262	23.414	38.562	0.6001	10.1875	839.983	1853.193	310.454	244.134	538.6155	90.2308
18	69	1.007	181.036	69.0167	25.6182	13.498	14.463	4.0109	1.8409	15.75997047	4998.423	6993.91	4588.4	4.526	791.551	465.6129	26.475	40.222	0.4864	10.2294	1340.43	2114.659	288.004	387.415	611.1851	83.2397
19	69	1.011	179.827	87.9736	30.5688	13.469	14.423	3.1919	1.4602	12.52770784	3833.282	4316.54	3388.48	3.183	673.936	515.9169	31.788	58.291	0.8728	10.0114	2121.75	4073.539	59.6449	625.067	1200.062	17.5713
20	69	0.993	180.761	0	0	14.394	14.337	3.9373	1.8082	14.51642224	4517.977	5400.96	3868.78	6.174	776.64	506.578	11.789	19.644	3.5891	8.75627	531.046	1032.795	3263.3	180.994	352.0032	1112.22
21	69	0.995	202.655	8.8953	3.9255	14.701	15.775	4.6218	2.1252	16.70504135	5115.972	5827.14	4306.55	4.587	866.537	526.604	12.054	18.682	0.6046	10.273	730.221	1258.191	3759.57	212.28	365.7641	1092.93
22	69	1.009	203.763	25.9511	10.2567	15.027	16.105	4.8588	2.2335	17.17545677	5357.472	6277.56	4198.26	5.734	891.204	518.521	13.641	19.642	0.3334	10.3811	1301.13	1334.035	2959.25	373.26	382.6986	848.928
23	69	1.007	210.173	39.6546	14.5506	15.386	16.478	5.1421	2.3613	17.73454556	5486.976	6607.72	4361.61	6.594	921.595	510.407	15.239	21.034	0.3028	10.4358	1098.16	1156.559	2421.93	314.565	331.2924	693.755
24	69	1.002	265.964	71.8849	19.6141	18.7005	20.0743	7.0245	3.2339	19.98333612	6683.571	8352.59	5257.29	8.494	1160.29	526.685	18.287	22.803	0.3767	10.4672	679.008	1108.121	1624.37	195.2	318.5604	466.97
25	69	1.007	293.672	99.7739	23.5572	20.9001	22.473	7.8836	3.6081	19.9491698	6046.989	7212.2	4930.35	5.871	1283.8	507.536	24.774	31.858	0.2788	10.5752	1178.64	1260.331	517.127	337.225	360.5976	147.957
26	69	1.004	271.032	108.8756	26.8905	19.1708	20.626	7.0979	3.2761	19.74747345	6344.456	9222.39	5795.39	6.478	1168.31	521.268	25.614	38.061	0.4879	10.3647	1516.1	2059.554	276.344	438.219	595.3021	79.8756
28	69	0.989	186.2746	0	0	13.453	14.458	3.6427	1.6702	14.34643393	4718.231	5470.84	3987.61	4.592	802.483	507.987	11.377	18.592	6.0932	7.31488	352.22	926.742	3173.67	140.348	369.2748	1264.6
29	69	1.001	184.323	37.2381	15.4307	13.568	14.581	4.0096	1.8419	15.6871785	5176.588	5975.22	4007.98	6.518	818.117	492.201	16.925	20.381	0.5904	10.0482	691.75	1499.611	2541.5	200.956	435.6416	738.313
30	69	1.004	183.778	36.9627	15.3836	13.5564	14.578	4.0293	1.8492	15.76282795	5063.052	6004.74	4005.3	6.466	818.048	492.2305	15.959	20.864	0.5291	10.0563	881.87	1539.358	2387.84	255.415	445.8423	691.588
31	69	1.0001	184.244	38.0574	15.7438	13.5497	14.522	4.0496	1.8565	15.83287923	4398.939	5634.71	3691.31	5.186	816.413	499.679	15.664	24.275	0.5938	10.0315	581.05	1470.524	2030.34	168.825	427.2632	589.919
32	69	1.0001	182.783	38.2082	15.9076	13.5346	14.5417	3.9908	1.8312	15.63453539	3945.021	4562.82	3363.29	4.872	803.678	511.116	16.089	26.714	0.5507	10.0562	537.134	1270.776	1587.92	155.735	368.4439	460.396
33	69	0.994	183.727	38.1286	15.8113	13.4619	14.4784	3.9727	1.8234	15.65201357	3550.349	4132.7	2962.48	5.431	787.329	522.209	16.781	28.497	0.6523	10.0115	407.74	1114.359	1270.65	118.812	324.7143	370.257
34	69	0.994	183.715	37.9619	15.7549	13.4614	14.4536	3.8708	1.7737	15.22595571	3209.966	3841.82	2638.1	5.491	774.621	529.581	16.535	30.191	0.6855	10.0087	394.419	1085.563	1041.82	115.119	316.8431	304.075
35	69	1.003	181.277	35.4356	14.9883	13.5207	14.5041	4.2141	1.9349	16.53689517	5777.417	6704.96	4310.72	6.396	814.621	482.218	16.598	19.461	0.5932	10.0496	904.722	1613.711	2430.38	262.861	468.8525	706.131
36	69	1.005	180.713	35.7563	15.1393	13.5163	14.4491	4.2108	1.9341	16.53543893	5660.001	6641.22	4323.62	6.711	814.284	480.5091	15.882	19.972	0.5625	10.0713	1006.61	1722.501	2349.74	292.021	499.7053	681.671
37	69	1.0002	181.3719	35.9789	15.1791	13.5127	14.4772	4.2484	1.9508	16.68265764	4741.541	5752.63	3958.97	6.386	816.508	490.0392	15.586	24.465	0.6265	10.0803	635.632	1469.618	2008.11	184.982	427.6885	584.399
38	69	0.995	182.146	36.4725	15.3071	13.5083	14.4695	4.2046	1.9305	16.51443554	4155.999	4922.88	3485.7	5.176	806.982	502.609	15.819	29.376	0.6691	10.0656	474.559	1338.688	1474.69	138.397	390.4058	430.068
39	69	0.9995	181.0221	37.0646	15.5988	13.5014	14.5253	4.1171	1.8899	16.17538574	3755.162	4394.89	3221.44	5.651	794.063	513.088	-16.252	31.637	0.5737	10.1113	610.485	1433.917	1050.37	177.202	416.2149	304.886
40	69	1.0004	179.8731	37.7003	15.9126	13.4916	14.4093	4.0343	1.8506	15.85052774	3415.913	4163.9	2956	5.501	780.385	522.8769	16.801	33.424	0.5696	10.1224	608.723	1420.913	813.522	176.655	412.3571	236.089
41	69	1.011	177.5821	49.9295	20.2327	13.4305	14.4317	4.0262	1.8473	15.89424395	4019.957	5055.82	3378.73	5.321	791.156	493.4301	20.807	27.756	0.2632	10.0586	2641.8	1464.247	747.129	755.283	418.624	213.602
42	69	0.997	182.5145	48.7322	19.4493	13.4216	14.4305	4.1149	1.8884	16.25864414	4169.074	4964.76	3543.35	5.357	802.077	492.9889	18.932	27.159	0.6144	10.041	516.892	1209.597	1074.11	150.336	351.8072	312.4
43	69	0.997	182.2977	49.2409	19.6224	13.4182	14.4239	4.1151	1.8877	16.25673552	4141.283	4835.42	3502.58	5.382	800.976	493.6011	18.435	27.326	0.6205	10.0492	491.088	491.0875	1076.34	142.874	142.8741	313.144
44	69	0.996	181.9849	50.0408	19.9117	13.4118	14.4281	4.0777	1.8708	16.11888208	3897.879	4604.76	3241	5.681	795.044	499.5566	18.842	28.782	0.6317	10.0267	498.934	1182.794	895.533	145.237	344.3054	260.685
45	69	1.0008	182.3258	50.3811	19.9791	13.4882	14.5102	4.0637	1.8629	15.95990019	3555.752	4160.24	2967.8	5.522	788.613	509.6818	18.904	30.922	0.5101	10.0966	619.675	1229.081	641.344	179.309	355.6456	185.579
46	69	1.004	181.4006	49.2797	19.6997	13.4895	14.5105	3.9542	1.8131	15.53175498	3241.525	3818.38	2740.58	6.011	774.454	516.8323	13.232	32.792	0.4486	10.1266	684.827	1266.807	480.749	197.565	365.4596	138.691
47	69	1.004	179.4596	51.8436	20.7036	13.3379	14.2882	4.1371	1.8994	16.45597436	4438.894	5264.44	3729.36	5.371	803.948	487.1837	-20.051	29.362	0.5392	10.025	770.225	1622.844	918.857	223.19	470.2556	266.26
48	69	1.005	179.0745	52.1879	20.8499	13.3218	14.3398	4.1347	1.8981	16.46458563	4452.643	5497.48	3683.85	5.479	802.825	485.5315	19.019	29.189	0.569	10.0148	802.027	1635.645	929.103	232.746	474.6595	269.623
49	69	1.0006	179.6781	52.9797	21.0515	13.2991	14.2692	4.1255	1.8925	16.44403006	4422.738	5424.58	3639.94	5.362	801.505	485.6405	18.051	29.412	0.6563	9.9951	629.356	1575.212	959.48	183.425	459.0935	279.639
50	69	1.005	178.4889	54.4521	21.6007	13.3828	14.3246	4.1085	1.8864	16.2885125	4170.899	5011.87	3369.88	5.772	800.517	493.8678	17.685	31.196	0.4621	10.1152	883.857	1610.923	1610.92	255.151	465.0403	465.04
51	69	1.005	178.3972	54.7211	21.6933	13.3684	14.3534	4.0359	1.8518	16.00697525	3802.594	4555.79	3253.53	6.056	788.491	502.1343	18.751	33.565	0.4936	10.0894	818.417	1544.526	544.569	236.625	446.561	157.449
52	69	1.009	177.5903	55.6043	22.0408	13.3528	14.3586	3.9332	1.8036	15.60854813	3486.128	4255.12	3119.35	5.776	772.933	510.8261	18.681	35.959	0.4493	10.0824	1160.49	1724.362	377.112	334.801	497.4761	108.796

Table D- 7: Fuel Composition Used Within Full Study

Channel 2, CP-4900 Backflush Column Module, 10m PPQ Results

Pk #	*Name*	*Retention Time*	*Area*	*Concentration*
1	Nitrogen	0.370	505706	**0.639**
2	Methane	0.375	59211614	**93.365**
3	CO2	0.419	1846487	**2.038**
5	Ethane	0.472	11237534	**11.351**
Totals			72801341	**107.392**

Channel 3, 4m 5CB Unheated Injector Results

Pk #	*Name*	*Retention Time*	*Area*	*Concentration*
3	Propane	0.213	3544540	**1.572**
4	iso-Butane	0.247	423929	**0.158**
5	n-Butane	0.273	731937	**0.269**
6	iso-Pentane	0.360	234194	**0.077**
7	n-Pentane	0.401	334441	**0.109**
12	n-Hexane	0.677	245697	**0.072**
	n-Heptane			**0.000 BDL**
Totals			5514738	**2.258**

ABREVIATIONS AND SYMBOLS

Abbreviation	Term
AHRR	Apparent Heat Release Rate
aTDC	After Top Dead Center
bTDC	Before Top Dead Center
CA50	Crank Angle of 50% Heat Release
C-EGAI	Controlled End Gas Auto Ignition
CIM	Combustion Intensity Metric
CFR	Cooperative Fuel Research Engine
CFD	Computational Fluid Dynamics
CO	Carbon Monoxide
CO2	Carbon Dioxide
COV	Coefficient of Variance
CR	Compression Ratio
EGAI	End Gas Auto Ignition
EGR	Exhaust Gas Recirculation
EPA	Environmental Protection Agency
f-EGAI	Fractional End Gas Auto Ignition
FFT	Fast Fourier Transform
FTIR	Fourier Transform Infrared Spectroscopy
GAP	Graphical Application Programmer
H2O	Water

H2O2	Hydrogen Peroxide
IMEP	Indicated Mean Effective Pressure
KOCA	Knock Onset Crank Angle
LECM	Large Engine Control Module
MFB	Mass Fraction Burned
NG	Natural Gas
NMEP	Net Mean Effective Pressure
NOx	Oxides of Nitrogen
O	Atomic Oxygen
O2	Oxygen
OH	Hydroxide
PID	Proportional – Integral – Derivative
PMEP	Pumping Mean Effective Pressure
RPM	Revolutions Per Minute
RSM	Response Surface Method
SI	Spark Ignited
TDC	Top Dead Center
THC	Total Hydrocarbons
TPA	Three Pressure Analysis
VFD	Variable Frequency Drive
VI	Virtual